Tampere University

Scandem 2022
Book of Abstracts

ISBN 978-952-03-2484-1, Tampere

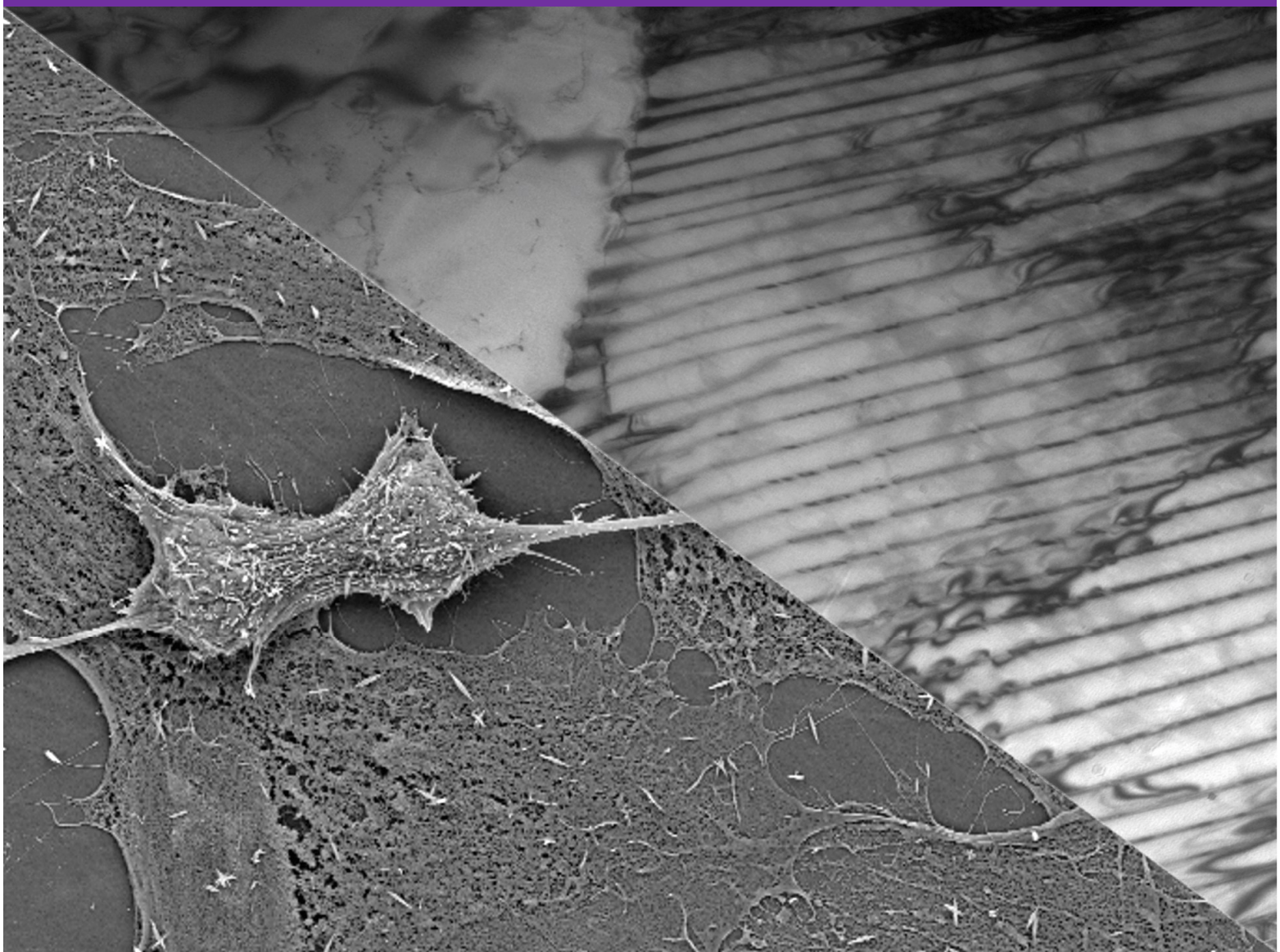

Tampere University

Scandem 2022
Book of Abstracts

Editors

Mari Honkanen

Justus Rantala

Turkka Salminen

Kati Valtonen

Minnamari Vippola

ISBN 978-952-03-2484-1, Tampere

Tampere University

Scandem 2022
20.-22.6.2022
Tampere Microscopy Center

Local organizing committee in Tampere University

Prof. Minnamari Vippola
Dr. Mari Honkanen
Dr. Turkka Salminen
Dr. Kati Valtonen
Dr. Teemu Ihalainen

Scientific Committee

Materials Science:
Professor Minnamari Vippola (TAU)
Professor Thomas Willum Hansen (DTU)
Senior Scientist Hua Jiang (Aalto)
Staff Scientist Turkka Salminen (TAU)
Staff Scientist Kati Valtonen (TAU)
Life Science:
Professor Sarah Butcher (University of Helsinki)
Professor Varpu Marjomäki (University of Jyväskylä)
Research Director Eija Jokitalo (University of Helsinki)
Academy Research Fellow Teemu Ihalainen (TAU)
Associate Professor Nonappa (TAU)
Senior Scientist Mari Honkanen (TAU)

Table of Contents

Life science:

Materials science:

Company presentations:

1. Genomic relationship between American lymegrass species and their Eurasian and Asiatic relatives

Kesara Anamthawat-Jónsson[1]

[1]*Institute of Life and Environmental Sciences, University of Iceland, Askja – Sturlugata 7, Reykjavík IS-102, Iceland*

Corresponding author: kesara@hi.is

Leymus Hochst. (lymegrass) is a genus of about 50 polyploid perennial grass species in the wheat tribe Triticeae. Type species is the octoploid *Leymus arenarius* (**Figure 1**). Lymegrass is an ecologically important plant due to the ability to bind soil and sand with its extensive rhizome system. Some species are forage grasses. Lymegrass has its distribution over the temperate regions of the Northern Hemisphere. Ten species are found in North America, nine species in Europe and Eurasia (including Russia, Siberia, Mongolia and Russian Far East) and the rest (over 30 species) occurs in Central Asia and China. We investigated three species from western North America, i.e., *L. cinereus*, *L. innovatus* and *L. triticoides*, in comparison with three species from Eurasia and Central Asia, i.e., *L. chinensis*, *L. multicaulis* and *L. racemosus*.

Figure 1. Leymus arenarius (sea lymegrass) on the coast of Reykjanes Peninsula on 20th June, 2018, at midnight.

We used the method of fluorescence in situ hybridization (FISH) to identify the Ns genome, with an aim to trace evolutionary relationships among these *Leymus* species. Ns genome belongs to the diploid genus *Psathyrostachys* Nevski, the ancestor of all polyploid *Leymus* species. We isolated Ns specific DNA sequences from *Psathyrostachys*, to be used as probes in the FISH experiments. Two repetitive sequence families were obtained: PshA (five 384-745 bp DraI plasmid clones) from *Ps. huashanica* (China) and PsjD (six 570-625 bp ScaI clones) from *Ps. Juncea* (Russia). The sequence analysis showed over 90% homology within family.

PshA and PhjD probes were first used to hybridize in Southern blot experiments to *Dra*I digested total genomic DNA of the six *Leymus* species under study, the two *Psathyrostachys* species, as well as reference Triticeae species, including barley, rye and wheat. The results showed that PshA and PsjD probes hybridized only to *Psathyrostachys* and *Leymus*, confirming that they are Ns genome specific sequences. Among these Ns species, however, the two probes showed differential hybridization. While PshA is present in American *Leymus* species, PsjD is prevalent among Eurasian/Asiatic species.

FISH experiments revealed physical location of PshA and PsjD sequences on chromosomes. The PshA family was localized in the subtelomeric heterochromatic blocks in chromosomes of *Ps. huashanica* (diploid, 2n=14): total 22 blocks, on both arms of ten chromosomes (5 pairs) and one arm of two chromosomes (one pair). This PshA was also localized to about 22 blocks in *L. innovatus* (tetraploid, 2n=28), and similar localization in the other American species. The PsjD family was also localized in the subtelomeric heterochromatic blocks on chromosomes of *Ps. juncea* (diploid, 2n=14), but only at 14 sites, on both arms of four chromosomes (two pairs) and one arm on six chromosomes (three pairs). The same pattern was detected in FISH experiments of PhjD on *L. multicaulis* and other Eurasian/Asian species.

The American *Leymus* species under study are allotetraploid containing half of its Ns genomes deriving from the diploid *Ps. huashanica*, which has a very restricted distribution, only in a mountain area in NW China. On the other hand, the *Leymus* species from Eurasia and Central Asia appear to be allotetraploid containing half of its Ns genomes deriving from or related to *Ps. juncea*, which occurs in the same distribution range as the Eurasian/Asian *Leymus* species.

Acknowledgements: I sincerely thank Dr Snædís Björnsdóttir for the cloning and sequencing experiments, Dr Ægir Thór Thórsson for FISH experiments and Dr Sæmundur Sveinsson for Southern blot experiments. We express our gratitude in memory of Dr Björn Salomon (Swedish Agricultural University) who provided us with most of the accessions used in this study.

2. Democratizing deep learning for image segmentation with DeepMIB

Ilya Belevich[1], Eija Jokitalo[1]

[1]*Electron Microscopy Unit, Institute of Biotechnology, PO Box 56 (Viikinkaari 9), University of Helsinki, 00014, Finland*

Corresponding author: ilya.belevich@helsinki.fi

Deep learning approaches are highly sought after solutions for coping with large amounts of collected datasets and becoming an essential part of imaging workflows. However, in most cases, deep learning is still considered as a complex task that only image analysis experts can master. In my talk, I will present DeepMIB [1], a user-friendly software package that is capable of training convolutional neural networks for segmentation of multidimensional microscopy datasets (Figure 1).

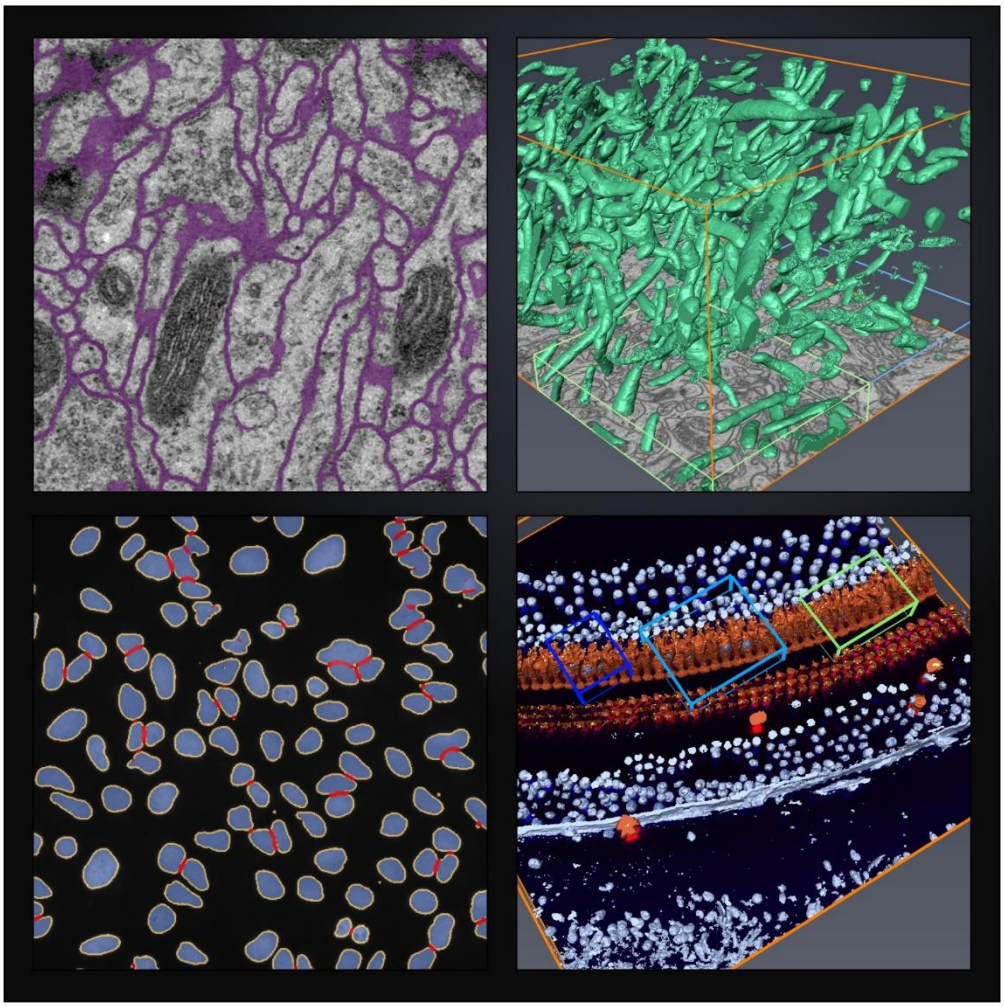

Figure 1 Application of DeepMIB for image segmentation of 2D and 3D light and electron microscopy datasets.

I will demonstrate its successful application for segmentation of 2D and 3D electron and multicolor light microscopy datasets with isotropic and anisotropic voxels. DeepMIB is available as an open-source multi-platform Matlab code and as compiled standalone

application for academic research on Windows and MacOS. It is easy to install and its usage does not require any computer programming skills. DeepMIB is suitable for researchers interested of bringing a power of deep learning into own image segmentation workflows. DeepMIB is bundled with Microscopy Image Browser (MIB) [2], forming a powerful suit to address all aspects of an imaging pipeline starting from basic processing of images (e.g., filtering, normalization, alignment) to manual, semi-automatic and fully automatic segmentation, proofreading of segmentations, their quantitation and visualization.

[1] A I. Belevich, E. Jokitalo, PLoS Comput Biol. 2021 Mar 2;17(3):e1008374.

[2] I. Belevich, M. Joensuu, D. Kumar, H. Vihinen E. Jokitalo, PLoS Biology 2016 Jan 4;14(1):e1002340.

3. Investigating the physiology of retinal pigment epithelium with immunogold electron microscopy

Julia Fadjukov[1*], Viivi Karema-Jokinen[1*], Satu Hakanen[2], Maija Vihinen-Ranta[2], Teemu Ihalainen[1], Soile Nymark[1]

[1]Tampere University, Tampere, Finland,

[2]University of Jyväskylä, Jyväskylä, Finland,

Corresponding author: Julia.johansson@tuni.fi

The light sensing photoreceptors are under constant renewal and this process is crucial for their survival. This renewal occurs daily and involves a sequence of regulated steps during which the spent photoreceptor outer segments are taken up and digested by the retinal pigment epithelium (RPE) [1]. The aim of this study was the investigate the possible roles of voltage-gated sodium channels in this renewal pathway that is also known as phagocytosis. This was carried out by using human embryonic stem cell (hESC)-derived RPE. The localization of photoreceptor outer segments (POS) and the channels were studied by incubating hESC-derived RPE with purified POS particles. To offer a more detailed view of their localisation, this was carried out with immunoelectron microscopy where the sodium channels were labelled with nanogold particles, and the samples were processed for pre-embedding electron microscopy. The imaging was carried out with transmission electron microscope (TEM).

These experiments showed co-localization between certain subtypes of sodium channels and photoreceptor outer segment marker opsin. Moreover, it showed that sodium channels undergo a change in the cellular localization during the renewal process [2]. While their localization was heavily in the junctions in the control conditions, during phagocytosis the junctional localization decreased, and signal showed a more diffuse distribution in the cell membrane. Furthermore, the nanogold particles were also found adjacent to the outer segments. Our data strongly indicates that voltage-gated sodium channels are involved in the phagocytosis pathway. Further studies are needed to fully evaluate the concerted functioning of these channels in the regulation of the phagocytic process, and in the RPE physiology overall.

[1] R. W. Young, “The daily rhythm of shedding and degradation of rod and cone outer segment membranes in the chick retina.,” *Invest Ophthalmol Vis Sci*, vol. 17, no. 2, pp. 105–16, Feb. 1978.

[2] J. K. Johansson *et al.*, “Sodium channels enable fast electrical signaling and regulate phagocytosis in the retinal pigment epithelium,” *BMC Biology*, vol. 17, no. 1, p. 63, Aug. 2019, doi: 10.1186/s12915-019-0681-1.

4. The BUILD project: Proof-of-Concept study for high-resolution correlative multimodal imaging of mouse brain

Fernandez-Rodriguez J.[1], Axer M.[2], Micaroni M.[1], Camacho R.[1], Amunts K.[2], Handschuh S.[3], Gloesmann M.[3], De Felipe J.[4], Merchan-Perez A.[4], Eberle A.L.[5], Garbowski T.[5], Ruland S.[2], Jaeger C.[6], Casares A.[6]

[1]Centre for Cellular Imaging, Shalgrenska Academy, University of Gothenburg, Sweden
[2]Institute of Neuroscience and Medicine, Forschungszentrum Jülich, Germany
[3]VetCore/Imaging, University of Veterinary Medicine, Vienna, Austria
[4]Laboratorio Cajal de Circuitos Corticales, Universidad Politécnica de Madrid, Spain
[5]Carl Zeiss MultiSEM GmbH, Oberkochen, Germany
[6]Carl Zeiss Microscopy GmbH, Oberkochen, Germany

Corresponding author: Julia.fernandez-rodriquez@cci.sahlgrenska.gu.se

The future of bioimaging is in the synergy between modalities, in the hard-to-navigate waters of the interdisciplinary divide. While 'omics' communities attempt to reduce complexity through advances in single-cell technologies, imaging communities are attempting to broaden their existing single-cell technologies to tackle the complex spatial systems biology of three-dimension (3D) models or entire organs (e.g., the brain), and pathological tissues such as tumors. Given the age-old trade-off between sample size and resolution, and between imaging structure and function, these challenges will only be met by designing new and more automated *Correlative Multimodal Imaging (CMI)* workflows that daisy-chain microscopes together to capture images of nanoscale biological processes across scales within a single organism.

The CMI approach aims at gathering information from a specimen with multiple imaging modalities that – when combined – create a highly informative, composite view of the specimen. It is a holistic approach that spans a large spatial resolution range from from mm to nm, and provides complementary information about the structure, function, dynamics, and the molecular composition of the sample. CMI is of strategic importance to a large and wide group of national and international life scientists, supporting many research activities, such as, to characterise synaptic changes and pathological protein aggregation underlying neurological diseases. In this context we have created in 2019 a European consortium, *Big mUltimodal hIgh-resolution atLas Data Management, BUILD*, to design a proof-of-concept approach to study and understand the brain's nerve fiber architecture and the resulting structural connectivity (e.g., to address diseases that affect myelination, such as MS). During the study the same sample was shipped to the different expert facilities all over Europe. We first prepared and visualized a mouse brain section with a low-resolution polarized microscopy, (Figure 1A). The same brain section was sent to a second facility where is prepared for scanning electron microscopy and X-ray tomography (1B). We then defined the volume of interest with X-ray tomography (1C), creating a reference 3D image dataset. After a successful evaluation of the X-ray the images were correlated with different scanning electron microscope systems to image the volume at high resolution for advanced analysis (SEM single and multi-beam systems and FIB-SEM, see Figure 1 D-F). Finally, datasets will be transferred to the Fenix infrastructure for segmentation analysis test and final storage. Thus, the combined usage of these interdisciplinary approach will finally enable the generation of unique brain atlases of different species, such non-human and human primates.

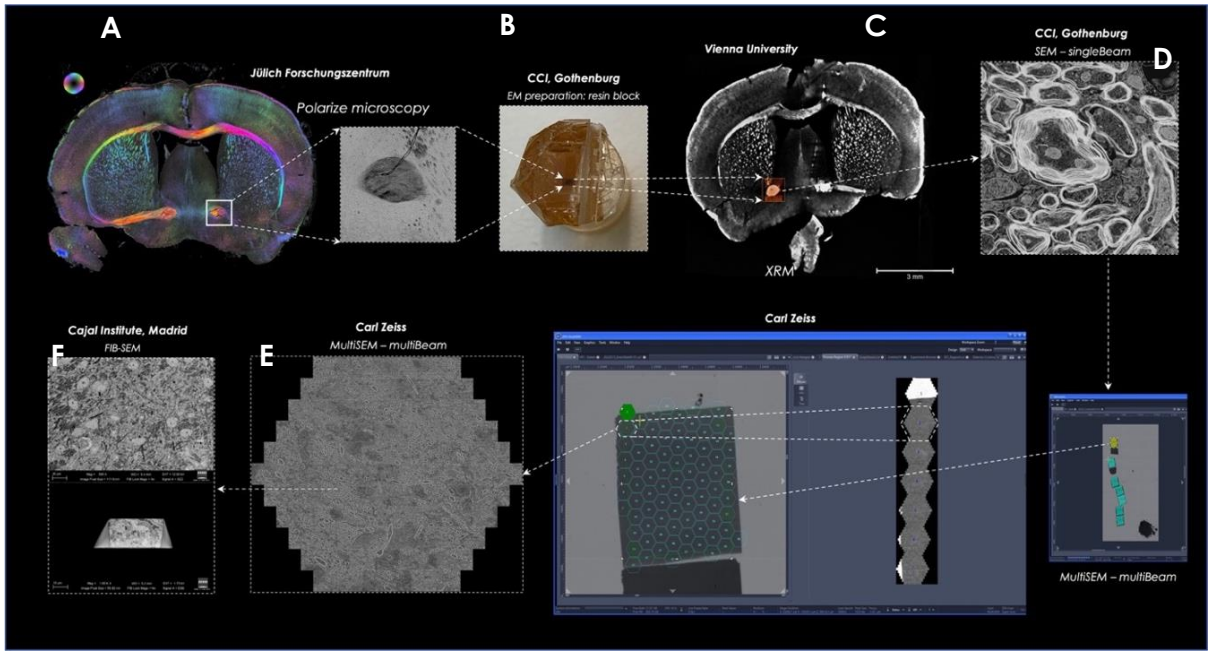
A
Jülich Forschungszentrum
Polarize microscopy
B
CCI, Gothenburg
EM preparation: resin block
C
Vienna University
XRM
3 mm
CCI, Gothenburg
SEM – singleBeam
D
Carl Zeiss
MultiSEM – multiBeam
Carl Zeiss
MultiSEM – multiBeam
E
Cajal Institute, Madrid
FIB-SEM
F

5. Optimising Image Analysis of Membrane Hydration Using Solvatochromic Fluorophores

Ainsley Huang[1], Jeremy Adler[2] and Ingela Parmryd[1]

[1]*Institute of Biomedicine, University of Gothenburg, Gothenburg, Sweden*

[2]*Department of Immunology, Genetics and Pathology, Uppsala University, Uppsala, Sweden*

Corresponding author: chi-wen.huang@gu.se

Fluorescence microscopy is important in studies of membrane order and dynamics. With the special characteristics of emission peak shifting when exposed to environments with different polarities, solvatochromic flurophores like laurdan and c-laurdan are frequently used in membrane order studies. In model membranes mimicking the lipid arrangement of natural cell membranes, the lipid bilayer can separate into two distinct liquid phases known as the liquid ordered (Lo) and disordered phases (Ld). The Lo phase is enriched in saturated sphingolipids and cholesterol has tighter lipid packing whilst lipids are more loosely packed in Ld phase. In cells, Lo phase is commonly referred to as lipid rafts. Phase alternation in model and cellular membranes from Lo to Ld phase causes a red shift in their emission spectra. Generalised polarisation is calculated from the differences in intensities at specific regions or wavelenghts of the two fluorescence emission spectra and used to quantify changes in membrane order.

Images acquired by fluorescence microscopy are inevitably degraded by blurring and Poisson noise. The blurring due to convolution of the true objects by the point spread function (PSF) of the whole imaging system. To enable the extraction of more accurate information, a deconvolution process can be applied before any image analysis. Image deconvolution is a restoration procedure to enhance the resolution of an image. By partially relocating the blurred photons back to their original positions, the deconvolution process generates an image more representative of the original object.

In this study, we have examined how GP-values in the plasma membrane of live Jurkat cells are affected by image deconvolution and the selection of the region of interest (ROI) for the plasma membrane. While maintaining the relative intensities in the two channels, we have addressed how the adjustment of a critical user input in the Huygens deconvolution software the “signal to noise ratio (S/N)” for deconvolution procedure affects GP-values (Fig. 1). The GP-values displayed significant differences between the deconvolved and the raw images, which demonstrates the effect of deconvolution. To determine the ideal SN combinations from both channels for application in future experiments, the SN groups having the smallest standard deviations of their mean GP-values were determined. The images deconvolved at SN=8 were selected for further ROI analysis due to its membrane being more smooth, visible and can be distinguishable from the internal membranes. To assess how ROI selection changes GP-values, firstly, the plasma membrane was identified as the brightest line of pixels around the cell edge and then different ROIs were created by moving the original ROI one to seven pixels inwards or outwards from the plasma membrane. As the ROI was shifted towards cytoplasm, the GP-values decreased until they reached a plateau reflecting the lower membrane order of intracellular membranes compared with the plasma membrane. Noticeably, the GP-values were significantly different for all 15 ROI positions, which indicates the importance of an accurate ROI selection when determining the GP-values. By optimizing the deconvolution procedure and the ROI selection, membrane properties defined by GP analysis will report of cellular events more accurately.

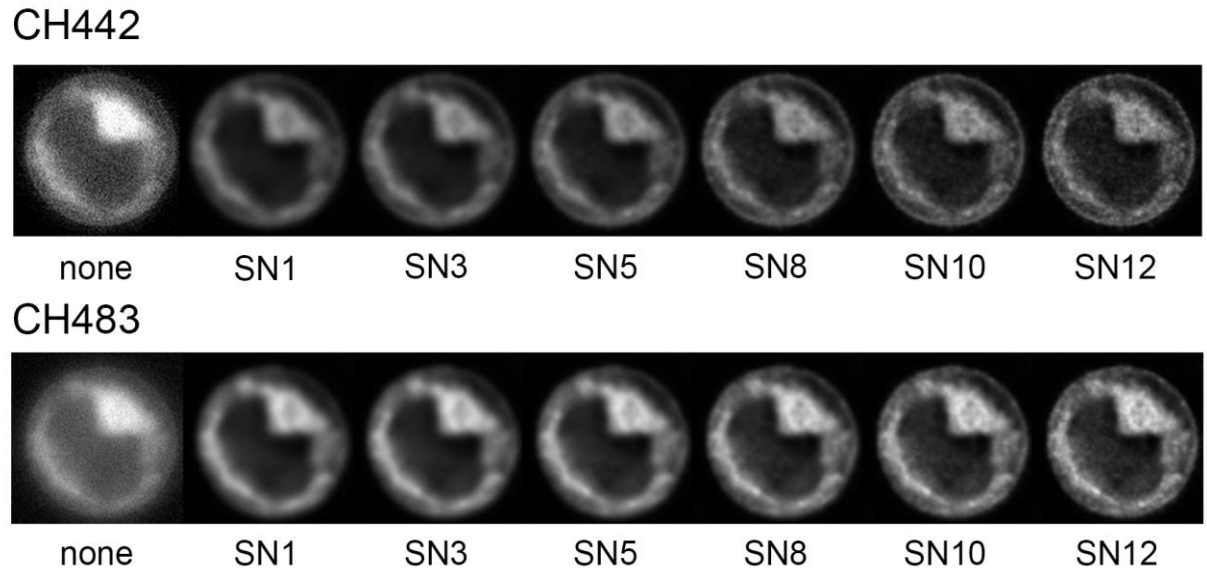

Figure 1. Illustration of image deconvolution using different signal to noise ratios. What representations of the cell staining should be analysed for reliable results?

6. Modular Vaccine Platform Based on the Norovirus-Like Particle

Lampinen Vili[1], Heinimäki Suvi[1,2], Laitinen Olli H[1], Pesu Marko[1], Hankaniemi Minna M[1], Blazevic Vesna[1,2], Hytönen Vesa P[1].

[1]*Faculty of Medicine and Health Technology, Tampere University, Tampere, Finland*

[2]*Vaccine Development and Immunology/Vaccine Research Center*

Corresponding author: vili.lampinen@tuni.fi

Virus-like particle (VLP) vaccines have recently emerged as a safe and effective alternative to conventional vaccine technologies. In addition to using VLPs as vaccines against the viruses they derive from, their strong immunogenic effects can be harnessed for making vaccines against other pathogens by decorating VLP surface with antigens from the pathogen. We covalently decorated the robust norovirus-like particle with two conserved influenza antigens using SpyCatcher/SpyTag conjugation technology (PMID: 22366317), and tested for the immunogenicity of the resulting vaccine candidates in BALB/c mice.

SpyTagged noro-VLP was expressed with high efficiency in insect cells and purified using industrially scalable methods. Like the native noro-VLP, SpyTagged noro-VLP is stable for months when refrigerated in a physiological buffer. We studied the morphology and size of the tagged and decorated noro-VLP with transmission electron microscopy and compared the results to dynamic light scattering. The conserved influenza antigens were produced separately as SpyCatcher fusions in E. coli before covalent conjugation on the surface of noro-VLP. Producing the antigenic pathogen fragments and the VLP platform separately makes vaccine development rapid and convenient. The noro-VLP had a high adjuvant effect, inducing high titers of antibody production against proteins presented on its surface. The modular noro-VLP vaccine platform presented here offers a rapid, convenient and safe method to present various soluble protein antigens to the immune system for vaccination and antibody production purposes.

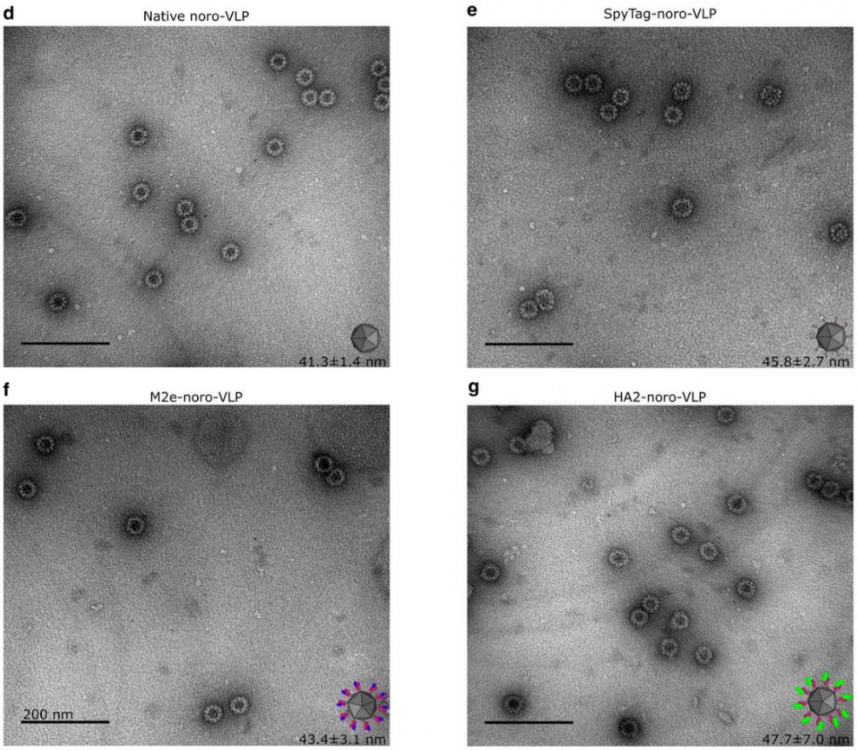
d
Native noro-VLP
41.3±1.4 nm
e
SpyTag-noro-VLP
45.8±2.7 nm
f
M2e-noro-VLP
200 nm
43.4±3.1 nm
g
HA2-noro-VLP
47.7±7.0 nm

7. Application of Nanochannel Liquid Cell for Liquid Phase Electron Microscopy

Tayyaba Malik[1], Emil Christian Stillhoff[1], Mads Søndergaard Larsen[1], Murat Nulati Yesibolati[1] and Kristian Mølhave[1]

[1]*DTU Nanolab, National Centre for Nano Fabrication and Characterization, Technical University of Denmark, 2800 Kgs. Lyngby, Denmark*,

Corresponding author: taymal@dtu.dk

Liquid Phase Electron Microscopy (LPEM) is a developing method that is used to obtain the structural information about materials with atomic scale resolution in liquids, studying reactions such as nucleation and growth from dynamic process and observe polymers and biological specimens in their original liquid environment [1]. Different systems used for LPEM are commercial clamped liquid cell, graphene liquid cell and here we present a novel Nanochannel LPEM cell.

We are combining the best features of existing systems into a single nanofluiduc system with chips that have four inlets/outlet ports that can be connected with micro- and nanochannels in different ways to channels suspended on a membrane for imaging. The channels are primarily made of silicon nitride. The thickness of silicon nitride varies from 10-50 nm and the channels thickness is defined during the chip fabrication which varies from 60-500 nm. The nanochannels themselves have a high flow resistance, and the chips are typically designed with two larger by-pass microchannels that allow flushing and injecting samples easily to flush the nanochannels with new reagents and samples in seconds. The chips have a central opening with the suspended nanochannels, elongated in one direction (e.g. 50x200 µm) to allow EDX detection and tilting the sample, and a large area for imaging. The chips are square and can be mounted in any orientation in the holder as shown in figure 1 (a-c) and We have built holders as shown in figure 1(d) with four flow connections for flow studies in TEM.

The nanochannel design reduces outwards bulging to a few negligible nanometers, and we know the exact thickness of liquid and membrane. This made it possible to measure the mean free path [2] and mean inner potential [3] of water. Flow can be well controlled with parabolic Poiseuille flow profiles in the channel. Well-defined mixing is fast with diffusion on the length scales of the channels, can be done by joining two channels to meet a third. Through this we can introduce multiple reagents directly into the field of view at once. Radiolytic damage to the liquid sample is always a concern as the electron beam induces strong chemical reactions. When designed as parallel channels, the radiolytic damage in one channel has little influence on the separate nearby channels, making measurements repeatable in one TEM session. A wide variety of channel designs are available, and those helps to run the different LPEM experiments.

Nanochannel liquid cell has vast range of applications. For example, we have performed beam induced nucleation experiment, using 0.5mM $HAuCl_4$. The deposited particles can be imaged with lattice fringe resolution as shown in figure 2(A). The nanochannels offer the novel opportunity to mix liquids directly in the field of view and we can exchange the liquids in seconds and are able to control the flow of particles and liquids as well. The optical fluorescence image in figure 2(B) showing a constant concentration gradient achieved by flushing water and fluoresceine through a T-channel at constant pressure applied on inlets. Such capabilities open for studying different chemical reactions and knowing the concentration gradient profile. Crystal growth inside the nanochannel were also studied by growing glycine

crystals inside the nanochannel by drying concentrated solution and electron diffraction (ED) confirmed the pattern of a glycine crystal [4].

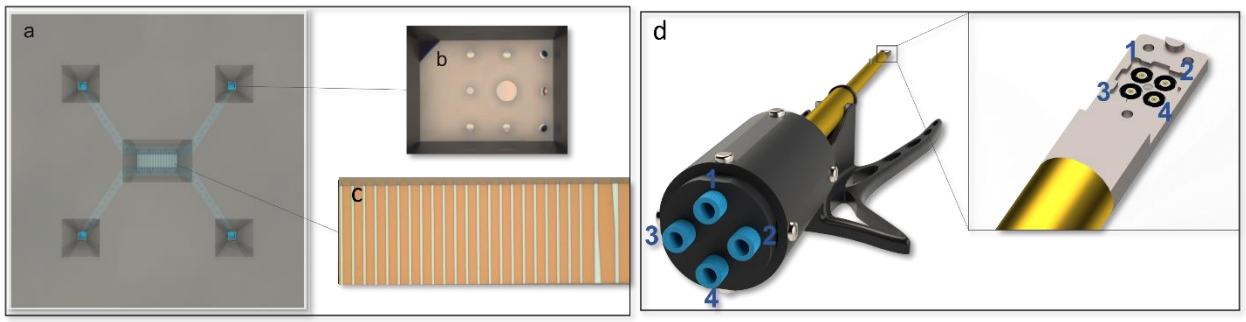

Figure 2 a) 3D image of Nanochannel chip. b) One of the inlet/outlets. c) Straight nanochannels. d) TEM holder having four flow connections

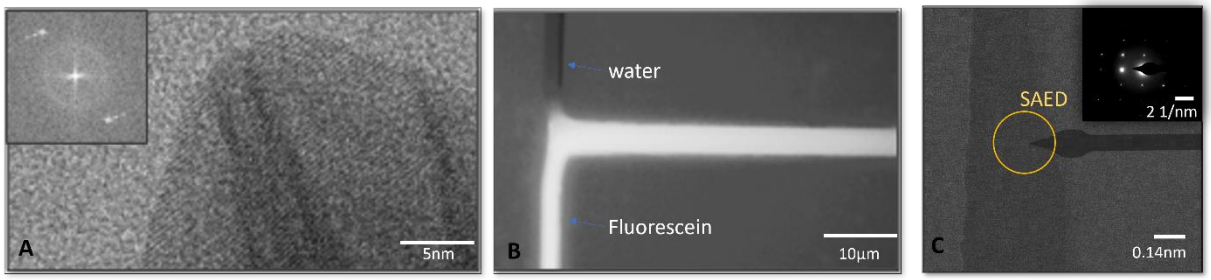

Figure 2 A TEM image showing atomic resolution of gold particle nucleated by $HAuCl_4$. B) Optical fluorescence microscope image of a T-channel, where water and fluroscine was mixed at constant pressure C) Bright field (BF) and Diffraction TEM image of glycine crystal formed inside nanochannel.

[1] Keskin, Sercan, Peter Kunnas, and Niels de Jonge. "Liquid-phase electron microscopy with controllable liquid thickness." *Nano Letters* 19.7 (2019): 4608-4613.

[2] Yesibolati, Murat Nulati, et al. "Electron inelastic mean free path in water." *Nanoscale* 12.40 (2020): 20649-20657.

[3] Yesibolati, Murat Nulati, et al. "Mean inner potential of liquid water." *Physical Review Letters* 124.6 (2020): 065502.

[4] Broadhurst, Edward T., et al. "Polymorph evolution during crystal growth studied by 3D electron diffraction." *IUCrJ* 7.1 (2020): 5-9.

8. Analysis of Membrane Order in Pollen Tubes – Methodological Challenges and Plant Unique Findings

Ingela Parmryd[1], Jeremy Adler[2], Carolin Fritz[3]

[1]*Institute of Biomedicine, University of Gothenburg, Gothenburg, Sweden*
[2]*Department of Immunology, Genetics and Pathology, Uppsala University, Uppsala, Sweden*
[3]*Department of Biology, Friedrich-Alexander-University Erlangen Nuremberg, Germany*

Corresponding author: ingela.parmryd@gu.se

The plasma membrane of mammalian cells is made up of two co-existing liquid phases, i.e. its lipid packing is not homogenous. There are more tightly packed nanometre size domains, commonly referred to as lipid rafts, which are made up of liquid ordered (Lo) phase where the acyl groups of the phospholipids are more tightly packed and extended than in the more abundant surrounding liquid disordered (Ld) phase. In pollen tubes, plant cells that grow rapidly (3-20 □m/min) upon germination, little is known about the membrane order and the existence of membrane domains. To address this we stained pollen tubes with the solvatochromic probe di-4-ANEPPDHQ, which undergoes a red emission shift for membranes in lo-phase compared to membranes in Ld phase, because the latter is more hydrated. The pollen tubes were imaged live by widefield microscopy using LED excitation, a 63X NA1.27 water objective and a dual viewer, the emission was split into two channels detected simultaneously using a CCD camera. Z-series were captured, deconvolved and the relative abundance of Lo- versus Ld phase was quantified using generalised polarisation (GP).

Pollen tubes differ considerably in their shape with some being straight and others substantially curved (Fig. 1). This calls for automation in the image analysis to ensure that comparable regions are analysed between pollen tubes. The challenges addressed by automation include the definition of the background, the plasma membrane and intracellular regions. The plasma membrane was delineated semi automatically. Firstly, sequential points along the plasma membrane were marked manually and, assuming the pixels denoting the plasma membrane are the locally most intense, accurately located by a local search along a short line segment perpendicular to the local orientation of the plasma membrane. Additional points were then created by interpolation and similarly optimized. The mapped plasma membrane was then used to identify the tip of the pollen tube, a tentative midline along the pollen tube. An area outside the pollen tube automatically defined and used to find the background, which was subtracted. Three distances within in the pollen tubes were calculated (i) from the tip along the plasma membrane, (ii) from tip inside the pollen tube and (iii) inwards from the plasma membrane. These distances were used to identify the apical region of vesicle accumulation (ARLA), whose membrane order was compared to that of three biologically relevant zones along the plasma membrane (Fig.1). Interestingly, the highest membrane order was observed in the ARLA and the tip zone of growing pollen tubes whereas the membrane order of the plasma membrane along the tube was lower than that of the ARLA. Pollen tubes thus differ from other eukaryotic cells, for which the plasma membrane has the highest order.

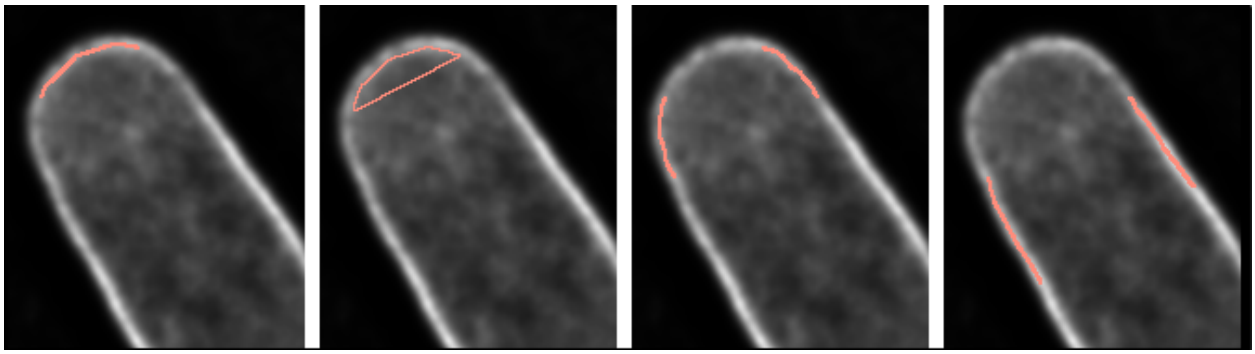

Figure 3. Illustration of the regions of interest in the pollen tubes for which GP-values were analysed.

9. Metabolic age-related hearing loss: Functional changes in the organ of Corti.

Sonal Prasad[1], Marja Pitkänen[1], and Anders Fridberger[1]

[1]*Department of Biomedical and Clinical Sciences, Linköping University, Linköping, Sweden*

Corresponding author: sonal.prasad@liu.se

Background: There are four different types of Presbycusis / Age-related hearing loss (ARHL), sensory, neural, mechanical and metabolic. The metabolic type is closely linked to stria vascularis degeneration and loud sound exposure. Ca^{2+} dependent proteins are implicated to be related to strial ion transport. We established that changes in Tectorial membrane (TM) Ca^{2+} and temporary hearing loss after loud sound exposure is related. As TM is an acellular structure that lacks active mechanisms for Ca^{2+} regulation which implies that Ca^{2+} pumps located elsewhere in the inner ear are physiologically important. The stria vascularis, TM attachment to the modulus, and the stereocilia of sensory cells are known to express Ca^{2+} transporters such as NKCC, TRPV5 and 6, PMCA1 pumps.

Hypothesis: There has been no clear evidence that how extracellular Ca^{2+} modulates the function of organ of Corti and hence Ca^{2+} transporters and ion channels could be physiologically relevant. We hypothesize that how sustained Ca^{2+} changes in both TM and extracellular fluids contributes to the development of metabolic ARHL. To test our hypothesis, infusions of Furosemide was used which interferes with adenylate cyclase and Na+/K+-ATPase and inhibits NKCC transporter in the stria vascularis and spiral ligament.

Methods: We investigated our novel hypothesis by a combined in vivo and in vitro approach using guinea pigs. In guinea pigs, cochleostomy was performed where osmotic mini pumps were used to deliver Furosemide (5 mg/ml) at the rate of 0.5 µl/hr to the cochlea through a basal opening. Hearing and organ of Corti functionality was assessed after 7 days using in vivo physiological recordings, ex vivo cochlear mechanics recordings, time-resolved confocal microscopy, fluorescence correlation spectroscopy and high-resolution confocal imaging.

Results: We found profound reduction in sound-evoked responses originated by different cell types in the cochlea shown through ABR, DPOAEs, CAPs, 3-tone suppression and decline in cochlear mechanics displayed through CM, SP, and EP with depressed bundle deflection. Morphological damages in the hearing organ (OHCs, SCs, IHCs, TM, RM, Stria) were observed (Fig. 1). Using FCS, we determined higher Ca^{2+} level in TM for operated reference animals while in TM and endolymph for Furosemide treated indicated lower Ca^{2+} level.

Conclusions: Collectively, the results demonstrates that how functional changes in the organ of Corti leads to sustained changes in the extracellular Calcium level contributing to metabolic ARHL.

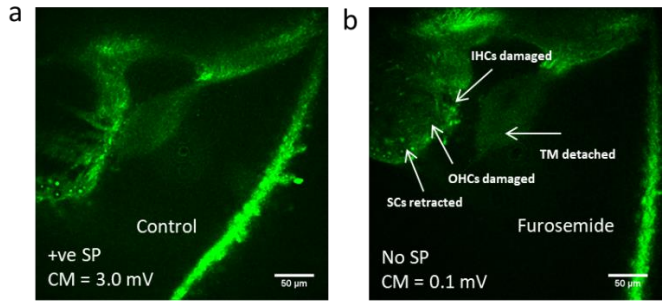

Figure 1: In control animals hair cells, supporting cells, RM and tectorial membrane looked healthy and intact and had positive SP and normal CM. While in Furosemide treated animals hair cells, supporting cells, RM and TM was damaged and detached and had negative SP and decreased CM.

10. Coherent lensless phase microscope with subpixel resolution

Igor Shevkunov[1], Peter Kocsis[1], Vladimir Katkovnik[1], and Karen Egiazarian[1]

[1]*Computational Imaging Group, ITC Faculty, Tampere University, Tampere, Finland,*

Corresponding author: igor.shevkunovl@tuni.fi

We have developed a lensless phase microscope for non-invasive real-time bio-samples investigations. It is based on a phase mask which encodes phase information of the sample into the observation. Phase imaging is realized by decoding these observations with a phase retrieval algorithm and state-of-the-art DCNN-based noise suppression techniques. Subpixel resolution of 2 um is obtained with a single observation registered by a sensor with a pixel size of 3.45 um.

Lensless real-time high-resolution phase imaging is an ill-posed and, therefore, challenging problem. In our previous publication [1], we have reported about the newly developed SSR-PR method which partly solves the problem. However, the reconstructed images of the SSR-PR method suffer from various types of noise in different regions: in the image center, it might be characterized as a low-level, non-white, spatially correlated noise, while closer to the edges the noise level increases and becomes almost white. In the literature, there was no existing solution to suppress these kinds of complex noises. However, recently in the paper [2] authors proposed estimating the noise level map for various kinds of noise by a designed deep convolutional neural network (DCNN) called PIXPNet. It is a fully blind predictor, trained with images without specific noise characteristics. Hence it is applicable for noise estimation in real-life images, contrary to the conventional CNN algorithms. We demonstrate a successful application of PIXPNet for the SSR-PR improvement.

The optical setup is shown in Fig. 1(a), it consists of 4 optical elements from left to right: a coherent illumination source, an object, a coding mask, and a sensor. First, the coherent light wavefront goes through the object collecting information about it, next, the wavefront goes through the known mask, which is the coding element, and after the coded wavefront is registered by the sensor as a coded diffraction pattern, see Fig.1(c). Mask is 2x2 mm2 with binary random phase

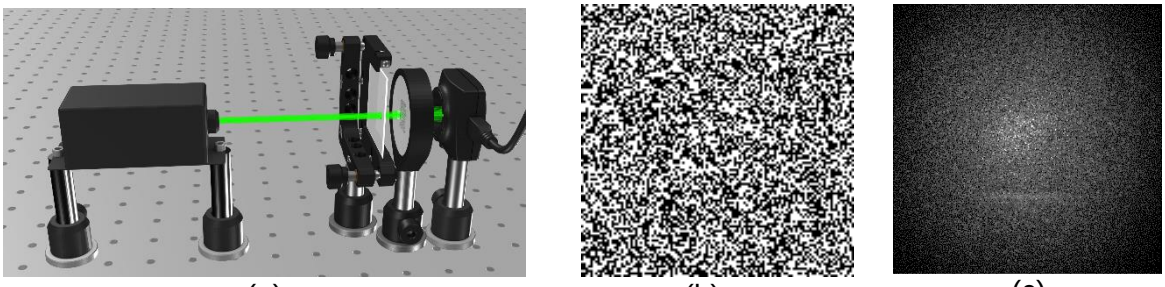

(a) (b) (c)

Figure 4 (a) SSR-PR optical setup. (b) Phase mask model of 2x2 mm^2. (c)The middle part (700x700 pixels) of the coded experimental observation.

pixels of 1.74 um. The used light wavelength is 532 nm, and the camera is a CMOS sensor with a pixel size of 3.45 um. The maximum resolution of the sensor is 2448 x 2048 pixels.

In Fig.2 we demonstrate the subpixel resolution of the SSR-PR method compared with the reference technique – Digital Holography (DH)[3] with the 40x objective lens. For this, a

calibrated resolution phase target (Phasefocus PFPT01-16-127 [4]) is used as a complex object, it is a piece of glass with etched lines of 127 nm depth. Phase images from DH and SSR-PR are recalculated into height maps and shown along with the cross-sections in Fig. 2. The achieved high quality of the SSR-PR approach, Fig. 2(b), is close to the quality of the DH, Fig. 2(a). SSR-PR overcomes the ill-posedness of the phase problem, suppresses noise, and resolves the thinnest lines of the object. These lines are the 3rd element of group 9 with a linewidth of 2 um, which is almost 2 times smaller than the sensor's pixel size.

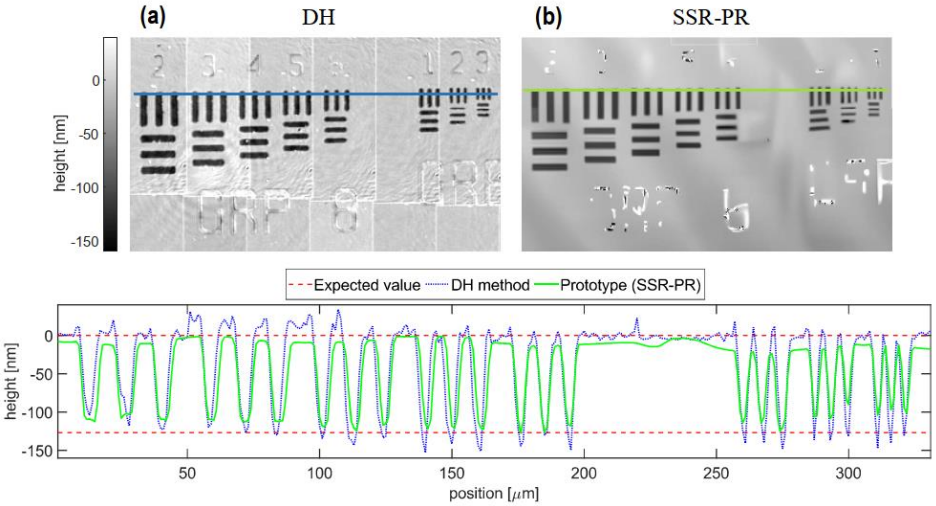

Figure 2 Test target height map reconstruction by DH with a 40x objective (a) and SSR-PR (b) methods. The corresponding cross-sections are shown at the bottom plot.

[1] P.Kocsis, I.Shevkunov, V.Katkovnik, H.Rekola, K.Egiazarian, "Single-shot pixel super-resolution phase imaging by wavefront separation approach" Opt. Express 29, 43662-78 (2021).

[2] M. Ponomarenko, O. Miroshnichenko, V.Lukin, K. Egiazarian "Blind estimation of noise level based on pixels values prediction". In: Proceedings of International Conference Computational Imaging XX, Electronic Imaging Symposium, Electronic Imaging 34, 1-5 (2022).

[3] V., Katkovnik, I. Shevkunov, N. V. Petrov, K. Egiazarian, High-accuracy off-axis wavefront reconstruction from noisy data: local least square with multiple adaptive windows. Opt. Express, 24(22), 25068-83 (2016).

[4] T.M. Godden, A. Muñiz-Piniella, J.D. Claverley, A. Yacoot, and M.J. Humphry. Phase calibration target for quantitative phase imaging with ptychography. Opt. Express 24(7), 7679-92 (2016).

11. SEM characterization of cell morphology on flat 2D substrates, more physiological 3D substrates and porous substrates for diverse cell cultivation applications

Anne Skogberg[1], Julia Pajorova[2], Satu Malinen[1], Lucie Bacakova[2] and Pasi Kallio[1]

[1]*BioMediTech Institute and Faculty of Medicine and Health Technology (MET), Tampere University, Tampere, Finland*

[2]*Department of Biomaterials and Tissue Engineering, Institute of Physiology of the Czech Academy of Sciences, Prague, Czech Republic*

Corresponding author: anne.skogberg@tuni.fi

Field Emission Gun Scanning electron microscopy (FEG-SEM) scanning of biomaterial-cell samples was performed to visualize both the biomaterial and the cell morphology at the same time. FEG-SEM was used to characterize cell morphology on different substrate topographies, including flat film-like two-dimensional (2D) surfaces, three-dimensional (3D) substrates with more physiological topography [1] and substrates with varying pore sizes. In addition to SEM studies, quantitative cell viability or cell proliferation experiments and other imaging techniques were performed in order to obtain more precise information of the cell morphology and thus draw conclusion of the suitability of the studied substrates on different cell cultivation applications. SEM gives additional information on the 3D morphology of the cells, while fluorescence microscopy gives important information on the studied inner cell structures. Therefore, these methods provide complementary information on the cell morphology, especially on more 3D surfaces.

This poster focuses on SEM studies of cell morphologies of adipose derived stem cells (ADSC), (Fig. 1), human dermal fibroblasts (HDF) [1], and a human retinal pigment epithelial (ARPE-19) cells on different surface topographies and different surface chemistries of cellulose nanofibril (CNF) -coated cellulose meshes and varying pore sized polyethersulfone (PES) membranes. Results show different cell responses on the different substrates, even when the substrates are prepared using the same material components. As a conclusion, SEM is a great tool to distinguish differences in cell morphology and cell survival in various topographically diverse substrates. Especially when the viability results between different samples are similar, SEM may reveal remarkable differences in cell morphologies between different cell substrates. However, SEM is not meant to be used alone but as a complementary method to other imaging techniques and quantitative assays in studying cell-biomaterial interactions.

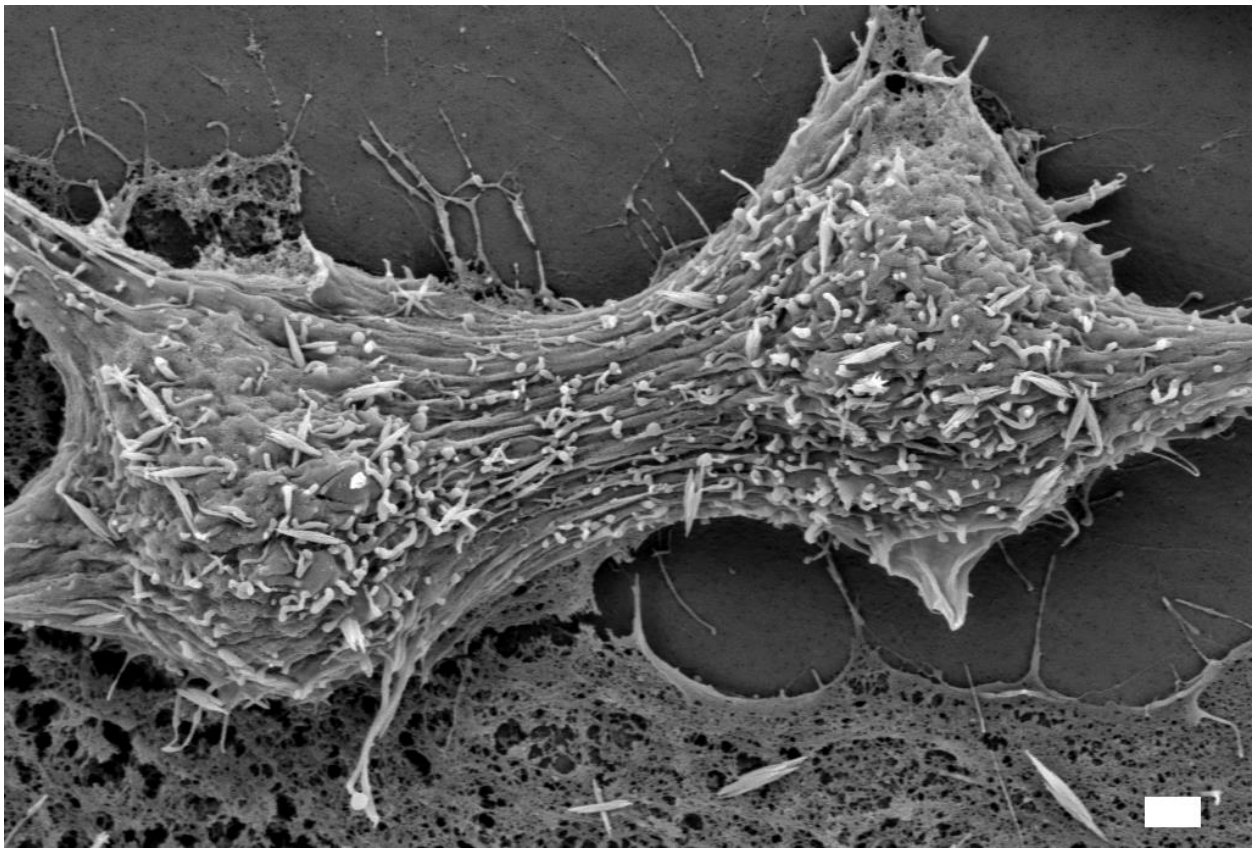

Figure 5 Dividing ADSCs on flat 2D CNF-coated cellulose mesh. Scale bar = 1 µm.

[1] J. Pajorova, A. Skogberg, D. Hadraba, A. Broz, M. Travnickova, M. Zikmundova, M. Honkanen, M. Hannula, P. Lahtinen, M. Tomkova, L. Bacakova and P. Kallio, *Biomacromolecules*, 2020, **21**, 4857–4879.

The work was supported by EU H2020-FETOpen (PRIME project, grant number 964712 to AS, SM, and PK).

12. Thin section TEM analysis to study Golgi morphology and localization of Golgi proteins

Helena Vihinen[1] and Eija Jokitalo[1]

[1]Electron Microscopy Unit, Institute of Biotechnology, HiLIFE, University of Helsinki, Helsinki Finland

Corresponding author: helena.vihinen@helsinki.fi

The Golgi apparatus is a central organelle of the secretory pathway and it has an essential role in processing and sorting of secretory and membrane proteins. Whereas some plant cells can have several hundreds of individual Golgi stacks, the Golgi in most vertebrate cells contain 100-200 stacks that are connected by tubules into a single, contiguous, ribbon-like structure.

Fluorescence light microscopy (FLM) studies can be applied to estimate the quantity of the Golgi and analyze its relative location in the cells. However, the fine detailed structures of the Golgi *i.e.*, flattened cisternae, tubules and numerous vesicles, can only be verified by microscopy techniques with sufficient resolution *e.g.,* transmission electron microscopy (TEM). For TEM analysis, the specimens can be prepared using flat embedding *i.e.,* the cell mono layer is fixed and embedded into epoxy while the cells are still attached to the substratum, thereby maximizing the Golgi area. In addition, by flat embedding the cells remains at the same the orientation as in FLM making the correlation more comprehensive.

The novel 3D-EM techniques *e.g.,* serial block face and focused ion beam scanning electron microscopies enable collection of datasets covering entire Golgi from several cells. However, as the modelling of whole Golgi is laborious and tools for automated segmentation and quantitative analysis of 3D-models are still under development, thin section TEM remains as a valuable technique to study Golgi morphology and function [1]. In addition to providing the data from broader sample survey, stereological analysis from thin sections can be implemented with standard TEM-microscope without any investment on expensive devices required for 3D-EM. From thin section TEM micrographs, various aspects of the Golgi structure can be quantified by applying stereology *e.g.,* the distribution of Golgi membranes in different structural categories, the volumes of Golgi area, the length of Golgi stacks as well as the size and number of vesicles. Random sampling and anonymization are used to facilitate collecting and analyzing images blindly, thereby ruling out the possibility of being biased while collecting and classifying the structures. Here we demonstrate how Microscopy Image Browser -software (MIB) [2] can be used for anonymization and stereological analysis of Golgi morphology.

The location of various Golgi enzymes or structural proteins can be studies at EM-level using different staining methods. From many existing labelling methods, we here introduce DAB (3,3′-diaminobenzidine) cytochemical staining and pre-embedding immunolabeling (preIEM). In DAB cytochemical staining, DAB is oxidized by hydrogen peroxide in a reaction catalyzed by horseradish peroxide (HRP) or an engineered monomeric peroxidase reporter APEX2, which are cloned to the protein of interest. In pre-embedding immuno-EM the cells are mildly fixed by chemical crosslinking to preserve the morphology while maintaining the antigenicity, after which the cells are gently permeabilized, immunolabelled with primary and nano-gold conjugated secondary antibodies prior silver-enhancement and flat embedding. The

advantage of preIEM is that it can provide information of endogenous Golgi proteins in intact cells at the EM level. Labelling in preIEM is not stoichiometric due to signal enhancement, however, the labelling density can be estimated by applying systematic categorization of silver precipitates.

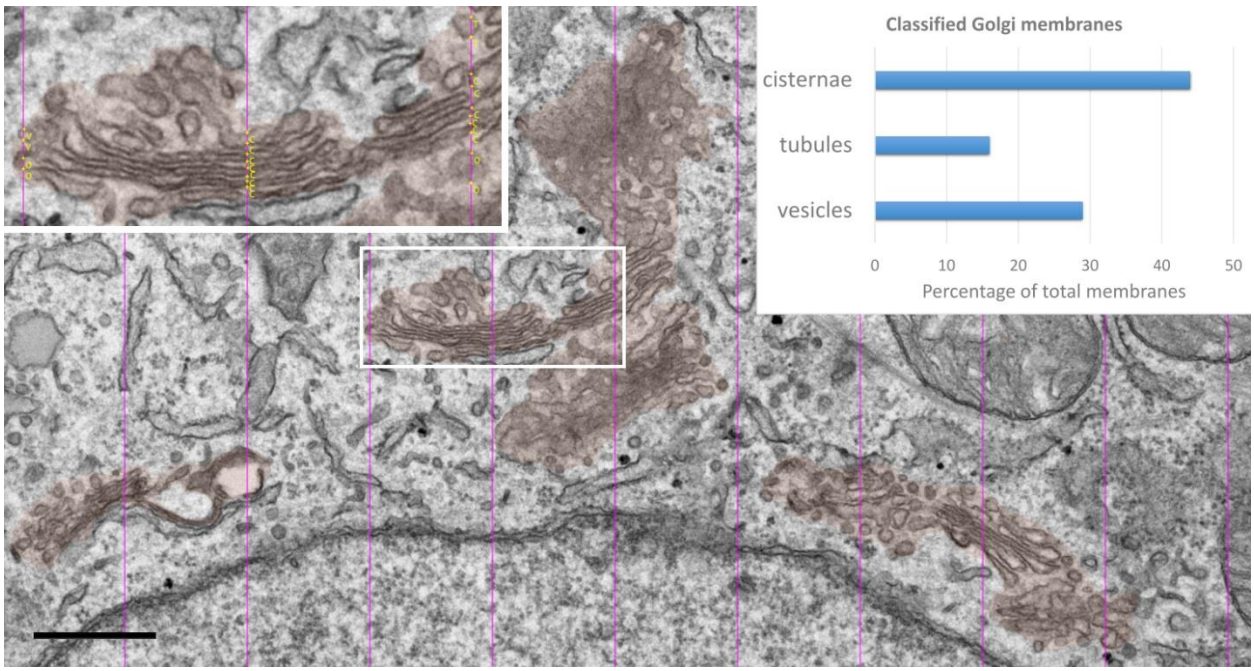

Figure 6 Morphological quantification of Golgi apparatus from a TEM micrograph using stereology. Golgi area in Huh7 cell is manually segment (light brown). The grid lines (purple) placed using the stereology tool in MIB-software are 500 nm apart, and each intersection between grid line and membrane in the Golgi area is assigned as tubule (T), vesicle (V), cisterna (C) or other (O) [3]. The relative proportion of each category of membranes can be reported as percentage of the total membrane. Scale bar 500 nm.

[1] Vihinen H., Jokitalo E., "Studying Golgi structure and function by thin section TEM", Accepted for publication in *Methods Mol. Biol.* 2022.

[2] Belevich I., Joensuu M., Kumar D., Vihinen H., Jokitalo E., "Microscopy Image Browser: a platform for segmentation and analysis of multidimensional datasets", *PloS Biol* **14**, doi: 10.1371/journal.pbio.1002340.

[3] Misteli T., Warren G., "COP-coated vesicles are involved in the mitotic fragmentation of Golgi stacks in a cell-free system", *J. Cell Biol.*, **125**, 269-282, 1994.

13. Fluorescence microscopy and SEM in the validation of a microplastic extraction method

Elina Yli-Rantala[1], Clara Lessa Belone[1], Marika Kokko[1] and Essi Sarlin[1]

[1]*Tampere University, Tampere, Finland*

Corresponding author: elina.yli-rantala@tuni.fi

The methods to extract microplastics (MPs) from complex environmental matrices are not established yet [1], and therefore each used extraction method should be validated by using reference MPs before the method is used for MP analysis. The validation preferably includes both determining the extraction efficiency of the method and examines the possible effects of the extraction method on reference MPs. The extraction efficiency is determined by inserting a known number of reference MPs to the sample, and after employing the extraction method, the captured reference MPs are counted [2]. Fluorescent reference MPs can be employed in the determination of the extraction efficiency [3], because the fluorescence effect assists in distinguishing the reference MPs from indigenous MPs that are most likely present in all environmental samples. The effect of the extraction method on MPs is important to verify especially in cases where the extraction method involves applying harsh chemicals to remove the organic matter from the sample to be analysed [2].

In our work, we optimised the digestion of total solids and organic matter of sewage sludge matrix for an improved extraction of MPs [4]. We employed two types of reference MPs in our study: fluorescent polyethylene (PE) microspheres in a nominal size range of 125–150 µm (Cospheric, CA, USA) and 0.7 mm long fibrous reference particles made of polyamide 6.6 (PA66) in fluorescent pink colour (Campbell Coutts Ltd., Hampshire, UK). The nominal diameter of the fibres was approximately 13 µm. For the determination of the extraction efficiency, a fluorescence microscope (Zeiss Axio Observer Z1, filter set 00) was employed to detect the reference MPs after the digestion process. In addition, reference MPs were imaged before and after the digestion using a scanning electron microscope (SEM, JSM-IT500, JEOL) to detect possible effects on the particle size and surface topography induced by the treatment.

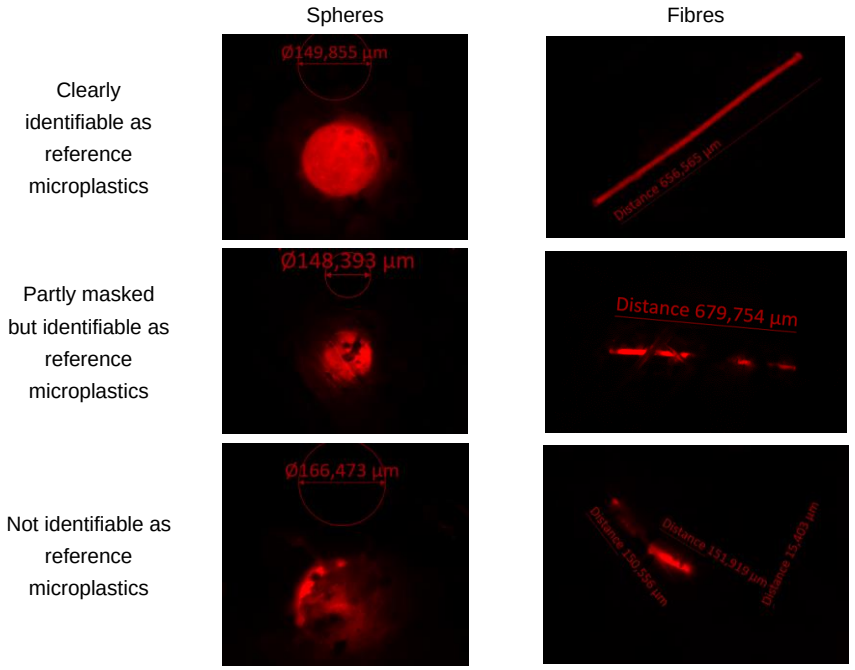

Figure 7. Fluorescent microscopy images of particles encountered in sludge samples after the digestion. Dimensions were measured to confirm or refuse the identification of reference microplastics.

The extraction efficiency was 84.0% ± 6.9% for reference spheres and 72.2% ± 6.6% for fibres. It was observed that besides the reference particles, there were also other fluorescent particles in the treated samples originating from sludge. This complicated the identification, as illustrated in Figure 1. The known approximate dimensions of the reference microplastics were used to confirm or refuse the identification in uncertain cases.

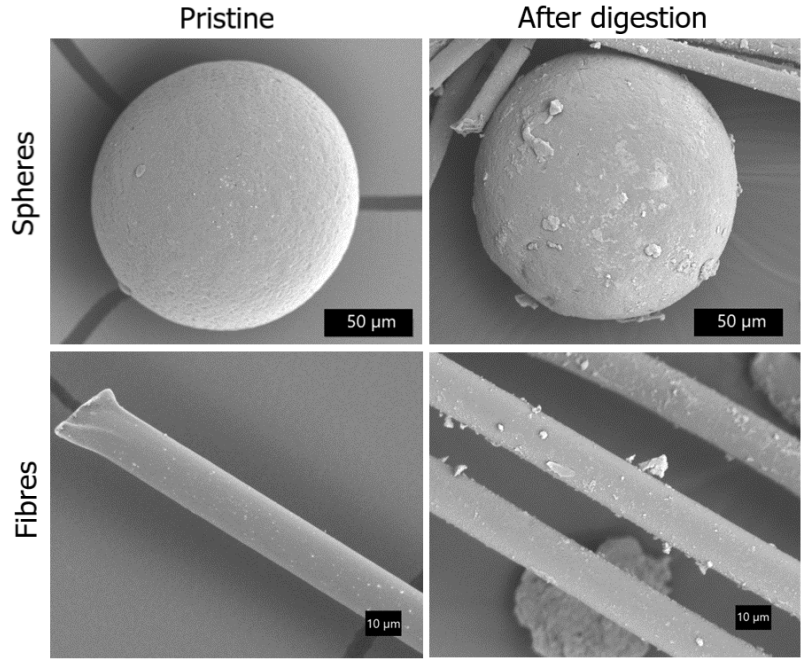

Figure 8. SEM images of microspheres and -fibres used as reference microplastics. Left column: pristine reference microplastics. Right column: reference microplastics after the optimised digestion process.

The digestion process did not have a notable effect on the surface topography of the reference MPs (Figure 2). The average diameter of microspheres was not significantly changed during the digestion process, and thus it was concluded that the digestion process did not induce a loss of material in the PE reference spheres. On the other hand, while the average width of PA66 fibres remained unchanged during digestion, there was a statistically significant reduction in the length which could be attributed to the digestion process or to the uncertainty in identifying reference fibres with SEM.

[1] R. R. Hurley, A. L. Lusher, M. Olsen, and L. Nizzetto, “Validation of a Method for Extracting Microplastics from Complex, Organic-Rich, Environmental Matrices,” *Environ. Sci. Technol.*, vol. 52, no. 13, pp. 7409–7417, 2018, doi: 10.1021/acs.est.8b01517.

[2] X. Li *et al.*, “Effects of chemical pretreatments on microplastic extraction in sewage sludge and their physicochemical characteristics,” *Water Res.*, vol. 171, p. 115379, 2020, doi: 10.1016/j.watres.2019.115379.

[3] E. G. Karakolis, B. Nguyen, J. B. You, C. M. Rochman, and D. Sinton, “Fluorescent Dyes for Visualizing Microplastic Particles and Fibers in Laboratory-Based Studies,” *Environ. Sci. Technol. Lett.*, vol. 6, no. 6, pp. 334–340, Jun. 2019, doi: 10.1021/acs.estlett.9b00241.

[4] E. Yli-Rantala, M. C. Lessa Belone, E. Sarlin, and M. Kokko, “Optimised reduction of total solids and organic matter of sewage sludge matrix for an improved extraction of microplastics,” *Sci. Total Environ.*, vol. 830, p. 154777, Jul. 2022, doi: 10.1016/J.SCITOTENV.2022.154777.

14. Dynamic strain aging in multiphase steels

Shahroz Ahmed[1], Jani Penttila[1], Jari Rämö[1], Mari Honkanen[2], Olli Oja[3], Veli-Tapani Kuokkala[1], and Pasi Peura[1]

[1] *Materials science and environmental engineering, Tampere University, Tampere, Finland*

[2]*Tampere Microscopy Center, Tampere University, Tampere, Finland,*

[3] *Product Development, SSAB Europe Oy, Hämeenlinna, Finland*

Corresponding author: shahroz.ahmed@tuni.fi

Mechanical properties and microstructures of a low carbon high aluminium manganese steel was investigated after intercritical annealing and quench and partition (Q&P) treatment. The Q&P heat treatments were conducted using three different intercritical annealing temperatures, two quench stop temperatures and three partitioning times.

Dynamic strain aging (DSA) was observed during tensile tests at room temperature in samples intercritically annealed close to A_1 transformation temperature; DSA serrations of the type A and type D were observed in the samples. The onset of DSA has been studied in ferritic steels [1]–[4], aluminium alloys [5]–[7]; it is reported that DSA is due to the interaction between moving dislocations and interstitial solute atoms during plastic deformation [6]–[9]. But studies related to DSA in multiphase steels are limited [10], [11]. The main focus of this work was to investigate the occurrence of DSA serrations in low carbon manganese steels undergone intercritical annealing and Q&P heat treatment.

Images from Digital Image correlation (DIC) showed Luder's bands at the start of plastic deformation while Portevin Le-Chatelier (PLC) bands were visible after yielding in the stress strain curve. EBSD micrographs (Fig 1) shows blocky retained austenite morphology in the samples intercritically annealed at low temperature, while the samples annealed at high temperature show lath type morphology.

Transmission electron microscopy (TEM) investigations were conducted to study the dislocation cells before and after tensile testing. TEM micrographs (Fig 2), obtained from the samples before and after tensile testing, show the presence of carbides at the grain boundaries of ferrite. The dislocation movement seen in Figure 2b, shows pinning of dislocations at the areas where there are no carbides. It is hypothesized that these areas are solute rich atmospheres and dislocations are pinned at the solute atoms in these areas.

Simulations from JMaTPro (version 12.4) shows that carbides inside ferrite are in the stage of dissolution between 640°C-750°C annealing temperature. The carbides are of the type M(C,N) and M_2(C,N) and upon dissolution they release C and N interstitials which can remain in ferrite. It is therefore speculated that DSA serrations is due to interaction between dislocations and C, N interstitials inside ferrite phase.

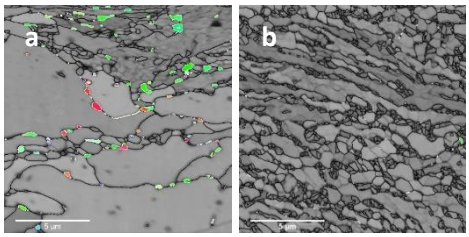

Figure 9: EBSD micrographs of samples after intercritical annealing Q&P heat treatment (a) intercritically annealed at 740°C (b) intercritically annealed at 780°C. Scale bar 5 µm.

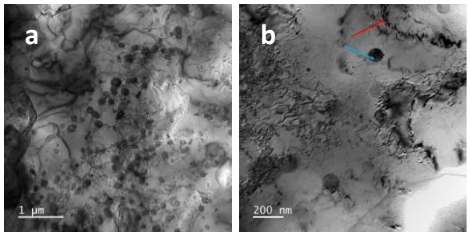

Figure 2: TEM micrographs of the sample showing DSA serrations (a) before tensile test, carbides of sizes 80-150 nm are seen in ferrite, (b) after tensile testing, red arrows indicate dislocation walls/cells and blue arrows indicate carbides.

[1] A. K. Schdev, “Dynamic Strain Aging of Various Steels” Metallurgical Transaction A, 13A, 1793–1797, 1982.

[2] A. K. Taheri, T. M. MacCagno, and J. J. Jonas, “Dynamic Strain Aging and the Wire Drawing of Low Carbon Steel Rods” ISIJ International, 35, 1532–1540, 1995.

[3] A. K. Taheri, T. M. Maccagno, and J. J. Jonas, “Effect of cooling rate after hot rolling and of multistage strain aging on the drawability of low-carbon-steel wire rod” Metall. Mater. Trans. A, 26, 1183–1193, 1995.

[4] D. Caillard and J. Bonneville, “Dynamic strain aging caused by a new Peierls mechanism at high-temperature in iron” Scr. Mater., 95, 15–18, 2015.

[5] B. Keisuke and O. Metals, “Portevin-Le Chatelier Effect in Aluminium- Magnesium Alloys ”, Trans. JIM, 10, 1969.

[6] P. G. McCormigk, “A model for the Portevin-Le Chatelier effect in substitutional alloys” Acta Metall., 20, 351–354, 1972.

[7] P. G. McCormick, “Theory of flow localisation due to dynamic strain ageing” Acta Metall., 36, 3061–3067, 1988.

[8] A. H. Cottrell, “A note on the Portevin-Le Chatelier effect” Philos. Mag. J. Sci., 44, 829–832, 1953.

[9] A. van den Beukel, “Theory of the effect of dynamic strain aging on mechanical properties” Phys. Status Solidi, 30,197–206, 1975.

[10] M. Callahan, O. Hubert, F. Hild, A. Perlade, and J. H. Schmitt, “Coincidence of strain-induced TRIP and propagative PLC bands in Medium Mn steels” Mater. Sci. Eng. A, 704, 391–400, 2017.

[11] B. Sun, N. Vanderesse, F. Fazeli, C. Scott, J. Chen, P. Bocher, M. Jahazi, S. Yue, “Discontinuous strain-induced martensite transformation related to the Portevin-Le Chatelier effect in a medium manganese steel” Scr. Mater., vol. 133, pp. 9–13, 2017.

15. Porous flame sprayed Al_2O_3 coating for slippery liquid infused surface

Betul Aktas[1], Reza Jafari[1], and Heli Koivuluoto[1]

[1]*Materials Science and Environmental Engineering, Faculty of Engineering and Natural Sciences, Tampere University, Tampere, Finland*

Corresponding author: heli.koivuluoto@tuni.fi

Thermal spraying is a cost-effective and practical surface engineering method to produce coatings with different thicknesses on several substrates by using a variety of different feedstock materials [1]. Thermal spraying combines kinetic and thermal energies to form the coating from feedstock material onto the substrate. The feedstock materials, e.g., ceramics, metals, polymers or composites are melted during the coating processing, and therefore, technically any material, which can be melted are good candidates for thermal spraying. Thanks to flexibility in the choice of feedstock materials and substrates, thermal spraying is being used in a wide range of applications, e.g., in corrosion protection, biomedical applications, anti-icing, and many more [2].

Flame spraying is one of the most common thermal spraying methods. The heat is generated by combustion of fuel gas, usually acetylene, and oxygen to melt the feedstock material and then, a molten material is accelerated and propelled onto the substrate, where it solidifies and form the coating. Depending on the process parameters selected, dense coatings can be produced as well as for the specific purposes, relatively porous structures can be obtained by flame spraying [2]. One interesting approach to manufacture, e.g., slippery and icephobic coatings, is to produce porous coatings by flame spraying for SLIPS (Slippery Liquid Infused Porous Surfaces) [3]. The main methodology behind SLIPS is trapping an immiscible lubricant, like oil, inside the porous structure to repel various types of substances, like water. It has been studied that SLIPSs can be used in different applications like corrosion protection, hydrophobic surfaces, and anti-icing surfaces, depending on the lubricant type and coating characteristics [4]. This work aims to produce porous ceramic coatings by flame spraying and evaluate suitability of their microstructures for SLIPS. Alumina (Al_2O_3) was selected as a feedstock material, and it was used as a form of flexi-cord wire, where faceted Al_2O_3 powders (Fig. 1a) were surrounded by a polymeric binder.

Flame sprayed alumina (FS Al_2O_3) coating was highly porous (Fig. 1b), which was the target in this study. The Al_2O_3 particles were molten and accelerated towards the surface of the grit-blasted stainless-steel substrate, forming a relatively thick ceramic coating. Typically flame sprayed coatings include pores, oxide inclusions and some other defects caused by the nature of the coating process [1]. The overall view of the polished cross-section of the coating (thickness ~380 µm, Fig. 1b) was taken using a backscattered electrons detector (BED) in a scanning electron microscope (SEM). It is possible to see internal porosities in the structure as well as open porosities to the surface. Higher magnification of the coating microstructure (Fig. 1c) highlights the random distribution of pores between the lamellar structure of the coating. Evidently, micron-sized pores and some cracks are formed at the splat boundaries of solidified molten particles, having a connection path through the coating towards the top surface. SEM micrograph (Fig. 1d) shows an open porosity to the surface structure which is appeared as the result of the molten particles impact and solidification. The morphology of feedstock material is changed to rounded splats in the flame spray process; however, build-up of splats can produce a relatively rough surface. Ideally, the lubricant can infiltrate inside

the coating and fill the internal porosities toward the provided diffusion path, and form lubricant micro-reservoirs inside the coating.

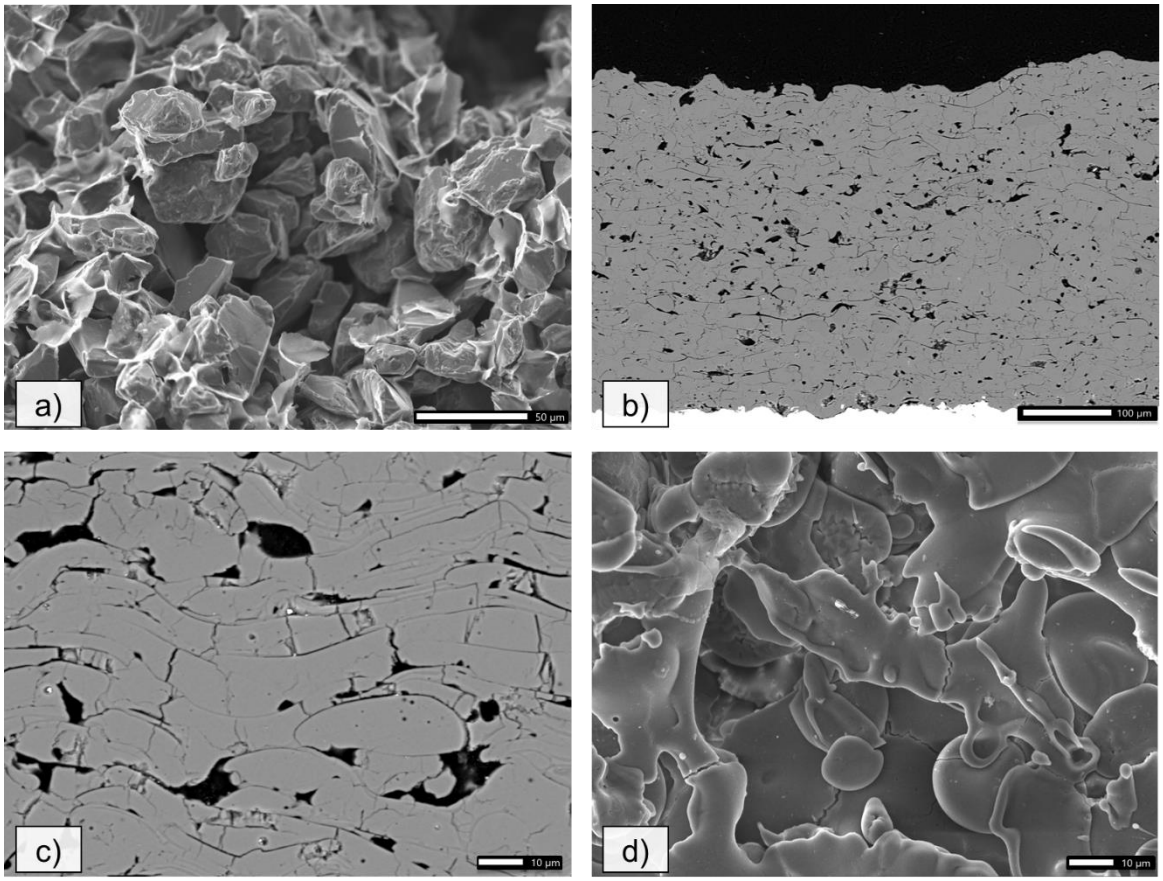

Figure 10 SEM images of a) morphology of flexi-cord feedstock, b) FS Al_2O_3 coating on grit-blasted stainless-steel substrate, c) microstructure of porous FS Al_2O_3 coating and d) surface structure of FS Al_2O_3 coating.

Flame spraying is the surface engineering method to produce relatively thick and porous coatings. FS Al_2O_3 coating was characterized by SEM to investigate the porous structure for the optimization of lubricating coating. In the scope of this research, porosity is an important feature, which is desired to further design of slippery surfaces, SLIPS, towards anti-icing applications.

[1] L. Pawlowski (Ed.), The Science and Engineering of Thermal Spray Coatings, 2nd Edition, Wiley, 2008, 656

[2] D. Tejero-Martin et al., Beyond Traditional Coatings: A Review on Thermal-Sprayed Functional and Smart Coatings, Journal of Thermal Spray Technology, 28 (2019) 598–644

[3] H. Koivuluoto et al., Thermally Sprayed Coatings: Novel Surface Engineering Strategy Towards Icephobic Solutions, Materials 13 6 (2020) 1434

[4] C. Huang, Z. Guo, Fabrications and Applications of Slippery Liquid-infused Porous Surfaces Inspired from Nature: A Review, Journal of Bionic Engineering, 16 (2019) 769–793

This research was funded by Academy of Finland, project "Thermally Sprayed slippery liquid infused porous surface – towards durable anti-icing coatings" (TS-SLIPS).

16. Local E-field manipulation of III-V nanowire catalysts in an Environmental Transmission Electron Microscope

Andersen CR[1, 2, 3], Tornberg M[2, 3], Jacobsson D[2, 3], Dick K A[2, 3] and Mølhave KS[1]

[1.] *National Centre for Nano Fabrication and Characterization, Technical University of Denmark, 2800 Kgs. Lyngby, Denmark*

[2.] *nCHREM and Centre for Analysis and Synthesis, Lund University, 22100 Lund, Sweden*

[3.] *NanoLund, Lund University, 22100 Lund, Sweden*

Corresponding author: chrisan@dtu.dk

The idea of studying the atmospheric effect on materials at the nanoscale was realized shortly after the invention of the electron microscope. It started with a so-called closed cell system allowing high pressures within a cell clamped by two thin windows with a purpose built sample holder. Later, Environmental Transmission Electron Microscopes (ETEM) were introduced with dedicated apertures allowing a gas injection directly into the microscope column.

By modifying the sample holders and sample carriers, it has been possible to control other parameters in the ETEM related to the sample such as temperature, substrate and electric bias. Today, these solutions are offered by commercial providers. However, they do not always offer the specific configurations needed for specific investigations.

At Lund University, we have an ETEM with purpose built gas handling system allowing high-resolution imaging of III-V crystalline growth at the nanoscale [1]. One of our research areas is bottom-up growth of III-V nanowires exploring the growth kinetics *in situ*.

In this project, we introduce microfabricated Si-cantilevers with a <111> crystal orientation in the ETEM (Fig 1a). Temperature is controled by resistive heating applying a bias on one cantilever, while we are also able to apply an external electric field having a bias between two cantilevers.

This system have many advantages: The crystal orientation of the cantilevers, which acts as nucleation substrate, ensures epitaxial growth of the nanowires giving a desirable growth direction for studying monolayer formation with an atomic resolution. A great thermal contact between sample and sample carrier allows temperature changes within milliseconds. Finally, it allows manipulation of the nanomaterials by applying an external electric field.

Here, we will present the results from our *in situ* studies of the E-field influence on catalyst droplets and the field influence on nanowire growth for fundamental understanding of the growth kinetics and for future III-V-Si-device engineering.

We show that the applied E-field elongates the catalyst droplet (Fig 1b-e), which we use to calculate the surface tension comparing our TEM results with simulations using COMSOL Multiphysics®. We also use the field to change the nanowire length (Fig. 1f-g) and diameter (Fig. 1h) as well as the catalyst position terminating the nanowire growth (Fig. 1j).

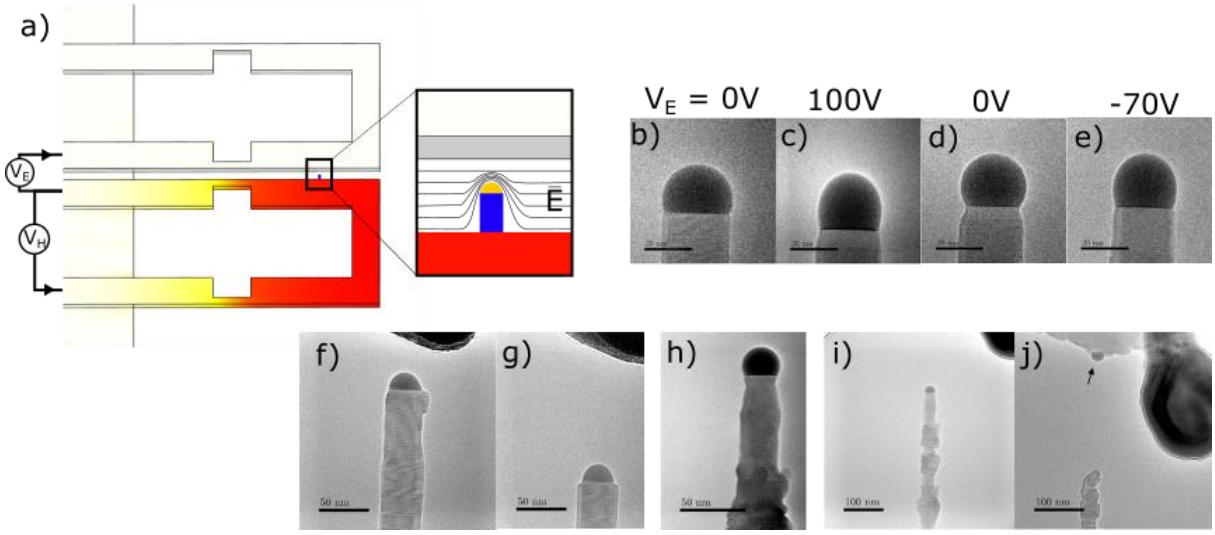

Figure 1. Illustration of cantilever device with an electric field applied onto a nanowire (inset). Different results from applying an electric field to the catalyst droplet without (b-g) and with (h-j) a Ga-atmosphere. (b-e) droplet deformation at increasing and decreasing applied bias. (g-h) etching of a nanowire at high negative field. (g) Nanowire narrowing during growth when applying a high positive field. (h-i) Growth terminated after applying a high electric field.

[1] Hetherington, C. J. D. *et al*, "In situ MOCVD growth of III-V semiconductor nanowires in the Lund ETEM". *Semicond. Sci. Technol.* **35**, 34004 (2020).

17. Indentation based stress relaxation tests – novel tests to study transient plasticity

Suprit Bhusare[1], Aloshious Lambai[1] and Gaurav Mohanty[1]

[1]*Engineering Materials Science, Faculty of Engineering and Natural Sciences, Tampere University, Tampere, Finland*

Corresponding author: suprit.bhusare@tuni.fi

Nanomechanical tests are moving beyond regular hardness and modulus measurements to encompass host of different mechanical properties like strain rate sensitivity, creep, and fracture toughness. Developing the capability to measure stress relaxation behavior of materials will be useful to not only extend the gamut of properties studied at the micro/nanoscale, but also to study fundamental time-dependent deformation behavior of materials. This poster will present, for the first time, the development of indentation-based stress relaxation tests that can reliably extract the activation parameters for deformation at micrometer length scales. The developed testing methodology, data analysis framework and the validation results on nanocrystalline metals will be presented. Nanocrystalline metals were selected for validation tests because they do not show size effects in indentation since hundreds of nanometer sized grains are interrogated in the indentation zone. Therefore, the micromechanical response can be considered to be “bulk” even in case of these small-scale tests. The indentation results were systematically compared with compression tests on micrometer sized pillars which have previously been shown to exhibit “bulk” scale behavior. A good match was found between both indentation and micropillar compression tests validating the developed testing methodology. This opens up the possibility to perform transient stress-relaxation tests on thin films and individual grains in future to systematically study the operative deformation mechanism(s) in a wide range of materials.

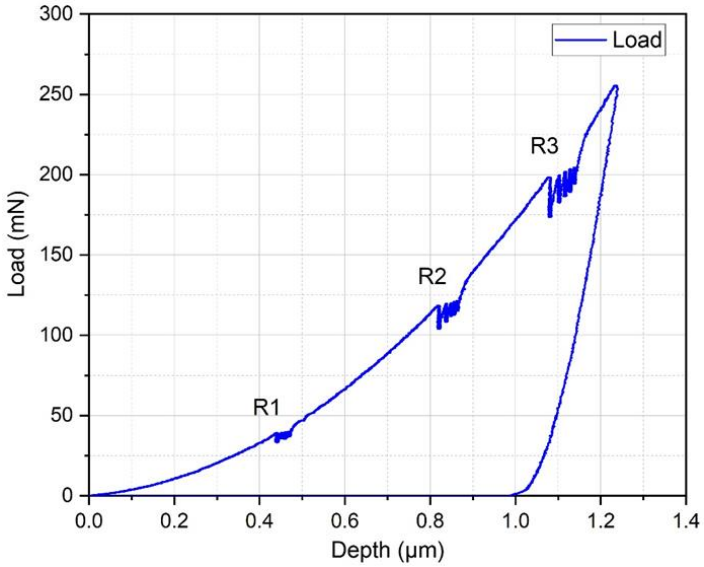

Figure 1. Example of an indentation stress-relaxation test

18. Atom transfer between precision nanoclusters and polydispersed nanoparticles: A facile route for monodisperse alloy nanoparticles and their superstructures

Paulami Bose[1], Papri Chakraborty[1], Jyoti Sarita Mohanty[1], Nonappa[2], Angshuman Ray Chowdhuri[1], Esma Khatun[1], Tripti Ahuja[1], Ananthu Mahendranath[1,3], and Thalappil Pradeep[1]

[1]*DST Unit of Nanoscience (DST UNS) and Thematic Unit of Excellence (TUE), Department of Chemistry, Indian Institute of Technology Madras, Chennai 600 036, India,*

[2]*Faculty of Engineering and Natural Sciences, Tampere University, P.O. Box 541, FI-33101 Tampere, Finland,*

[3]*Department of Metallurgical and Materials Engineering, Indian Institute of Technology Madras, Chennai 600036, India.*

Corresponding author: pradeep@iitm.ac.in

Reactions between atomically precise noble metal nanoclusters (NCs) have been studied widely in the recent past, but such processes between NCs and plasmonic nanoparticles (NPs) have not been explored earlier. For the first time, we demonstrate spontaneous reactions between an atomically precise NC, $Au_{25}(PET)_{18}$ (PET = 2-phenylethanethiol), and polydispersed silver NPs with an average diameter of 4 nm and protected with PET, resulting in alloy NPs under ambient conditions. These reactions were specific to the nature of the protecting ligands as no reaction was observed between the $Au_{25}(SBB)_{18}$ NC (SBB = 4-(*tert*-butyl)benzyl mercaptan) and the very same silver NPs. The mechanism involves an interparticle exchange of the metal and ligand species where the metal–ligand interface plays a vital role in controlling the reaction. The reaction proceeds through transient $Au_{25-x}Ag_x(PET)_n$ alloy cluster intermediates as observed in time-dependent electrospray ionization mass spectrometry (ESI MS). High-resolution transmission electron microscopy (HRTEM) analysis of the resulting dispersion showed the transformation of polydispersed silver NPs into highly monodisperse gold–silver alloy NPs which assembled to form 2-dimensional superlattices. Using NPs of other average sizes (3 and 8 nm), we demonstrated that size plays an important role in the reactivity as observed in ESI MS and HRTEM.

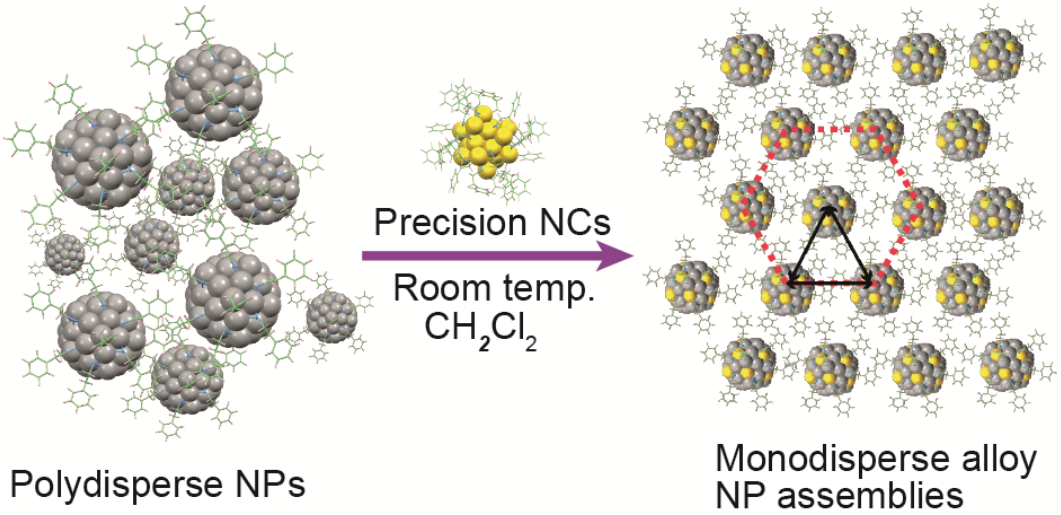

Figure 11 Schematic representation of the interparticle reaction between Ag@PET nanoparticles and $Au_{25}(PET)_{18}$ nanoclusters resulting in formation of monodispersed AgAu@PET nanoparticles.

[1] P. Bose, P. Chakraborty, J. S. Mohanty, A. R. Chowdhuri, E. Khatun, T. Ahuja, A. Mahendranath and T. Pradeep, *Nanoscale*, 2020,12, 22116-22128.

[2] I. Chakraborty and T. Pradeep , *Chem. Rev.*, 2017, 117 , 8208 —8271.

19. Low Voltage Scanning Electron Microscopy Analysis of Thin Film Microstructure.

Robert D. Boyd[1] and Tetsuhide Shimizu[2]

[1]Plasma & Coatings Physics Division, IFM Materials Physics, Linköping University, Linköping, 581-83, Sweden

[2]Department of Mechanical Systems Engineering, Graduate School of System Design, Tokyo Metropolitan University, Japan

Corresponding author: Robert.boyd@liu.se

Thin films (here defined as having a thickness of 1 nm to 5 µm) are critical components of many of today's technologies, from hard coatings to microelectronics. Their further development is essential to meet future societal challenges. Including photovoltaic cells for alternative energy generation, reducing the use of rare earth metals and the development of organic electronics. Understanding their microstructure, down to the nanoscale, is key in being able to predict their behaviour.

Scanning electron microscopy (SEM), developed in the 1960s and widely used in universities and industry, provides analysis at the micro through to the nanoscale. This technique is being continuously improved in areas such as better optics (for improved resolution), low voltage SEM (which uses low energy electrons, typically less than 1 kV) for analysing the surface structure, and the development of in-lens detectors that can detect low energy secondary and primary electrons [1]. These improvements now mean that SEM can provide analysis that would be otherwise impossible to obtain.

An example of this is shown in Fig. 1, where low voltage SEM combine with in-lens detectors can resolve the grain structure of 10 nm tungsten thin films. This grain structure is impossible to resolve using conventional SEM and transmission electron microscopy (TEM). The latter technique has been considered the technique of choice when investigating thin film microstructures.

Furthermore, the development of thin film based organic electronic based devices requires the use of polymer substrates. Traditional TEM and SEM approaches use high energy electrons and there is an open question on whether these can modify and damage such substates [2]. Low energy electrons used in LVSEM can analyse such materials with little or no damage [3]. Fig. 2 shows nanoparticles before and after they have been incorporated in an organic matrix. LVSEM can resolve particles outside and incorporated into the polymer matrix and the presence of pores.

Here the usefulness of LVSEM in determining the structure of film films will be demonstrated and discussed and will include topics such as topography and compositional and contrast, sample preparation and comparison with other techniques, in particular TEM.

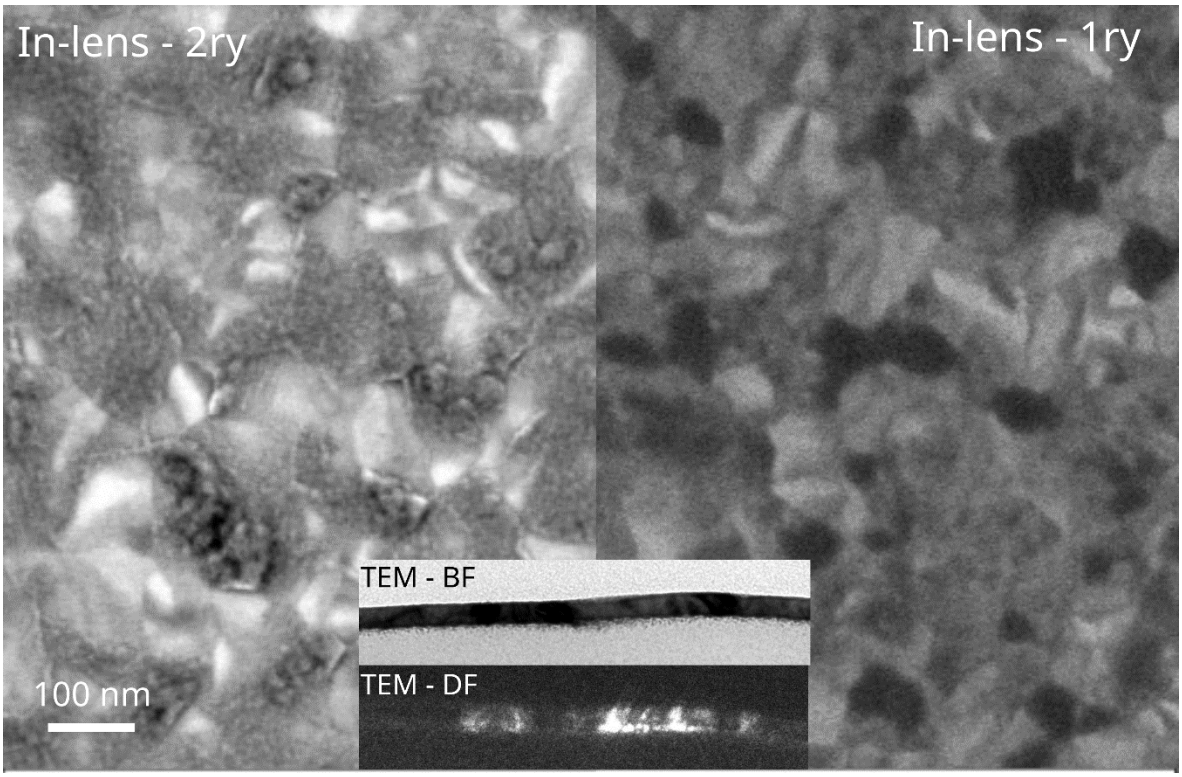

Figure 1: (Left) Secondary and (right) primary electron microscopy images of a 10 nm thick tungsten film. The grain structure of the film can be clearly resolved. The primary electron image gives compositional contrast. Cross sectional TEM analysis of the film (inset) was unable to resolve the film's microstructure.

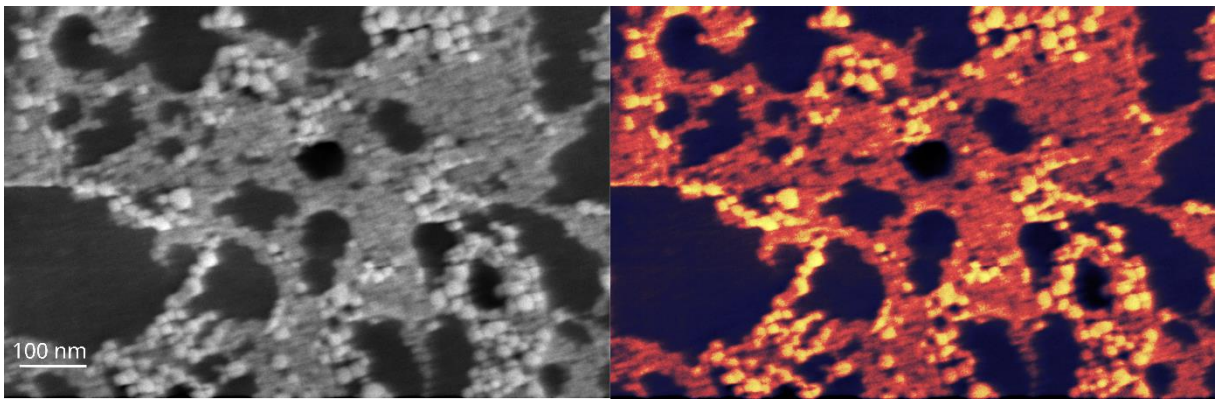

Figure 2: LVSEM Images taken using 0.5 kV electrons and are generated by combining the signals from the secondary and primary in-lens detectors of nanoparticles. (Left) the original and (right) an artificially coloured image. The polymer (blue), particles outside (yellow) and incorporated into (red) the polymer and a pore (black) can be resolved.

20. Plasticity of amorphous Al_2O_3 at room temperature

Erkka J. Frankberg[1,2,3], Janne Kalikka[4], Francisco García Ferré[3], Lucile Joly-Pottuz[2], Jiahui Zhang[5], Sergei Khakalo[6], Aloshious Lambai[1], Turkka Salminen[7], Jouko Hintikka[1], Mikko Hokka[1], Siddardha Koneti[2], Thierry Douillard[2], Bérangère Le Saint[2], Patrice Kreiml[8], Megan J. Cordill[8], Thierry Epicier[2], Douglas Stauffer[9], Matteo Vanazzi[3], Lucian Roiban[2], Jaakko Akola[4,10], Fabio Di Fonzo[3], Antti Kuronen[5], Gaurav Mohanty[1], Erkki Levänen[1] & Karine Masenelli-Varlot[2]

[1]Unit of Materials Science and Environmental Engineering, Tampere University, Tampere, Finland

[2]Université de Lyon, INSA-Lyon, UCBL, MATEIS, CNRS UMR 5510, Villeurbanne, France

[3]Center for Nano Science and Technology @PoliMi, Istituto Italiano di Tecnologia, Milano, Italy

[4]Computational Physics Laboratory, Tampere University, Tampere, Finland

[5]Department of Physics, University of Helsinki, Helsinki, Finland

[6]Integrated Computational Materials Engineering, VTT Technical Research Centre of Finland Ltd., Espoo, Finland

[7]Tampere Microscopy Center, Tampere University, Tampere, Finland

[8]Erich Schmid Institute of Materials Science, Austrian Academy of Sciences, Leoben, Austria

[9]Bruker Nano Surfaces, Bruker Inc., Eden Prairie, MN, USA

[10]Department of Physics, Norwegian University of Science and Technology, Trondheim, Norway

Corresponding author: erkka.frankberg@tuni.fi

Oxide glasses are an integral part of the modern world, but their usefulness can be limited by their characteristic brittleness at room temperature. Using in situ TEM (Fig. 1) and atomistic simulations (Fig. 2), we show that amorphous aluminum oxide can permanently deform without fracture at room temperature and high strain rate by a viscous creep mechanism [1]. These thin-films can reach flow stress at room temperature and can flow plastically up to a total elongation of 100%, provided that the material is dense and free of geometrical flaws coupled with an effective activation energy that allows sufficient bond-switching activity in the atom network. Our study demonstrates a much higher ductility for an amorphous oxide at low temperature than previous observations and we formulate a criterion that can help to find other oxides with similar behavior. This discovery may facilitate the realization of damage-tolerant glass materials that contribute in new ways, with the potential to improve the mechanical resistance and reliability of applications such as electronic devices and batteries. Moreover, the results indicate that amorphous oxides have potential to be used as high-strength, damage-tolerant engineering materials. The results reveal new aspects of glass thermodynamics below glass transition temperature and could lead to a new paradigm on how glass materials can be used in engineering. Follow up studies confirm that the available plasticity mechanisms can be scalable to thermodynamic bulk scale by using microcompression and large-scale atomistic simulations.

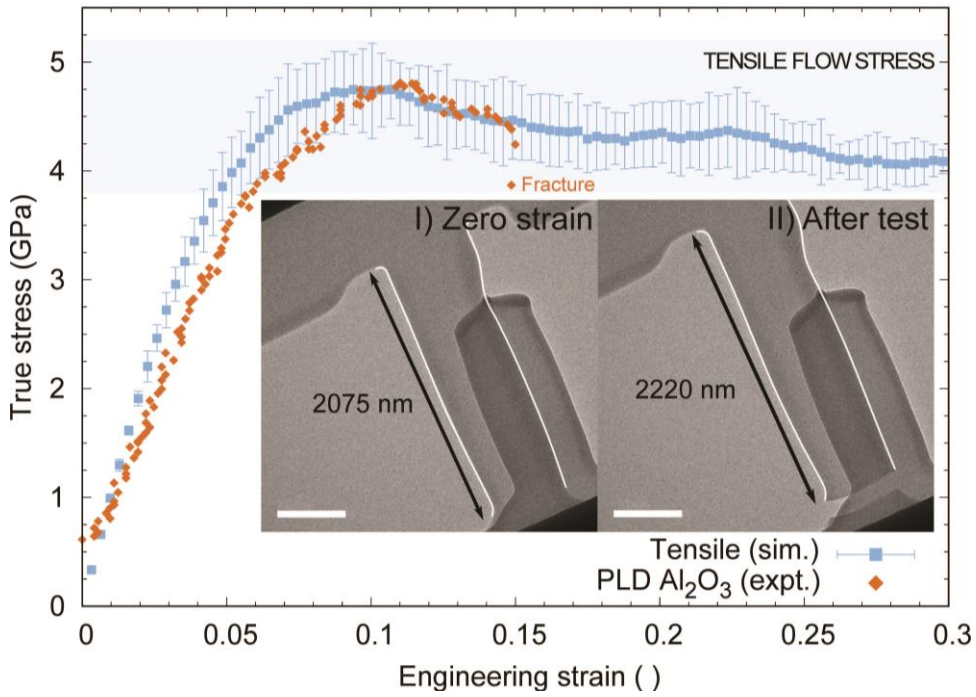

Figure 12 In situ mechanical response of amorphous aluminum oxide in tension as imaged inside a transmission electron microscope.

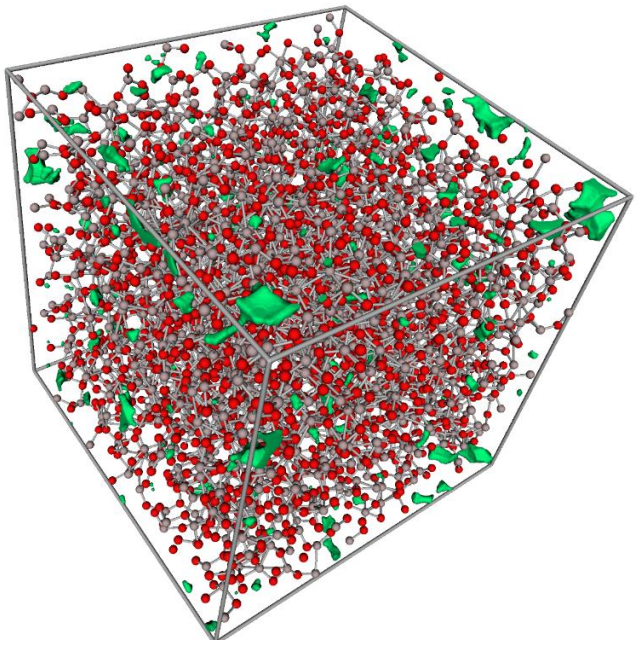

Figure 2 A molecular dynamic simulation of amorphous aluminum oxide, highlighting in green the cavity volumes located in the structure.

[1] Frankberg et al. “Highly ductile amorphous oxide at room temperature and high strain rate”, Science, 366:6467, 864-869, 2019.

21. Surface and subsurface modification of selective laser melting built 316L stainless steel by means of severe shot peening

Tejas Gundgire[1], Tuomas Jokiaho[1], Suvi Santa-aho[1], Timo Rautio[2], Antti Järvenpää[2], Minnamari Vippola[1,3]

[1] *Materials Science and Environmental Engineering, Faculty of Engineering and Natural Sciences, Tampere University, Tampere, Finland*

[2] *Kerttu Saalasti Institute, University of Oulu, Pajatie 5, 85500 Nivala, Finland*

[3] *Tampere Microscopy Center, Tampere University, Tampere, Finland*

Corresponding author: tejas.gundgire@tuni.fi

Metal additive manufacturing is a cutting-edge manufacturing technology which enables layer-by-layer production of complex shaped geometries. In addition to intricate shapes, it facilitates minimum material wastage, consolidated assemblies as well as topology optimization [1], [2]. However, the as-printed parts produced by laser powder bed fusion (LPBF) have poor surface finish compared to the conventional manufacturing methods such as hot or cold rolling [3]. Therefore, in the present work the as-printed LBBF 316L stainless steel components were subjected to severe shot peening (SSP) to improve the surface and subsurface properties.

The as-printed LPBF 316L parts were shot peened with 2 and 42 number of passes. The effect of SSP on the surface roughness as well as grain refinement was studied with the help of scanning electron microscopy, optical profilometry and electron backscatter diffraction (EBSD). In addition, the samples were analysed for residual stresses as well as microhardness in near surface areas. Subjecting the sample to SSP smoothened the surface by evening out un-melted powder particles (refer Fig.1). It resulted in significant improvement in the surface roughness value (Rz = 29 µm) compared to the as printed condition (Rz = 71 µm). Furthermore, SSP resulted in grain refinement depth of ~40 µm which was evident from the EBSD results. Moreover, beneficial large compressive residual stresses were also induced in near surface areas. The SSP caused work hardening and thereby significantly increased the hardness values in near surface areas. These advantageous improvements make SSP a reliable method for surface and subsurface modifications in LPBF built 316L stainless steel components.

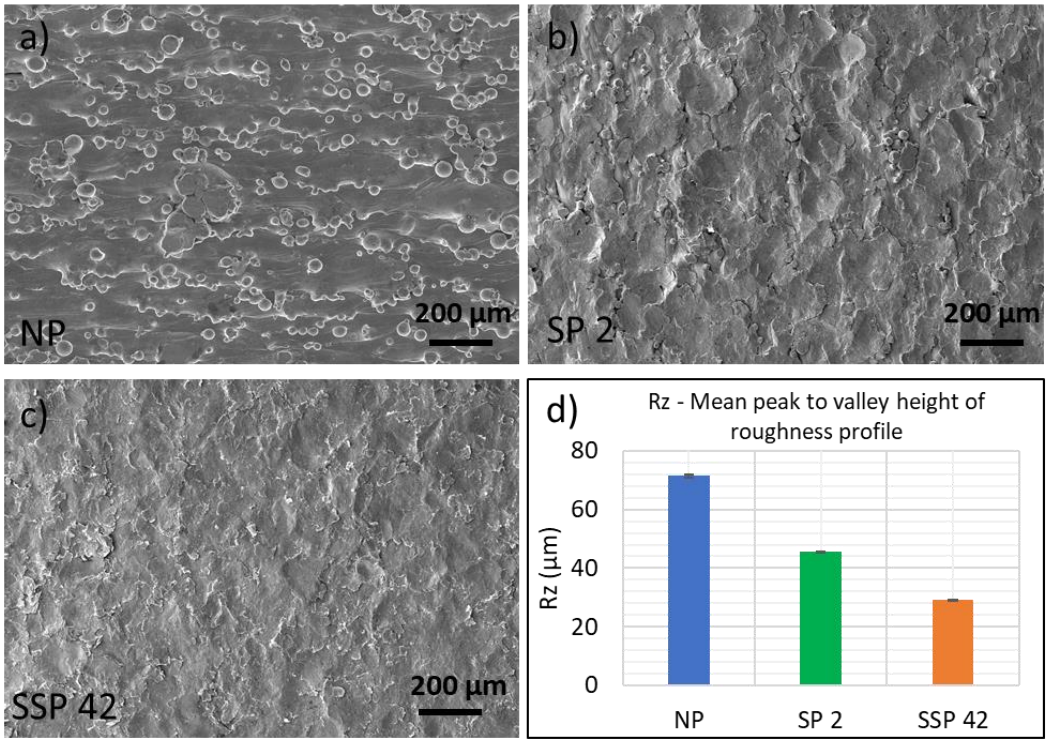

Figure 13 a, b, c) Topographic SEM images of not peened (NP), shot peened with 2 passes (SP 2) and severely shot peened with 42 passes (SSP 42) and d) Roughness (Rz) values of all the three samples .

[1] J. Gausemeier, N. Echterhoff, and M. Wall, "Thinking ahead the Future of Additive Manufacturing – Innovation Roadmapping of Required Advancements," *Univ. Paderborn Direct Manufacuring Res. Cent.*, p. 110, 2013, [Online]. Available: http://www.hni.uni-paderborn.de/en/pe.

[2] M. Attaran, "The rise of 3-D printing: The advantages of additive manufacturing over traditional manufacturing," *Bus. Horiz.*, vol. 60, no. 5, pp. 677–688, 2017, doi: 10.1016/j.bushor.2017.05.011.

[3] S. Santa-Aho *et al.*, "Additive manufactured 316l stainless-steel samples: Microstructure, residual stress and corrosion characteristics after post-processing," *Metals (Basel).*, vol. 11, no. 2, pp. 1–16, 2021, doi: 10.3390/met11020182.

22. Phase Mapping of Precipitates in Aluminium Alloys by SPED

Elisabeth Thronsen[1], Tina Bergh[2], Emil F. Christiansen[1], Tor Inge Thorsen[1,3,] A.T.J. van Helvoort[1], Randi Holmestad[1]

[1]*Norwegian University of Science and Technology (NTNU), Department of Physics, Høyskoleringen 5,7491 Trondheim, Norway,*

[2]*NTNU, Department of Chemical Engineering, 7491 Trondheim, Norway*

[3]*NTNU, SFI PhysMet, 7491 Trondheim, Norway*

Corresponding author: randi.holmestad@ntnu.no

In scanning precession electron diffraction (SPED) a convergent probe scans a 2D region of the specimen while a precessed diffraction pattern is recorded for every probe position, creating a 4D dataset from a relatively large area. Analyzing SPED data from age-hardenable aluminium (Al) alloys can provide good statistics of the relative phase occurrence of strengthening nanoscale precipitates in the aluminium matrix [1]. In this work, an Al-Cu-Li alloy was used as a model system to evaluate various data analysis methods. In this alloy, two precipitate phases with given orientation relationships (ORs) and distinguishable shapes exist. These are the tetragonal θ' phase (Al_2Cu), which forms plates on on $\{001\}_{Al}$ planes with OR $(001)_{\theta'} \parallel (001)_{Al}$, $\langle 100\rangle_{\theta'} \parallel \langle 100\rangle_{Al}$ and the hexagonal T1 phase (Al_2CuLi) which forms plates on $\{111\}_{Al}$ planes with OR $(001)_{T1} \parallel (111)_{Al}$, $\langle 110\rangle_{T1} \parallel \langle 112\rangle_{Al}$.

The data was acquired in a [001] zone axis for aluminium, using a JEOL 2100F equipped with a Nanomegas system and a QD Merlin direct electron detector. Because of the ORs between aluminium and precipitates, the data only contain five unique precipitate diffraction patterns- two from T1 and three from θ'. Figure 1 shows the virtual dark-field (VDF) image from a typical dataset along with examples of the five unique diffraction patterns. Different data analysis methods were tested on the dataset to assess their performance in terms of reliability, speed and objectiveness. The methods include non-negative matrix factorization, template matching, a vector-based approach, and artificial neural networks. The goal is to establish a robust and unbiased way to obtain phase maps of precipitate distributions in Al alloys. All data analyses are done in the open-source python library for multi-dimensional diffraction microscopy PyXem [4].

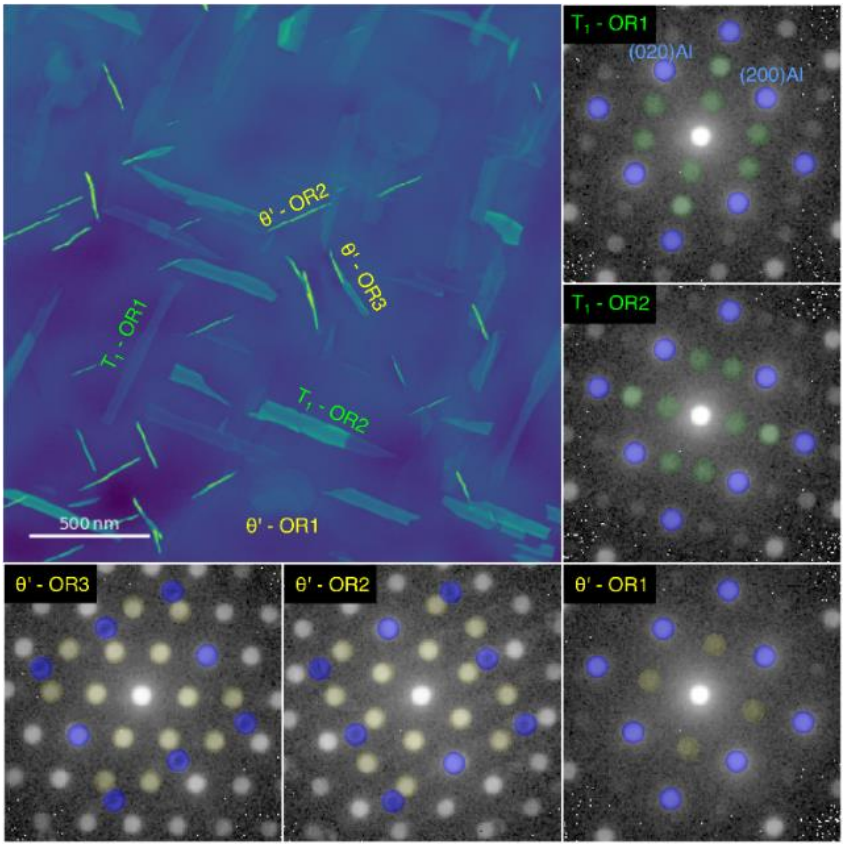

Figure 14 VDF image of a dataset from the Al-Cu-Li alloy acquired in [001]Al zone axis, with examples of the five unique precipitate diffraction patterns identified.

[1] Sunde, JK, Marioara CD, van Helvoort ATJ, Holmestad R, Mat. Char. 142, 458-469 (2018), 10.1016/j.matchar.2018.05.031

[2] https://github.com/pyxem/pyxem

[3] Acknowledgements: We thank Philip Crout and Paul A. Midgley, Department of Materials Science and Metallurgy, University of Cambridge, UK for collaborations through the ESTEEM3 project (grant no 823717). Data is acquired at the NORTEM infrastructure (project number 197405) Trondheim, Norway.

23. A microstructure-based approach towards cold sprayed composite coating quality assessment

Reza Jafari[1], Jarkko Kiilakoski[2], Mari Honkanen[3], Minnamari Vippola[1,3], Heli Koivuluoto[1]

[1] *Materials Science and Environmental Engineering, Faculty of Engineering and Natural Sciences, Tampere University, Tampere, Finland*

[2] *Saint-Gobain Coating Solutions, Avignon, France*

[3] *Tampere Microscopy Center, Tampere University, Tampere, Finland*

Corresponding author: reza.jafari@tuni.fi

Cold spraying as an emerging coating technology in the surface engineering field, can deposit a wide range of feedstock materials. Particularly, it is possible to yield an integrated deposit dense enough comparable to bulk materials. On the other hand, microstructure plays a crucial role in performance and properties of materials. The vitality of microstructural studies applies here as well; the assurance of cold sprayed coating quality is not feasible without a through characterization of the microstructure [1].

In the current research, the integrity of cold sprayed Al-based composite coating was assessed by employing structural characterization techniques. A high-pressure cold spray system was used to fabricate the composite coating from hard quasicrystalline powders premixed with Al-based powders on aluminium substrate. The same cold spray process parameters were also used to make an Al-based coating counterpart. The achieved coatings were exposed to cavitation erosion following the recommended procedure in ASTM Test Method G32-16 modified [2]. As the result of cavitation bubbles formation, micro-explosion over the surface of the coatings causes gradual damage to the coating. This process can be used to define the cohesion of the sprayed coating and highlight the weak spots in the microstructure after a certain exposure duration. Scanning electron microscopy (SEM) micrographs in Figure 1 from the coatings after 30 minutes of cavitation can be compared with the sprayed coatings before cavitation. Horizontal cracks generated at the grains and particle boundaries were remarkably eliminated in cross-sections when the quasicrystalline particles (bright phases) were embedded inside the coating. Topography images showed that the ultimate detachment of large segments of loosely connected powders could be responsible for the emergence of deep cavities of Al-coating; while a different kind of morphology can be seen over composite coating. An optical profilometer was also used to investigate the extent of the surface damage (Figure 1). In accordance with SEM images of the eroded surface, the cavitation erosion volume loss of the cold-sprayed Al-based coating with large and deep cavities was considerably higher than that of the Al-quasicrystalline composite coating.

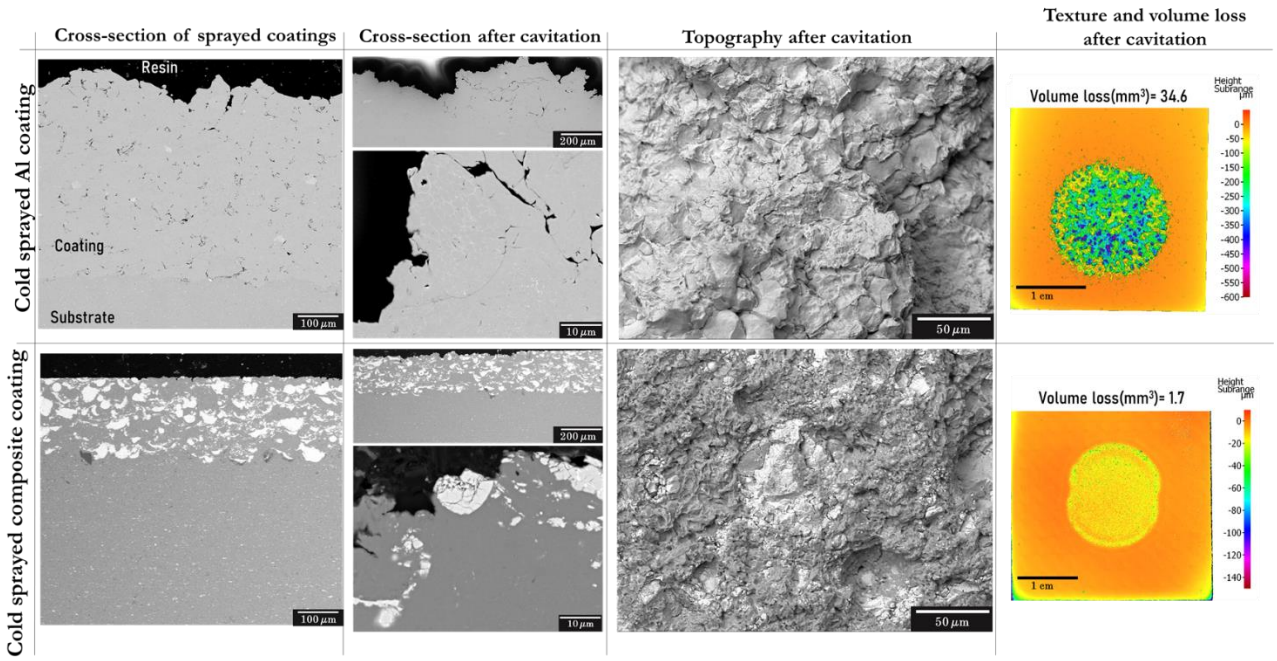

Figure 15 SEM images of tested cold sprayed coatings before and after 30 minutes exposure to cavitation erosion and 2D texture and volume loss from damaged area showing the extend of degradation.

To conclude, Al-quasicrystalline composite coating was made using cold spraying. The utilized microstructural characterization confirmed the positive role of hard quasicrystalline powders in the densification and enhanced microstructural integrity of the composite coating compared to Al-based coating counterpart.

[1] A. Srikanth, V. Bolleddu, A review on characteristics of cold sprayed coatings, Aust. J. Mech. Eng. (2020) 1–17. https://doi.org/10.1080/14484846.2020.1794504.

[2] W. Conshohocken, Standard Test Method for Cavitation Erosion Using Vibratory Apparatus G 32, in: Annu. B. ASTM Stand., 2010: pp. 1–18. https://doi.org/10.1520/G0032-16.

24. Microstructural details of high-pressure cold-sprayed aluminium alloy coatings

Heli Koivuluoto[1], Mari Honkanen[2], and Gaurav Mohanty[1]

[1]*Materials Science and Environmental Engineering, Faculty of Engineering and Natural Sciences, Tampere University, Tampere, Finland*

[2]*Tampere Microscopy Center, Tampere University, Tampere, Finland*

Corresponding author: heli.koivuluotol@tuni.fi

Cold spraying is one of the thermal spray coating production technologies, which enables us to produce dense and thick metallic coatings for different industrial sectors, e.g., in aviation and manufacturing industries. Additionally, it is suitable coating technology for repair and restoration applications. High coating quality and performance can be achieved with the selection of optimized feedstock materials together with cold spray processing parameters. Coating formation bases on plastic deformation of powder particles impacting the substrate surface [1] and therefore, microstructural characterization is needed to evaluate coating qualities. Especially, when the similar coating material is sprayed on similar substrate materials for repairing, it is needed to understand coating structure, microstructural characteristics and an interface between the coating and substrate.

This research focused on microstructural analysis of high-pressure cold-sprayed (HPCS) aluminium alloy Al2024 coating on similar substrate material. In addition to scanning electron microscope (SEM) analysis of the cross-sectional coating structures, electron backscattering diffraction (EBSD) was used to evaluate deformation of Al2024 particles and their interface between coating and similar substrate. The coatings were highly deformed as can be detected from the particle shapes. Original powder particles were spherical but very flattened in the coating structure as can be noticed from a band contrast (BC) map of the coating (Fig. 1a). A high level of plastic deformation is required during particle impacts [2] in cold spraying to achieve high quality coatings. EBSD analyses revealed high particle deformation as well as localized deformation of grains inside the particles as presented in an inverse pole figure (IPF) map in different sized small areas (Fig. 1b). Coating is fully dense and black areas in the EBSD images are so highly deformed areas or very fine grains that they cannot be indexed. Typically, grains are most highly deformed with strongly elongated shape and positioned close to the particle boundaries and impacting interfaces.

During the particle impacts in cold spraying, substrate deformed as well, which can be observed in BC map from the coating-substrate interface (Fig. 1c). The interface between coating and substrate is very critical part of the coating system because it defines the adhesion of the coating. If this adhesion is low, then coating can more easily delaminated form the substrate surface. In our research, the interface was very tight due to the severe plastic deformation, which can be noticed from IPF map (Fig. 1d). If this is evaluated with SEM without etching, the interface between cold-sprayed aluminium alloy on aluminium alloy substrate would not be detectable, indicating excellent bonding due to the plastic deformation.

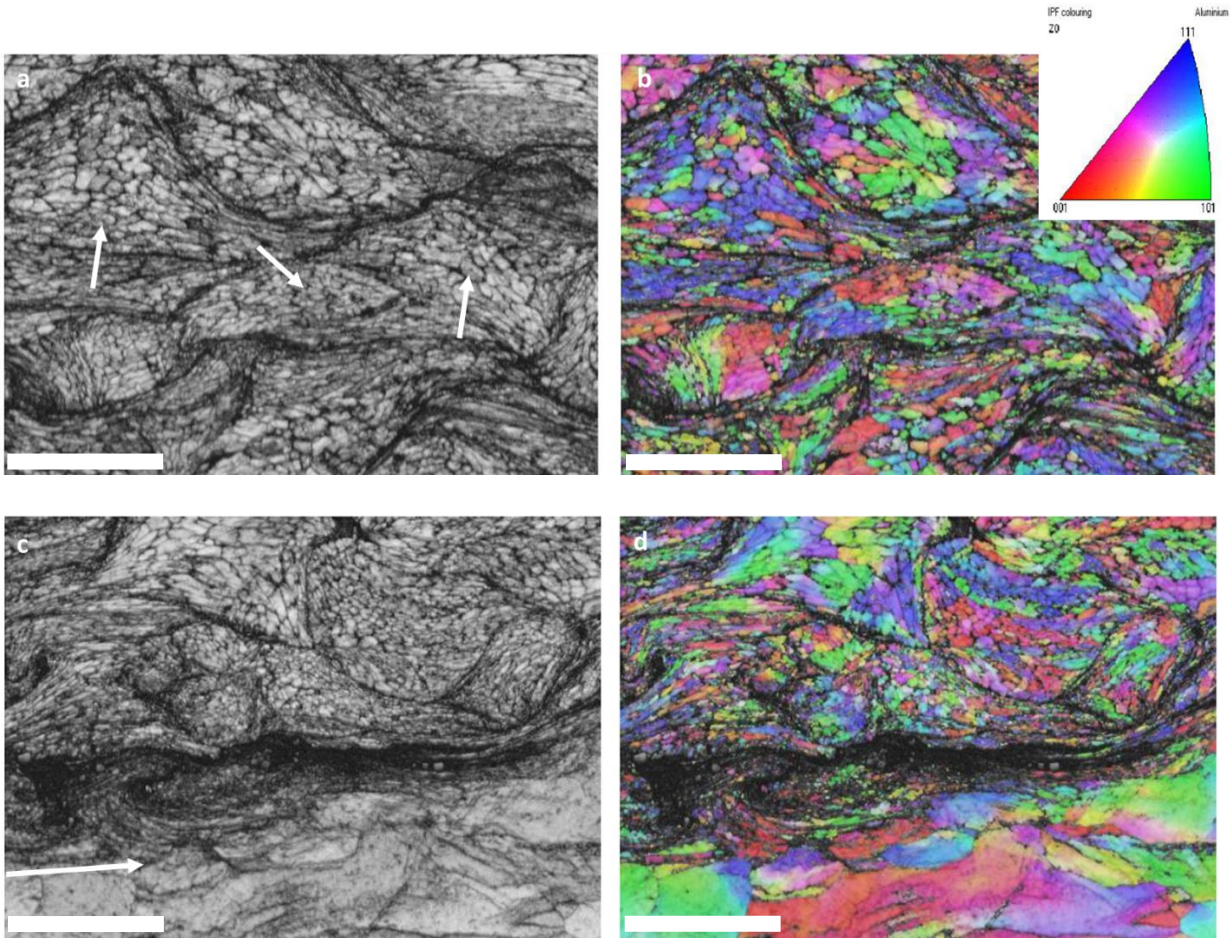

Figure 16 EBSD data of HPCS Al2024 coating on Al2024 aluminium substrate. a) BC map of coating (arrows show examples of deformed particles), b) IPF orientation map of coating, c) BC map of coating-substrate interface (arrow shows interface) and d) IPF orientation map of coating-substrate interface. Scale bar is 20 µm.

During the particle impacts, thermal softening takes place and assists the metal-metal bonding between particles or between particles and substrate. This is very advantageous for repairing applications and guarantees the high performance of the coating together with reliable industrial level coating formation for different components and parts. If a component is repaired instead of replacing it with a new part, we can have huge economic savings and cause lower environmental impact and improve sustainability in the future.

[1] P. Cavaliere (Ed.), Cold-Spray Coatings: Recent Trends and Future Perspectives; Springer International Publishing, Berlin, Germany (2018) 570

[2] M.R. Rokni et al., Microstructure and mechanical properties of cold sprayed 6061 Al in As-sprayed and heat treated condition, Surface and Coatings Technology, 309 (2017) 641-650

SEM-EBSD work made use of Tampere Microscope Center facilities at Tampere University, Tampere, Finland. The Scientific Advisory Board for Defense (MATINE), Finland is acknowledged for the funding of the work.

25. High strain rate testing of ultra fine grained aluminium at micro and macro length scales

Aloshious Lambai[1], Jari Kokkonen[1], Mikko Hokka[1], Veli-Tapani Kuokkala[1], Gaurav Mohanty[1]

[1]*Materials Science and Environmental Engineering, Faculty of Engineering and Natural Sciences, Tampere University, Tampere, Finland*

Corresponding author: aloshious.lambai@tuni.fi

Key Words: High strain rate testing, Micro vs macro comparison, ultrafine grained materials, activation volume, strain rate sensitivity

There are rapid advances in microscale testing enabling both nanoindentation and micropillar compression to be performed at high strain rates, exceeding 1 s^{-1}.[1][2] However, till date, there is no systematic comparison of the microscale test results with other established macroscale high strain rate methods, for e.g. Split Hopkinson Pressure Bar (SPHB) tests that can achieve > 1000 s^{-1} strain rates[3]. This poster will present a comparison study between micro- and macro-length scale testing using an ECAP ultra fine grained (UFG) aluminium sample. The experiments were performed in uniaxial compression using cylindrical geometries at macroscale (~16mm diameter and ~8mm thick) and microscale (micropillar ~10µm diameter and ~15 µm height). The average grain size of the UFG aluminium is around 1-2 µm, which includes a significant number of grains even in microscale testing (a micropillar contains >500 grains). Due to small grain size and interrogating large number of grains, no size effects are expected and the yield strength can be assumed to be controlled by the grain size predominantly. Microscale testing was performed from 10^{-3} s^{-1} to 750 s^{-1} and macro scale tests from 10^{-2} s^{-1} to 10^{3} s^{-1}. Additionally, strain rate jump tests were performed at both length scales to obtain strain rate sensitivity (SRS) exponent and activation volumes for deformation. The SRS exponents obtained in both cases were found to be in excellent agreement. The activation volumes obtained from both the scales lie in the range of 90-150 b^3 indicating similar dominant deformation mechanisms. No change in deformation mechanisms were observed from 10^{-2} s^{-1} to 10^{3} s^{-1} strain rates. This study provides confidence on the reliability of microscale high strain rate test techniques and paves the way for routine tests at high strain rates.

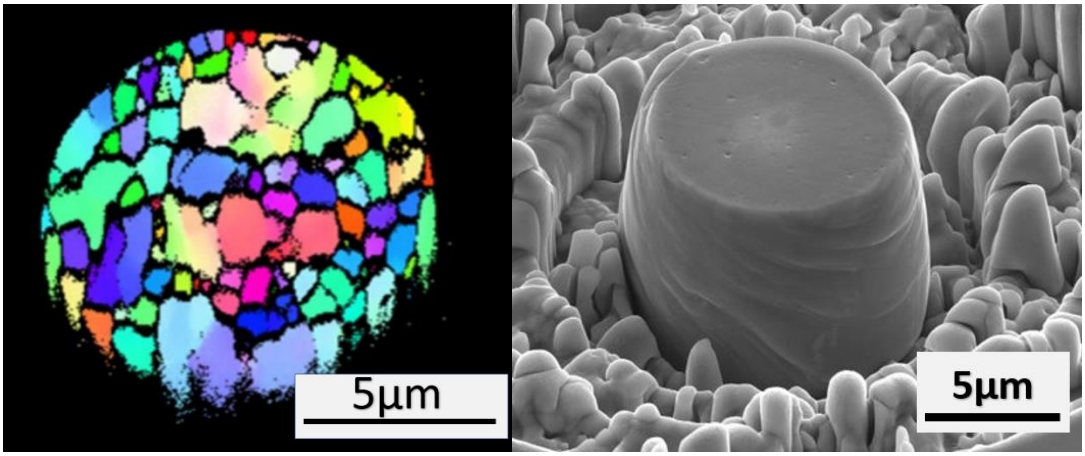

Fig1 a) Microstructure of the top surface of ufg al pillar using EBSD b) Micropillar post compression at 750/s strain rate.

[1] G. Guillonneau *et al.*, “Nanomechanical testing at high strain rates: New instrumentation for nanoindentation and microcompression,” *Mater. Des.*, vol. 148, pp. 39–48, 2018, doi: 10.1016/j.matdes.2018.03.050.

[2] R. Ramachandramoorthy *et al.*, “High strain rate in situ micropillar compression of a Zr-based metallic glass,” *J. Mater. Res.*, vol.36, no.11, pp. 2325–2336, 2021, doi: 10.1557/s43578-021-00187-5

[3] M. Hokka *et al.*, “Characterization of the mechanical behavior of ultrafine- grained metals using digital image correlation,” vol. 05005, 2010, doi: 10.1051/epjconf/20100605005.

26. Simulating Electron-Holography with FEM for charge analysis

Mads S. Larsen[1], Murat N. Yesibolati[2], and Kristian S. Mølhave[3]

[1]*Ph.D. Student, Technical University of Denmark, 2800 Kgs. Lyngby, Denmark*

[2] *Associate Professor, Technical University of Denmark, 2800 Kgs. Lyngby, Denmark*

[3]*Professor, Technical University of Denmark, 2800 Kgs. Lyngby, Denmark*

Corresponding author: maslar@dtu.dk

Understanding the charges surrounding nanoparticles and walls when immersed in liquids is crucial to understand the dynamics, the stability, and the solid-liquid interactions from the DLVO theory [1,2]. This is also crucial when one needs to assess the influence of the channel wall when working in a confined space, such inside a nanochannel when understanding particle motion near a wall. Not only is the diffusion limited [3], but also the electrostatic interactions increases due to the charges of both the wall and the particle itself according to the DLVO theory [2]. At the Technical University of Denmark (DTU), the Molecular Windows Group (MoWin) are working on a better understanding to answer some of these questions. We are utilizing electron holography (EH) on an Analytical Transmission Electron Microscope at 300kV for the experimental data, which has been further processed via custom made Python scripts based on the Gauss theorem [4] to get charge densities of individual nanoparticles together with the wall surrounding the liquid, and so far preliminary results are of coming in.

To backup experimental data numerical simulations based on the experiments are made via a Finite Element Method (FEM) using COMSOL 6.0 [5]. We utilize the electrostatic module and by linear projection of the potential map, an artificial hologram is produced. For a test simulation, we loaded 1000e- on a 100nm gold nanoparticle (AuNP) floating in free space. The phase shift is then further processed to obtain the charges, and in a way confirm that the scripts work as intended, but also to ensure the simulations behave as intended, see Figure 1. Afterwards the AuNP was immersed in 200nm water, which shows that the charges are screened quite extensively by the liquid, see Figure 2. Interestingly, the two implementations of the Gauss theorem do not agree, which in this case is due to the meshing size, but in experimental data may be due to issues with phase unwrapping of the complex wave.

The FEM simulations stand as a benchmark for all the holographic experiments conducted of particles and walls immersed in liquids, which in turn enables for a clear understanding of the obtained results. It is also straightforward to produce even more complex simulations. Overall, it is used together with the experiments to obtain better understanding of the charge accumulation surrounding particles in liquids. In the future, collaboration with researchers from the Ernest Ruska Centre (ER-C) will be done in the same manner, due to the higher resolution compared to what is available at DTU, overall explaining the charge and potentials in liquids using EH, which is one of the unanswered questions working with liquids in electron microscopes.

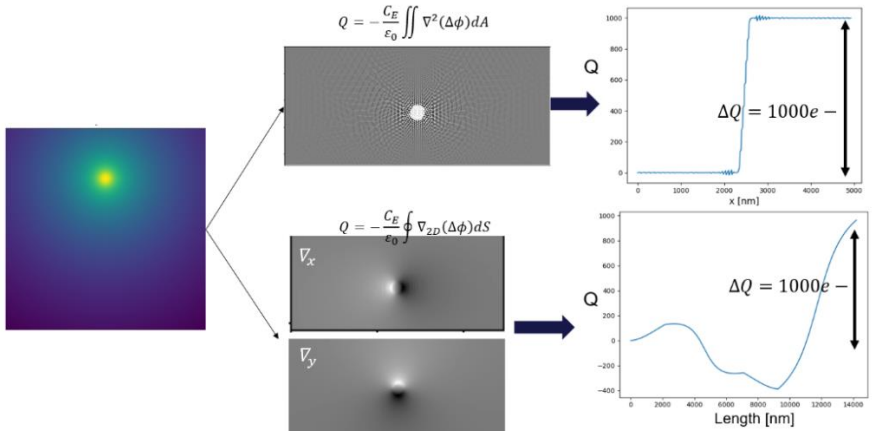

Figure 17 FEM study of a 100nm AuNP loaded with 1000e-, floating in free space. The arrows indicate the implementation of the Gauss theorem based from [4] in two ways to count the charges, either from the areal average of the Laplacian ($\nabla^2(\Delta\phi)$) or via the contour around the particle of the gradient of the phase ($\nabla(\Delta\phi)$).

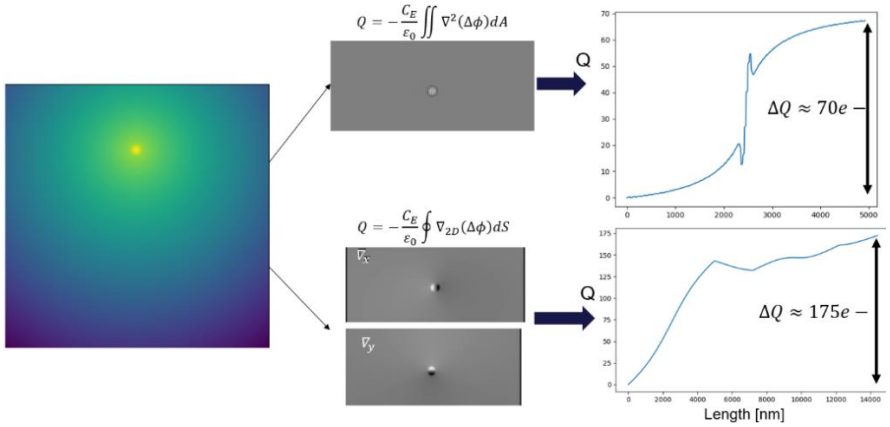

Figure 2 FEM study of a 100nm AuNP loaded with 1000e-, immersed in 200nm water. The arrows indicate the implementation of the Gauss theorem based from [4] in two ways to count the charges, either from the areal average of the Laplacian ($\nabla^2(\Delta\phi)$) or via the contour around the particle of the gradient of the phase ($\nabla(\Delta\phi)$).

[1] *Larsson, Mats, Adrian Hill, and John Duffy. "Suspension stability; why particle size, zeta potential and rheology are important." Annual transactions of the Nordic rheology society 2012: 6.*

[2] Adamczyk Z., WerońskiE P., “Application of the DLVO theory for particle deposition problems”, Advances in Colloid and Interface Science, 83, 137-226, 1999

[3] Yesibolati M.N et al., “Unhindered Brownian Motion of Individual Nanoparticles in Liquid-Phase Scanning Transmission Electron Microscopy”, Nano Letters 2020, 20(10), 7108-7115, 2020

[4] Beleggia M., “Direct measurement of the charge distribution along a biased carbon nanotube bundle using electron holography”, Appl. Phys. Lett., 98, 243101, 2011

[5] COMSOL Multiphysics® v. 6.0, www.comsol.com. COMSOL AB, Stockholm, Sweden

27. Scanning Droplet Tribometer for Rapid Surface Wetting Mapping

Mika Latikka[1]

[1]*Department of Applied Physics, Aalto University, Espoo, Finland*

Corresponding author: mika.latikka@aalto.fi

Wetting, i.e. the ability of a liquid to spread on a solid surface, is an omnipresent phenomenon. Consequently, surface wetting properties are crucial in a wide range of technologies, such as coatings protecting against adhesion, corrosion, contamination, bacteria and more, enabling fingerprint-repellent mobile phone touch screens, weatherproof structures and safe medical devices. While the conventional analytical tools are suitable for assessing wetting on most surfaces, they lack the spatial resolution and speed required for measuring surface wetting homogeneity and detecting miniscule wetting defects. The most common method, contact angle goniometry, requires several minutes for a comprehensive measurement on a single point on the surface. Furthermore, the technique is susceptible to optical errors, which prevent accurate measurements on highly liquid-repellent surfaces [1].

We have developed the Scanning Droplet Tribometer (SDT), which allows fast scanning (up to 1 cm/s) of surface wetting properties with a spatial resolution of 100 µm. This allows rapid 2D wetting mapping, which is not possible with conventional techniques. The method is based on scanning the sample surface with a millimeter-sized, magnetically actuated droplet containing minute amount (down to 0.02 vol%) of superparamagnetic nanoparticles. Due to the low concentration of the nanoparticles, the physical properties of the carrier liquid remain essentially unaltered [2]. Two permanent magnets, one above and one below the sample, are attached to a computer controlled linear stage. The magnets are moved to scan the sample with the magnetic droplet (Fig. 1). The droplet motion is recorded with a camera and the magnetic force affecting the droplet is calculated based on the droplet position as a function of time. This allows quantifying local friction between the droplet and the surface with sub-micronewton precision, and thus easy detection of any wetting inhomogeneity or defects on the sample.

The sensitivity of the SDT can be controlled by adjusting the magnetic nanoparticle concentration, which enables measurements on a wide range of samples, including on extremely water-repellent (i.e. superhydrophobic) surfaces (Fig. 2a). As the test droplet is controlled magnetically with no physical contact, measurements are possible also on inner surfaces of transparent tubes (Fig. 2b). The SDT can perform measurements, which are difficult with conventional techniques, such as quantifying subtle changes in wetting properties due degradation and contamination (Fig. 2c) or detecting tiny local wetting defects on coatings (Fig 2d). Due to its rapid measuring speed and accuracy, especially on liquid-repelling surfaces, the Scanning Droplet Tribometer can facilitate research and development of high-value surfaces, such as self-cleaning materials, biochips and sensors.

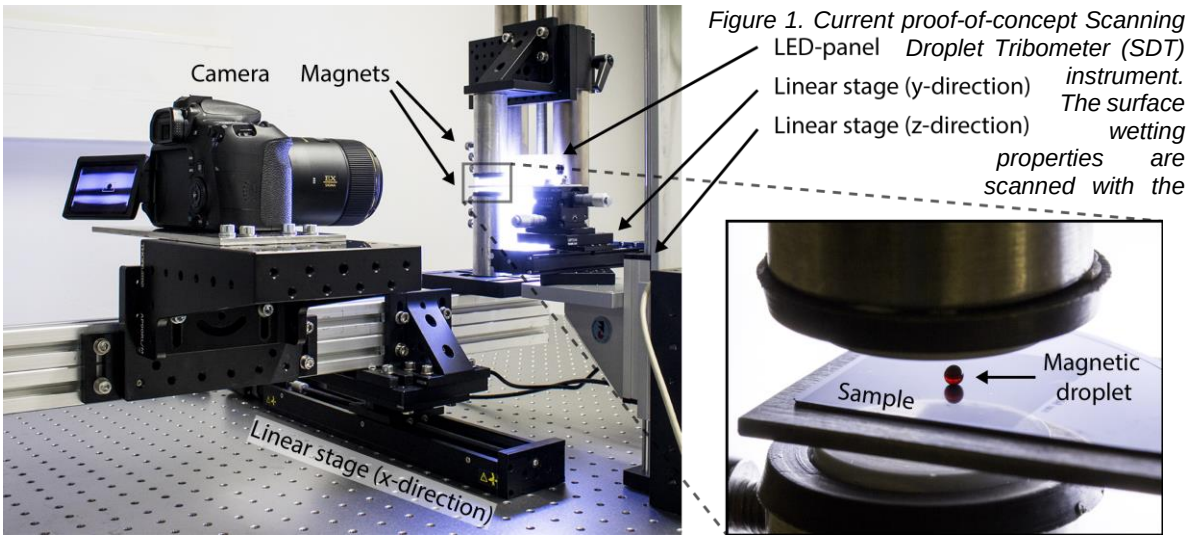

Figure 1. Current proof-of-concept Scanning Droplet Tribometer (SDT) instrument. The surface wetting properties are scanned with the magnetic droplet controlled by the magnets above and below the sample. Linear stages are used to control the positions of the magnets and the sample.

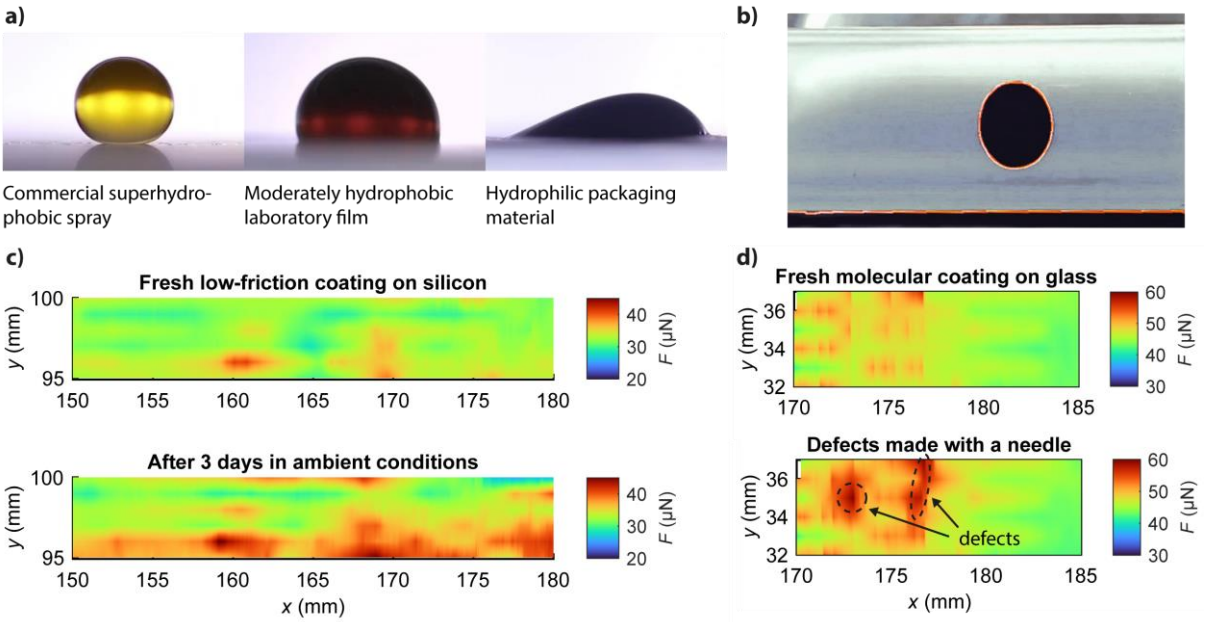

Figure 2. a) SDT can characterize a wide range of surfaces as the measuring sensitivity can be controlled by adjusting the magnetic nanoparticle concentration. b) Video frame from a wetting measurement of the inner surface of a transparent tube (bottom view). c) Wetting maps of a silicon wafer coated with a low-friction coating. SDT results show that the droplet friction increases when the surface is left in ambient conditions due to coating degradation and contamination. d) Wetting maps of a glass surface coated with a molecular coating. Needle was used to create miniscule defects on the coating, which can be measured with SDT but not be detected using optical methods due to the transparency of the coating.

[1] K. Liu, M. Vuckovac, M. Latikka, T. Huhtamäki, and R. H. A. Ras, "Improving surface-wetting characterization," *Science*, vol. 363, no. 6432, pp. 1147-1148, Mar. 2019.

[2] J. V. I. Timonen, M. Latikka, O. Ikkala, and R. H. A. Ras, "Free-decay and resonant methods for investigating the fundamental limit of superhydrophobicity," *Nat. Commun.*, vol. 4, no. 1, pp. 1-9, Sep. 2013.

28. Visualising the variable temperature oxidation of titanium nitride in the aberration-corrected environmental TEM

Ofentse A. Makgae[1], Filip Lenrick[2], Volodymyr Bushlya[2], Jon Andersson[3], Rachid M'saoubi[2,3] and Martin Ek[1]

[1]*National Centre for High-Resolution Electron Microscopy (nCHREM), Centre for Analysis and Synthesis, NanoLund, Lund University, Lund 221 00, Sweden.*

[2]*Division of Production and Materials Engineering, NanoLund, Lund University, Lund 221 00, Sweden.*

[3]*R&D Materials and Technology Development, Seco Tools AB, Fagersta 737 82, Sweden.*

Corresponding author: ofentse.makgae@chem.lu.se

Titanium nitride (TiN) nanocomposite thin films have been widely applied as protective coatings in metal machining[1], aviation[2], photonics[3], biomedical[4] and microelectronics[5], [6] industry. This is due to their excellent physicochemical properties such as hardness, thermal stability, oxidation resistance, and low electrical resistivity.[7] TiN undergoes structural dynamics under thermal annealing and oxidation, commonly involving residual stress relaxation, defects generation, recrystallisation, phase equilibrium/transition, diffusion, and interfacial reactions.[8], [9] Understanding the correlation between the mechanical properties and structural dynamics in TiN coatings near *operando* conditions is essential to designing and fabricating advanced, wear-resistant TiN-based materials. However, the direct visualisation of these dynamics at high spatial resolution is unachievable with *ex-situ* imaging and *in-situ* X-ray based techniques.[10]

Herein we report the direct visualisation of variable temperature treatment and oxidation of TiN coating from room temperature to 1000 °C using aberration-corrected environmental transmission electron microscopy (ETEM) with energy dispersive X-ray analysis (EDX). The recorded ETEM movies and calculated power spectra of the TiN coating show crack formation and propagation through the microstructure in a vacuum, up to ~550 °C, with no observable changes in the TiN rock-salt phase. Beyond 550 °C, the microstructure exhibits onset signs of thermal damage up to ~750 °C, followed by crystallisation from 800 °C to 1000 °C. The high-temperature crystallinity is retained upon cooling back to 31 °C with no signs of reversible structural dynamics to the coating before heating. In contrast, the presence of oxygen results in the phase transition of TiN grains to TiO_2 at ~600 °C, where the oxidation proceeds from the grain boundaries and cracks in the microstructure. Subsequently, complete oxidation is realised at ~750 °C, where the microstructure comprises TiO_2 nanoparticles. From 800 °C to 1000 °C, the growth of the rutile-TiO_2 nanoparticles in the coating through crystal merging, diffusion and recrystallisation is observed. Finally, the study provides unique insight into the real-time structural dynamics underpinning the properties of TiN coatings, including wear- and oxidation resistance.

[1] K. Tuffy, G. Byrne, and D. Dowling, “Determination of the optimum TiN coating thickness on WC inserts for machining carbon steels,” *J. Mater. Process. Technol.*, 155–156, 1861–1866, 2004.

[2] V. R. Parameswaran, J. P. Immarigeon, and D. Nagy, “Titanium nitride coating for aero engine compressor gas path components,” *Surf. Coatings Technol.*, 52, 251–260, 1992.

[3] H. Reddy, U. Guler, Z. Kudyshev, A. V. Kildishev, V. M. Shalaev, and A. Boltasseva, “Temperature-Dependent Optical Properties of Plasmonic Titanium Nitride Thin Films,” *ACS Photonics*, 4, 1413–1420, 2017.

[4] S. Datta, M. Das, V. K. Balla, S. Bodhak, and V. K. Murugesan, “Mechanical, wear, corrosion and biological properties of arc deposited titanium nitride coatings,” *Surf. Coatings Technol.*, 344, 214–222, 2018.

[5] M. Wittmer and H. Melchior, “Applications of TiN thin films in silicon device technology,” *Thin Solid Films*, 93, 397–405, 1982.

[6] V. Merie, M. Pustan, G. Negrea, and C. Bîrleanu, “Research on titanium nitride thin films deposited by reactive magnetron sputtering for MEMS applications,” *Appl. Surf. Sci.*, 358, 525–532, 2015.

[7] L. Gao *et al.*, “Thermal stability of titanium nitride diffusion barrier films for advanced silver interconnects,” *Microelectron. Eng.*, 76, 76–81, 2004.

[8] L. Hultman, “Thermal stability of nitride thin films,” *Vacuum*, 57. Elsevier Ltd, 1–30, Apr. 01, 2000.

[9] H.-Y. Chen and F.-H. Lu, “Oxidation behavior of titanium nitride films,” *J. Vac. Sci. Technol. A Vacuum, Surfaces, Film.*, 23, 1006, 2005.

[10] C. Kainz, N. Schalk, C. Saringer, and C. Czettl, “In-situ investigation of the oxidation behavior of powdered TiN, Ti(C,N) and TiC coatings grown by chemical vapor deposition,” *Surf. Coatings Technol.*, 406, 126633, 2021.

29. Perovskite nanocrystals under the Transmission Electron Microscope: towards reliable data

Anastasia Matuhina[1], G. Krishnamurthy Grandhi[1], Maning Liu[1], and Paola Vivo[1*]

1 Hybrid Solar Cells, Faculty of Engineering and Natural Sciences, Tampere University, P.O. Box 541, FI-33014 Tampere University, Tampere, Finland

Corresponding author: Paola.Vivo@tuni.fi.

Perovskite nanocrystals (NCs) is a big group of materials, which attracts a lot of attention of the researchers due to their high commercialization potential in the optoelectronic field. Colloidal synthesis of NCs is a flexible and convenient approach for tuning the obtained properties, therefore making perovskite NCs appealing for applications in LED, lasers, solar cells, etc. However, there are still challenges to overcome, such as poor phase stability and the high toxicity of the lead in the composition, which triggers the ongoing studies. Accordingly, to ensure progress in this direction, it is essential to develop reliable methods of characterization. Comparably insufficient attention in the perovskite community is given to the appropriate practices of transmission electron microscopy (TEM) when in the reality the one is facing the challenges during the sample preparation, measurement, and interpretation of the results.

In fact, the major drawbacks of the perovskite NCs are also reflected in the TEM measurements. Low phase stability leads to the fast degradation in the ambient condition during the storage and the sample preparation. The Pb^{2+} species (which are typically in a crystal structure of the top-performing NCs) can be reduced to Pb^0 by irradiation with high-energy electrons, driving the deterioration of the original NCs and complicating the analysis [1]. But arguably one of the most affecting ones is the presence of the organic ligands (fatty amines) in the samples. Acting as the solvent, reducing, and coordinating agent, its utilization is necessary in the colloidal NCs synthesis. Moreover, in the ready-made samples, the ligands form a so-called shell, which coats the NCs. And while this shell serves as a protective layer, shielding the NCs from the detrimental factors, it strongly affects the quality and the reliability of the TEM images. Typically employed ligands contain hydrocarbon chains, causing contamination due to the combustion of hydrocarbons, which results in the formation of dark areas during the imaging [2]. Accordingly, the removal layer of the ligands is challenging since it will mean accelerated degradation and might cause irreversible changes to the NCs during the process.

Here we summarize our experience from the TEM study on a series of the perovskite NCs including well-studied and new compositions. We provide some hints for collecting reliable TEM data. The results of our work will hopefully assist the community in overcoming the current challenges of the TEM measurements of the perovskite NCs and will be valuable for the other studies performed for similar materials.

[1] Z. Dang *et al.*, “In Situ Transmission Electron Microscopy Study of Electron Beam-Induced Transformations in Colloidal Cesium Lead Halide Perovskite Nanocrystals,” *ACS Nano*, vol. 11, no. 2, pp. 2124–2132, 2017, doi: 10.1021/acsnano.6b08324.

[2] Ayache, Jeanne, et al. *Sample preparation handbook for transmission electron microscopy: techniques*. Vol. 2. Springer Science & Business Media, 2010.

32. Recent advances in in-situ micromechanical testing inside Scanning Electron Microscopes (SEM)

Aloshious Lambai[1], Suprit Bhusare[1], Rahul Cherukuri[1] and Gaurav Mohanty[1]

[1]*Engineering Materials Science, Faculty of Engineering and Natural Sciences, Tampere University, Tampere, Finland*

Corresponding author: gaurav.mohanty@tuni.fi

Recent advances in materials for structural applications have pushed the need for mechanical testing at the micro- and nano-meter length scales. This has spawned a host of micro-scale mechanical tests techniques, most of which are directly adapted from conventional tests for small length scales, for e.g. miniaturized tension and compression tests, indentation tests, etc. Among these, nanoindentation has emerged as the most widely used and versatile test technique for mechanical testing of thin films, miniaturized devices and materials at small length scales over the past three decades, partly due to ease of testing and minimal sample preparation. The addition of in-situ observation of the material deformation characteristics in the SEM and TEM enables researchers to draw conclusions on the operative deformation mechanisms, an important criterion for structural materials design.

This talk aims to introduce the emerging test techniques in the field of in-situ micron scale testing with special emphasis on nanoindentation, micropillar compression and micro-cantilever fracture tests in the SEM. Focused Ion Beam (FIB) is typically used for preparing micropillars, cantilevers, and other test geometries at specific sites like grains of known orientation, grain/phase boundaries, etc. Case studies of in-situ mechanical tests will be presented to illustrate reliable extraction of mechanical properties like yield strength, fracture toughness, time dependent plasticity (creep, relaxation and strain rate sensitivity) and fatigue properties at the micron scale. Recent advances in the field like high-speed mapping high strain rate testing and combining micron scale mechanical tests with x-rays, Raman and EBSD will also be presented. Finally, a brief overview of the state of the art and future research directions will be discussed.

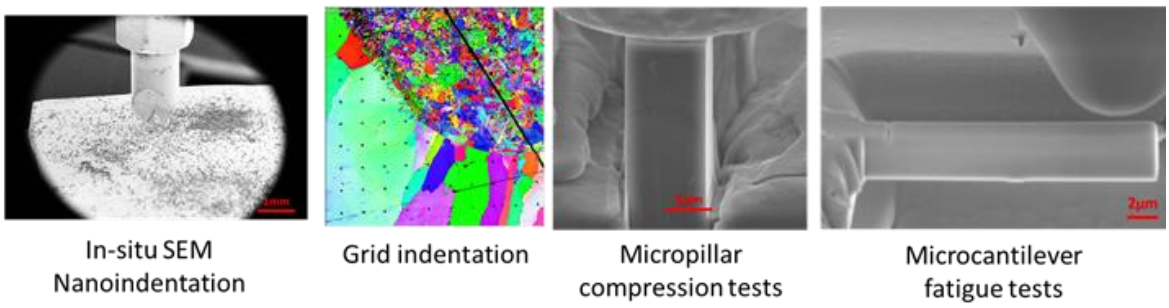

Figure 1. In-situ SEM micromechanical tests

33. Electrochemical Scanning Electron Microscopy

M.N. Yesibolati[1], E. Jensen[1], R. Møller-Nielsen, S. Canepa, H. Sun, and K. S. Mølhave[1]

[1]*DTU Nanolab, National Centre for Nano Fabrication and Characterization, Technical University of Denmark, 2800 Kgs. Lyngby, Denmark*,

Corresponding author: krmo@dtu.dk

Liquid Phase Transmission Electron Microscopy (LPTEM) is a rapidly growing area of research providing unprecedented insights into liquid phase processes with even atomic scale resolution [1]. To date, the systems for performing electrochemical experiments in situ TEM have shown limited resolution, as they typically provide liquid layer thicknesses from 0.2-4 µm. It seems many studies could be performed with reasonably matching resolution in a scanning electron microscope (SEM) instead, which would also offer other advantages:

A custom-built electrochemical system for in situ SEM (ECSEM) shown in Fig. 1 has proven very useful for studying a range of different processes [2]. It consists of a silicon chip with 5 or more microelectrodes lithographically defined on a silicon nitride membrane typically 30-50 nm thick, providing resolution of about 30 nm in the liquid. Four liquid ports make it possible to create flow to introduce dispersion of particles, reagents or flush our radiolytic species to limit the influence on the studied chemical processes from beam induced reactions. The ports can also be used to mount commercial reference electrodes, such as Ag/AgCl, which is not possible in LPTEM systems, and to use large counter electrodes such as Pt meshes. For high resolution optical microscopy, the top lid shown in Fig. 1B allows using water or oil immersion objective lenses.

LPTEM studies are typically strongly influenced by the very limited space between the two membranes encapsulating the thin liquid layer in such systems and hence provide limited mass transport. The open ECSEM design with >100 µm liquid beneath the microelectrodes relieves this limitation. It is possible to perform e.g. electrolysis with gas evolution as shown in Fig. 1C in 0.1M H_2SO_4, where the bubbles continuously form and diffuse away. In LPTEM systems, such bubbles would typically be stuck in the confined space, making continued measurements impossible. The ECSEM design also provides a well-defined ‘bulk‘ boundary condition for diffusion, and unlike our previous LPTEM studies of dendritic growth showing very inhomogeneous growth due to the LPTEM diffusive supply limitations [3], the ECSEM makes very quantitative measurements possible as the electrochemical system performs reliably with homogeneous dendritic growth of Cu from $CuSO_4$ solution as shown in Fig 1D. The multiple electrodes makes series of experiments possible in one experimental setting. They also make it possible to perform 4-point measurements, e.g. of conductance of a thin film conductor while biasing it to study deposition, pitting or corrosion.

Overall, such ECSEM systems enable rapid in situ optical and SEM experiments with reliable repeated electrochemical studies on multiple electrodes with the necessary control of mass transport as well as bulk diffusion boundary conditions, and also provide reliable electrochemical potential measurements and biasing with both reference and counter electrodes.

We expect such systems can provide new insights to complex nanoscale electrochemical processes. When found necessary further LPTEM studies can be done with higher resolution as the available electrochemical LPTEM systems improve.

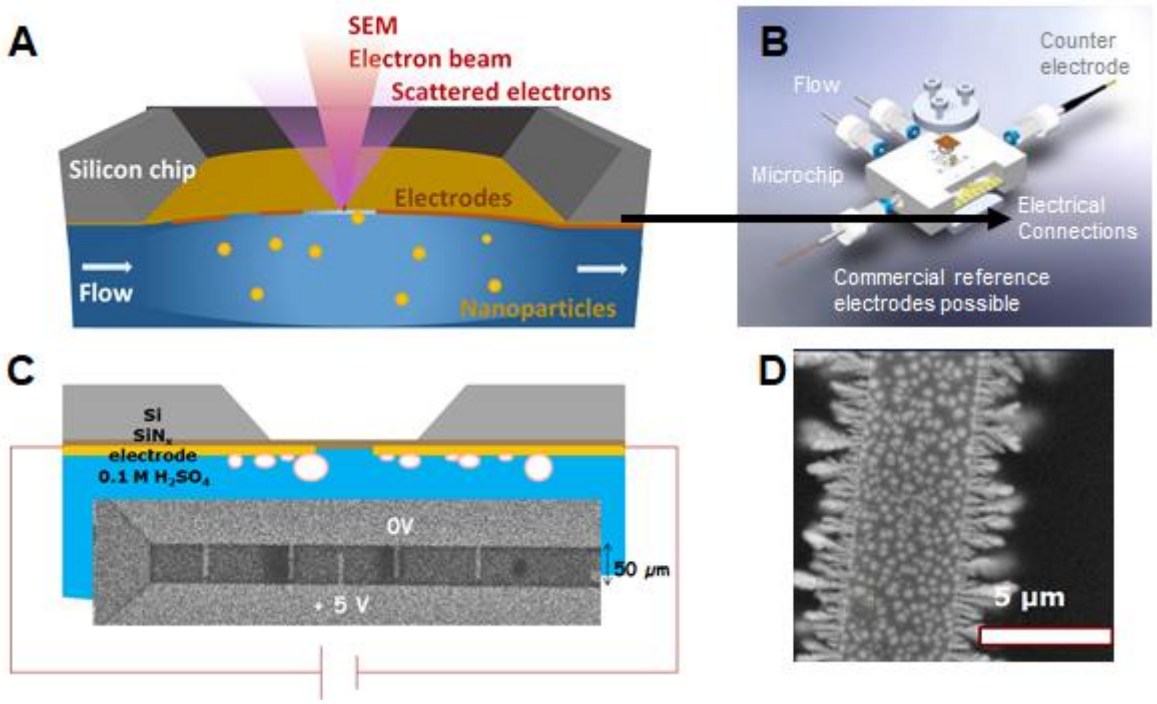

Figure 18 A) Schematic of the setup. B) 3D rendering of the ECSEM system. C) setup and ECSEM image of electrolytic formation of gas bubbles. D) Cu dendrites growing on microelectrode from $CuSO_4$ solution.

[1] F.M. Ross, Science 2015, 350 (6267), aaa9886

[2] Jensen et al. Ultramicroscopy 2013, 129, 63

[3] Zhao J. et al. Mater. Chem. A, 2017, 5, 11905

34. High resolution SEM/EDS study of stainless steel oxidation at high temperatures

Thao Nguyen[1] and Jyrki Juhanoja[1]

Top Analytica Oy, 20540 Turku, Finland

Corresponding author: thao.nguyen@topanalytica.com

Austenitic stainless steels are widely used in industries, like in fossil fuel power stations for tubes and pipes due to their excellent mechanical properties and corrosion resistance at high temperature. The good corrosion resistance of stainless steels is based on the formation of a very dense and thus protective chromium oxide (Cr_2O_3) on the steel surface. However, in some cases the protection is lost due to mechanical or chemical damage on the protective oxide layer. In order to overcome these problems, several ways to improve the mechanical and chemical stability have been studied, including mechanical treatments, optimized peroxidation or alloying the steel with minor elemental additives.

In this development work it is essential to have characterization methods which show how the physical and chemical properties are correlating with the mechanical properties and corrosion resistance. The method to be used for the characterization should be fast, reliable, and preferably with analytical resolution on the nanometer scale.

Scanning electron microscopy (SEM) with energy dispersive spectroscopy (EDS) is the one of most used technique in this field, but the analytical resolution is in the order of micrometer when the method is used in the conventional way (i.e., analyzing with K-lines and with relatively high voltages 15-20 kV). The analysis volume can be minimized down to 20-50 nm if lower voltages are used [1]. This makes the use of K-lines of main steel components (Cr, Fe and Ni) impossible, and the analyses must be done by using L-lines. The other problem arises from the fact that the emitted number of X-rays is low, and this may hinder the making the X-ray maps (increasing the accelerating voltage of using a longer mapping time is not a resolution due to decreased resolution or sample drift when working with high magnification).

In our studies, we use the Bruker FlatQUAD detector which has the highest collection angle for X-rays of the EDS detectors (high solid angle 1.1 sr with FlatQUAD, compared to 0.04 sr with an ordinary SDD-detector with 60 mm^2 chip). Our system is further modified with a thinner protection foil than the standard Flatquad detector, which improves the detection efficiency at low energies < 1 keV. As a result of higher resolution in mapping analysis, the double layer structures are observed in oxidized AISI 304L steel and Inconel 625 steel (Fig. 1 and Fig. 2).

Other critical step is the sample preparation. Our samples are prepared by using cross-section polisher with Ar-ions. Compared to the mechanical polishing methods the advantage is better polishing quality with less material mixing and retaining the porosity and crystallinity, which is important if Electron backscatter diffraction (EBSD) measurements are planned to perform.

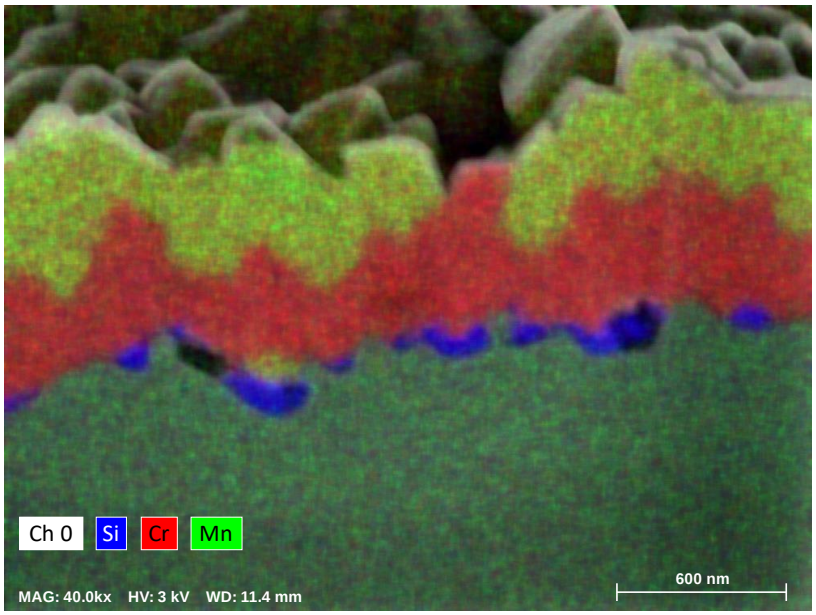

Figure 19. Oxidation of AISI 304L steel 750°C, 24 h. The double layer structure chromium oxide Cr_2O_3 on the bottom and manganochromite Mn_2CrO_4 on the top. On the steel-oxide interphase a SiO_2-layer has been formed.

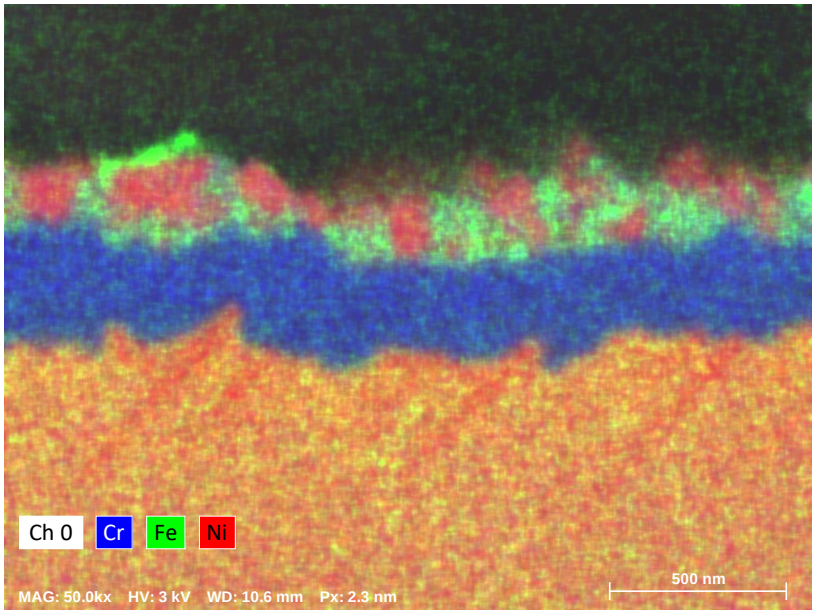

Figure 20. Oxidation of Inconel 625 steel 750°C, 24 h. The double layer structure is visible but now the upper layer on the top of Cr_2O_3 is separated to Ni- and Fe-rich phases.

[1] Small J. A., The Analysis of Particles at Low Accelerating Voltages (≤ 10 kV) With Energy Dispersive X-Ray Spectroscopy (EDS), Journal of research of the National Institute of Standards and Technology, 107(6), 555–566, (2002)

35. Atomic-scale study of planar defects in transition metal diboride coatings

Justinas Palisaitis[1], Martin Dahlqvist[1], Lars Hultman[1], Ivan Petrov[1,2,3], Johanna Rosen[1] and Per O.Å. Persson[1]

[1]*Thin Film Physics Division, Department of Physics, Chemistry and Biology (IFM), Linköping University, SE-581 83 Linköping, Sweden,*

[2]*Frederick Seitz Materials Research Laboratory and Department of Materials Science, University of Illinois, Urbana, Illinois 61801, USA,*

[3]*Department of Materials Science and Engineering, National Taiwan University of Science and Technology, Taipei 10607, Taiwan*

Corresponding author: justinas.palisaitis@liu.se

Transition metal diborides (TMB_2) received increasing attention as the next generation materials for hard coating/high temperature applications. Synthesis of TMB_2 coatings is, however, complicated because they are line-compounds that do not allow point defects to accommodate for slight off-stoichiometry. E.g. a ratio of B/TM>2, leads to the formation of a secondary B-rich phase, which is separated from the growing compound [1]. A recent breakthrough in achieving full control of the B/TM ratio during the deposition process has resulted in synthesis of novel coatings with ratios B/TM<2, that possess high crystal quality and hardness [2-4]. The realization of B-deficient TMB_2 films widens the compositional range and thus, design and synthesis of films with performance-tailored microstructures. At the same time, it raises fundamental questions on the atomic structure integrity of such TMB_2 coatings and how the off-stoichiometry is accommodated in the film.

In this contribution, we present and compare the atomic arrangement and chemistry of different planar defects present in TM-based diboride coatings. The description of defects throughout a wide elemental and compositional range are based on observations made in under-stoichiometric: ($TiB_{1.44}$, $Zr_{0.70}Ta_{0.30}B_{1.50}$, $TiB_{1.90}$, $CrB_{1.90}$) and over-stoichiometric ($CrB_{2.10}$, $ZrB_{2.40}$, $Ti_{0.79}Al_{0.21}B_{2.70}$) coatings. Atomically resolved scanning transmission electron microscopy (STEM) imaging, electron energy loss spectroscopy (EELS) elemental mapping, and first principles calculations have been applied to elucidate the atomic structures of the observed planar defects denoted as antiphase boundary (APB).

Fig. 1 shows a plan-view high-resolution STEM image from $CrB_{1.9}$ coatings, which reveals coexistence of various APB defects residing on the {1-100} planes and interconnected in various configurations.

The characteristic stoichiometry variations (without (APB-1) or with (APB-2i-iii) local deviation), atomic structures, interconnections and circumstances leading to the formation of these APB-defects together with their formation energies will be presented.

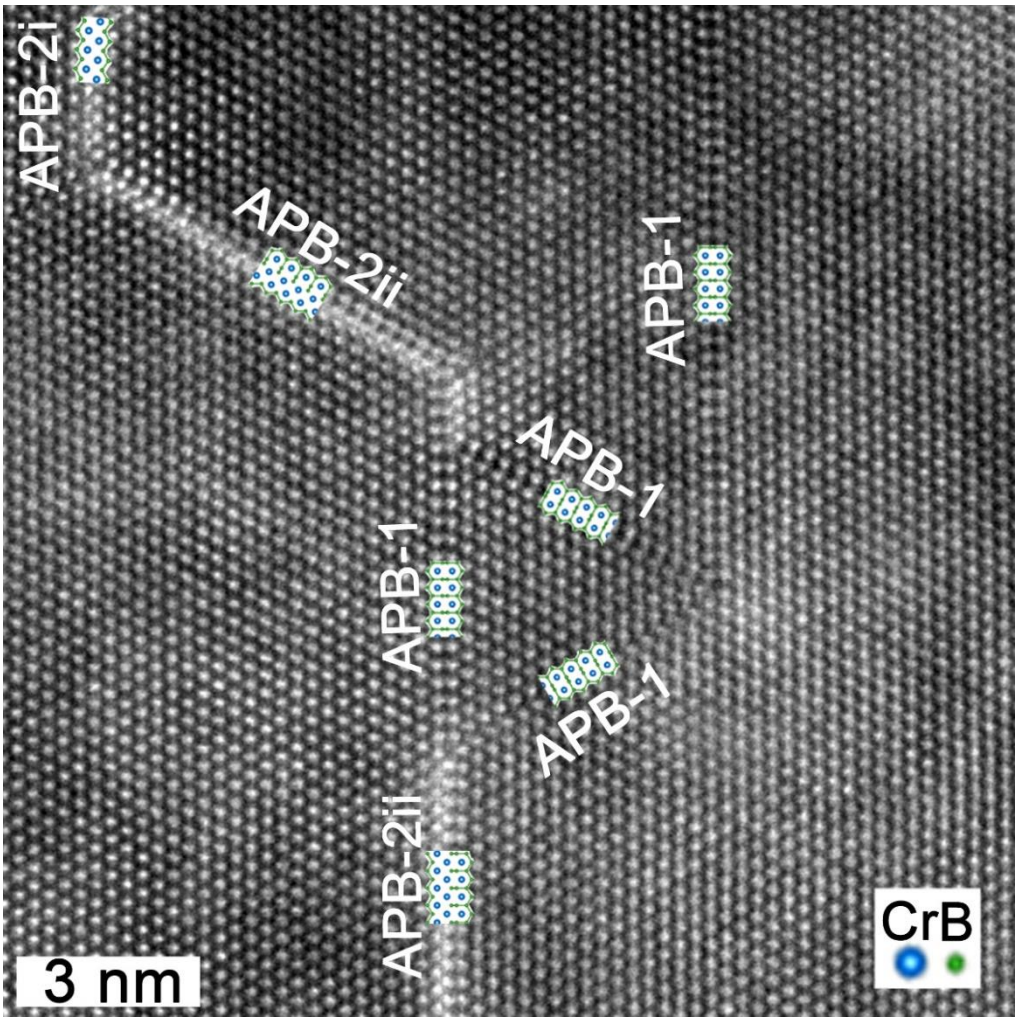

Figure 21 The coexistence of APB-1, APB-2i, and APB-2ii defects in the $CrB_{1.9}$ coating.

The authors acknowledge the Swedish Research Council for funding under grant no. 2016-04412. Knut and Alice Wallenberg Foundation for support of the electron microscopy laboratory in Linköping, a Fellowship/Scholar grant and a project grant (KAW 2015.0043). Swedish Foundation for Strategic Research (SSF) through the Research Infrastructure Fellow program no. RIF 14-0074 and project funding (EM16-0004). Swedish National Infrastructure for Computing (SNIC) at the National Supercomputer Centre (NSC) and the PDC Center for High Performance Computing partially funded by the Swedish Research Council through grant agreement no. 2018-05973. Swedish Government Strategic Research Area in Materials Science on Functional Materials at Linköping University (Faculty Grant SFO-Mat-LiU No 2009 00971). Megan Dorri, Allen J. Hall, Nils Nedfors and Jimmy Thörnberg are acknowledged for providing samples.

[1] P.H. Mayrhofer, et al, *Appl. Phys. Lett*., 86, 3, 2005.

[2] I. Petrov, et al, *J. Vac. Sci. Technol. A*., 35, 050601, 2017.

[3] M.M. Dorri, et al, *Scripta Mater*., 200, 113915, 2021.

[4] J. Palisaitis, et al, *Acta Mater*., 204, 116510, 2021.

36. Magnetic Force Microscopy in the Service of High Entropy Alloys Exploration

Anthoula Poulia[1], Amin S. Azar[2], Calliope Bazioti[1], Aleksander Amble Larsen[1], Joachim Seland Graff[3], Branson Belle[3], Patricia Almeida Carvalho[3], Pavlo Mikheenko[1], Spyridon Diplas[3] and Anette Eleonora Gunnæs[1]

[1]*Department of Physics, University of Oslo, Norway*

[2] *Effee Induction AS, Ålesund, Norway*

[3]*SINTEF Industry, Oslo, Norway*

Corresponding author: anthoula.poulia@smn.uio.no

Advanced soft magnetic materials are crucial for renewable electric energy generation, towards reducing the CO_2 emissions. Since current soft magnetic materials are approaching their performance limit, the field is calling for a disruptive technology that involves modern materials and novel methodologies. In the Magnificent project, we aim to develop soft magnets based on High Entropy Alloys (HEA), processed by laser metal deposition (LMD) method. HEAs can be prepared in a broad range of forms and properties, which institutes in multiple structural, magnetic, high-temperature, and oxidation-resistant applications. Due to their unique properties, these materials are in the spotlight for both academia and industry.

In this work, $FeCoNi(AlMn)_x$ alloys were evaluated in terms of structural and magnetic properties. Phase constitutions, either affected by compositional or structural changes, were explored as they are key factors in determining the magnetic performance of the materials studied. The alloys exhibited good soft-magnetic behaviour, being easily magnetized to the saturated state with coercivity values of <1000 A/m. Magnetic screening through Magnetic Force Microscopy (MFM) confirmed the importance of structure evolution in defining the magnetic properties of the alloys. Complementary imaging of the magnetic domain structure combined with the crystal-structure orientation information from Electron Backscattered Diffraction explained the trends in the magnetic behaviour, as a function of the alloy composition.

37. Differentiating Polyamorphous SiO_2 by SPED, PDF and Blind Source Separation algorithm

Andreas Rosnes[1], Emil Frang Christiansen[1], Hogne Lysne[1], Turid Reenaas[1] Randi Holmestad[1]

[1]*Department of Physics, Norwegian University of Science and Technology (NTNU), Trondheim, Norway*

Corresponding author: andrrosn@ntnu.no

Amorphous and nanomaterials lack the long-range order of crystals which makes it an experimental challenge to study the atomic arrangement with high precision. The transmission electron microscope (TEM) is a powerful tool to study local structures due to the electrons high-resolution and strong interaction with matter providing a lot of signals from a minuscule area. The lack of long-range order breaks down the crystallographic approach, and therefore an alternative method is required for describing the structure. A pair distribution function (PDF) provides a statistical weighted sum of correlated distances in the structure, in its simplest form, telling us the likelihood of finding an atom a certain distance away from a central atom. A combination of TEM and PDF can provide additional information on such materials. Recent work has successfully differentiated amorphous nanophases via blind source separation (BSS) of a mixed signal of independent phases from a four-dimensional scanning TEM experiment (4D-STEM) [1], and the field has experienced a rapid development in recent years [2]. BSS is an effective tool to separate a mixed signal in large datasets into independent sources (components) and their weighting in the set (loading maps).

This work evaluates the robustness of BSS by studying a cross sectional focused ion beam (FIB) prepared lamella of layered independent SiO_2 amorphous phases by scanning precession electron diffraction (SPED). Virtual bright-field imaging (VBF) and virtual annular dark-field imaging (VADF) together with PDF from the different layers were compared to the components and their loading maps of the decomposed SPED dataset. The decomposition was obtained by independent component analysis (ICA). The results are presented in an overview figure (Figure 1). The ICA components appear similar to the traditional PDF analysis results, and the components loading maps match their VADF counterparts, demonstrating that ICA can extract physical information from the data.

The main difference between the layers is the shift of the Si-O pair distance from 1.59 to 1.75 Å. The origin of this is expected to be the shift from a tetrahedra coesite-like to an octahedra stishovite-like amorphous phase [3]. As a conclusion, ICA of SPED dataset is successful in differentiating the amorphous phases, but careful considerations and supplementary TEM techniques such as VADF were necessary to support the physical meaning of the components.

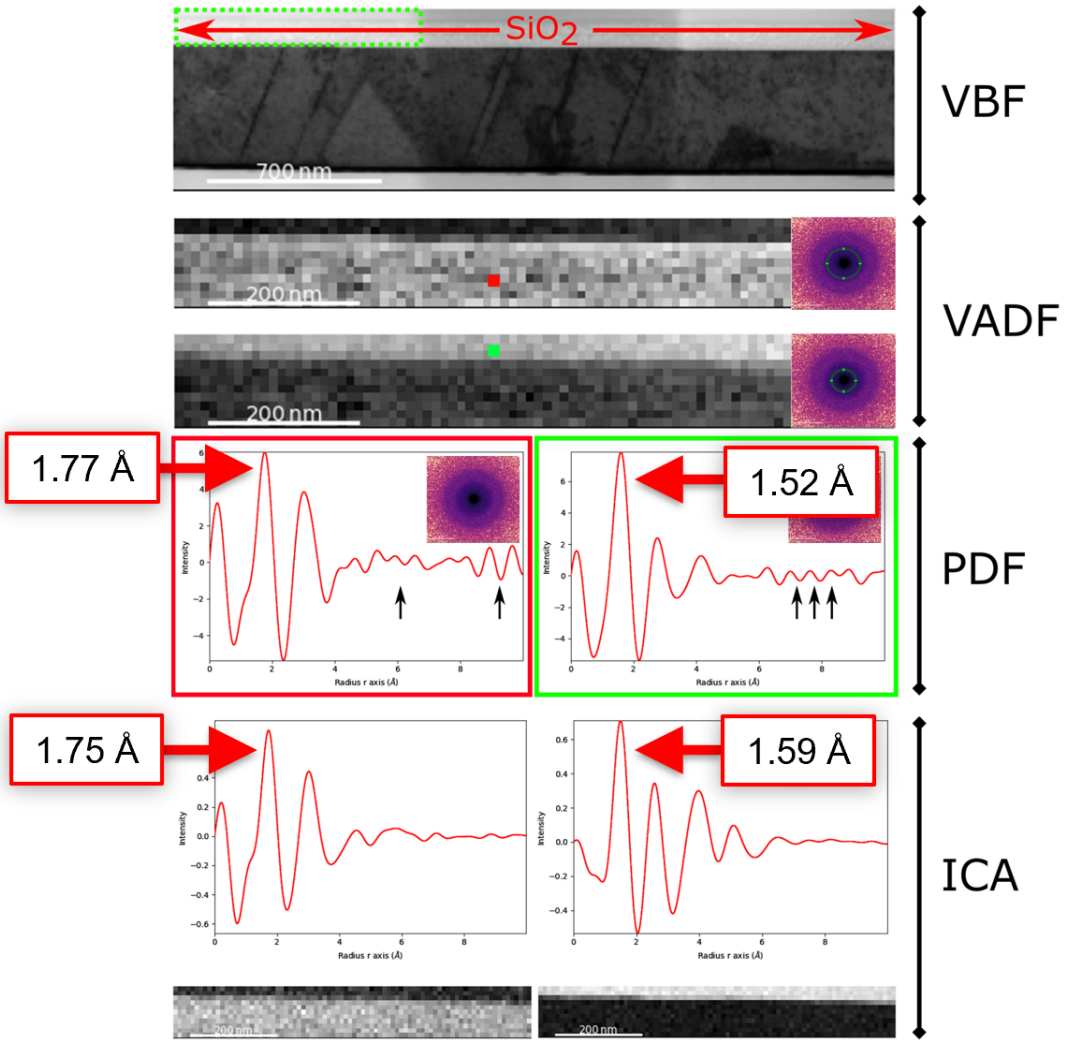

Figure 22 VBF image of a SPED dataset from a FIB lamella of the sample consisting of two different layers of amorphous SiO_2. The VADF is from the green dotted region and shows two distinct layers of amorphous SiO_2 structures. Manually picked out PDFs (red and green pixel) from the dataset are compared to two primary sources obtained from the ICA decomposition. The ICA components appear similar to the traditional PDF analysis results, and the component loading maps match their VADF counterparts, demonstrating that ICA can extract physical information from the data. The shift from 1.59 to 1.75 Å of the Si-O pair distance is expected to be due to a shift from the nature of the chemical bond from a tetrahedra coesite- to an octahedra stishovite-like amorphous phase.

[1] Mu X., Chen L., Mikut R., Hahn H., Kübel C., ”Unveiling local atomic bonding of amorphous nanophases via independent component analysis facilitated pair distribution function”, Acta Materialia, 212, 2021.

[2] Souza Junior J. B., Schlender G. R., Bettini J., Costa Nogueira I., Fazzio A., Leite E. R., ”Pair Distribution Function Obtained from Electron Diffraction: An Advanced Real-Space Structural Characterization Tool”, Matter, 4, 441-460, 2021.

[3] Polyakova I. G., “The Main Silica Phases and Some of Their Properties” in *Glass: Selected Properties and Crystallization*, Ed. Schmelzer J. W. P., De Gruyter, 2014. Pp. 197-268.

[4] Acknowledgements to FME SuSolTech (RCN 257639), NorFab (RCN 295864), NORTEM (RCN 197405), and Ox-IB (RCN 240466) for support and funding of this work.

38. In-situ Nanoscale Characterization of Electrical and Magnetic Properties of 3D Nanostructures by combination of AFM, SEM and FIB

C.H. Schwalb[1], H. Frerichs[1], S. Seibert[1], L. Stühn[1], M. Wolff[1], J. Ihrenberger[2], L. Seewald[2], R. Winkler[2], and H. Plank[2]

[1]*Quantum Design Microscopy GmbH, Darmstadt, Germany*

[2]*Institute for Electron Microscopy and Nanoanalysis, Graz Univ. Technology, Graz, Austria*

Corresponding author: schwalb@qd-microscopy.com

Combining different analytical methods into one instrument is of great importance for the simultaneous acquisition of complementary information. Especially the in-situ combination of scanning electron microscopy (SEM) and atomic force microscopy (AFM) enables completely new insights in the micro and nano-world. In this work, we present the unique in-situ combination of scanning electron and ion microscopy (SEM/FIB) and atomic force microscopy (AFM) for nanoscale characterization [1-2].

We will present a variety of case studies to highlight the advantages of interactive correlative in-situ nanoscale characterization for different materials and nanostructures. We show results for *in-situ* electrical characterization by conductive AFM for 2D materials as well as electrostatic force microscopy (EFM) of piezoceramic films that enables the precise analysis of grain boundary potential barriers in semiconducting $BaTiO_3$-based ceramics [3]. The grain boundaries were located by BSE-SEM and afterwards measured with in-situ EFM. The barriers were shown to be significantly thinner and more pronounced as the amount of SiO_2 was increased from 0 to 5 mol% (see Figure 1).

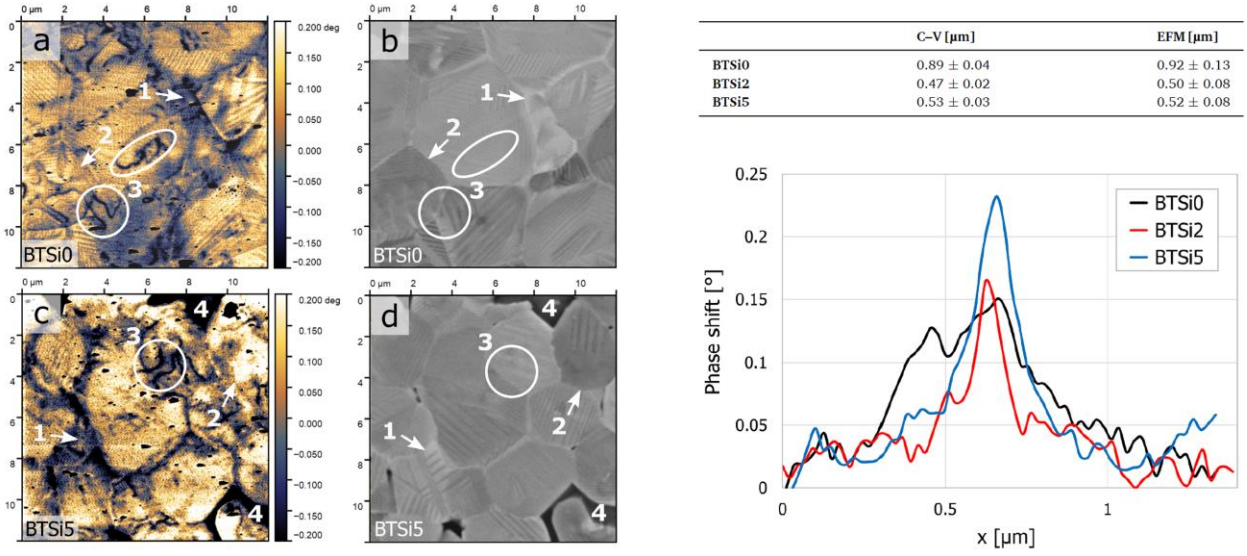

Figure 23: (Left) EFM signal of (a) BTSI0 and (c) BTSi5 and corresponding BSE-SEM images (b) and (d) of the exact same sample area. The EFM images were recorded with an external voltage of -3 V. (Right) Grain boundary potential barriers of $BaTiO_3$ based ceramics with varying SiO_2 content. Images extracted from [3]

In addition, we will present results for the in-situ characterization of magnetic nanostructures by combination of SEM and high-vacuum magnetic force microscopy (MFM). SEM enables to identify grain boundaries in order to measure the magnetic properties directly via MFM with nanometer resolution (see Figure 2).

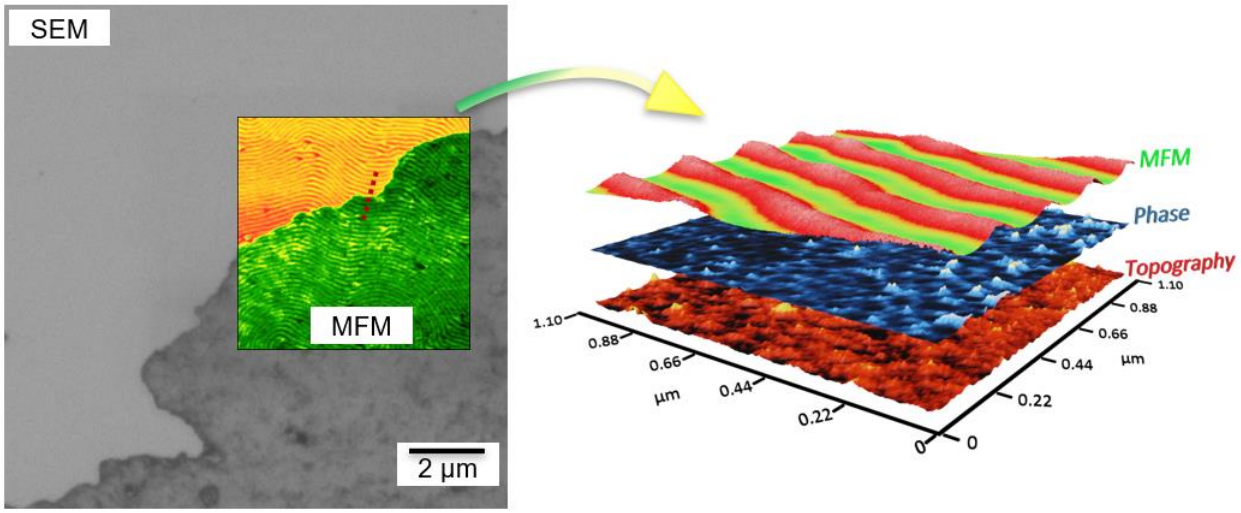

Figure 24: (Left) SEM image of multilayer magnetic sample with correlative MFM image at a grain boundary. (Right) AFM data overlay of topography, phase, and MFM signals.

[1] D. Yablon, et al., Microscopy and Analysis, **31** (2), 14-18 (2017)

[2] S.H. Andany, et al., Beilstein J. Nanotechnol., **11**, 1272-1279 (2020)

[3] J.M. Prohinig, J. Hütner, K. Reichmann, S. Bigl, Scripta Materialia, **214**, 114646 (2022)

39. Direct Observation of Facet, Morphology, and Phase Evolution in Photocatalytic Materials

Michael S. Seifner[1,3], Markus Snellman[2,3], Tianyi Hu[1,3], David Llorens Rauret[1,3], Ofentse A. Makgae[1,3], Daniel Jacobsson[1,3,4], Martin Ek[1,3], Knut Deppert[2,3], Maria E. Messing[2,3], Kimberly A. Dick[1,3]

[1]*Centre for Analysis and Synthesis, Lund University, Box 124, 22100 Lund, Sweden*

[2]*Solid State Physics, Lund University, Box 118, 22100 Lund, Sweden*

[3]*NanoLund, Lund University, Box 118, 22100 Lund, Sweden*

[4]*National Center for High Resolution Electron Microscopy, Lund University, Box 124, 22100 Lund, Sweden*

Corresponding author: Michael.Seifner@chem.lu.se

Corresponding author: Kimberly.Dick_Thelander@chem.lu.se

Recently, there have been substantial research efforts to create nanoparticle heterostructures by combining semiconductors with metals or other semiconductors to enhance their photocatalytic activity for specific chemical reactions [1]. Besides the materials' surface facets and their terminations, the interface design is essential for enhancing the photocatalytic activity in nanomaterial heterostructures [2]. Controlling the atomic structure of the heterointerface has a direct impact on the coupling of the components. Efficient component coupling can lead to an enhanced charge carrier separation, an essential step of the photocatalytic process.

The characterisation of nanomaterial heterostructures is usually performed after the synthesis making conclusions about the formation mechanism non-trivial or even impossible. However, understanding the formation of the materials is essential to obtain control over properties such as crystal structure, facet orientation, and morphology. The environmental transmission electron microscope (TEM) with an integrated metal-organic chemical vapour deposition (MOCVD) system at Lund University is an ideal tool to observe and study the evolution of such properties during the synthesis process [3].

This contribution reports the direct observation of nanoparticle heterostructures' facet, phase, and morphology evolution *via* high-resolution TEM imaging/movies and energy dispersive X-ray spectroscopy (EDS). The approach was to use Ag-Cu nanoparticles deposited on TEM heating chips *via* the spark ablation system as a materials platform to create Ag-Cu_3P, Ag-Cu_3As, and Ag-Cu_3P-GaP heterostructures by supplying precursors directly to the heated sample in the environmental TEM. Variation of process parameters, including the temperature and precursor flows, revealed the potential to initiate rearrangement processes to switch between different heterointerfaces, morphological changes, and phase transformations in the addressed materials systems.

This work highlights the potential of in-situ electron microscopy to help understand the formation of complex heterostructures and make progress in synthesising well-defined nanomaterials with a focus on facet-engineered surface and heterointerface design.

[1] Low J., Yu J., Jaroniec M., Wageh S., Al-Ghamdi A. A., “Heterojunction Photocatalysts“, *Adv. Mater., 29*, 1601694, 2017.

[2] Bai S., Wang L., Li Z., Xiong Y., “Facet-Engineered Surface and Interface Design of Photocatalytic Materials“, *Adv. Sci., 4*, 1600216, 2016.

[3] Hetherington C., Jacobsson D., Dick K. A., Wallenberg L. R., “In situ metal-organic chemical vapour deposition growth of III-V semiconductor nanowires in the Lund environmental transmission electron microscope“, *Semicond. Sci. Technol., 35*, 034004, 2020.

40. Cryo-electron microscopy of a thermotropic liquid crystal film dispersed with superparamagnetic nanoparticles

Baeckkyoung Sung[1,2]

[1]*KIST Europe Forschungsgesellschaft mbH, Saarbrücken, Germany,*

[2]*Division of Energy & Environment Technology, University of Science & Technology (UST), Daejeon, South Korea*

Corresponding author: sung@kist-europe.de

Inorganic nanoparticles dispersed in a liquid crystalline matrix can alter phase behaviour of the host liquid crystal (LC). From a structural viewpoint, it is well known that doped nanoparticles preferentially segregate at the LC defect sites [1]. In this presentation, we elucidate the local distribution and aggregated structure of oleic acid-coated superparamagnetic iron oxide nanoparticles (SPIONs; 5-6 nm in diameter) doped in the thin film of a nematic LC, 4-cyano-4'-pentylbiphenyl (5CB), utilising *in situ* cryogenic transmission electron microscopy (cryo-TEM), assisted with polarised optical microscopy (POM) [2]. The frozen thin film (50-150 nm in thickness) of a 5CB-SPION mixture was formed in a perforated carbon-coated grid, and was subsequently observed in a cryo-TEM, which was operated at 200 kV under low electron dose conditions (Fig. 1). The image data were quantitatively analysed to extract statistical information on the sizes of SPIONs and their agglomerates, as well as the inter-particle spacing of the agglomerated SPIONs [3]. We show that close-packed 30-40 SPIONs aggregated into a spherical morphology, and the aggregates combine into elongated and fractal-like clusters with a length of hundreds of nm (Fig. 1). With the SPION-doped LC matrix confined to a thin glass cell, we additionally explored the nematic-isotropic (N-I) phase transition, and suggest that local heterogeneity of LC textures as seen in POM was caused by the existence of SPION aggregate clusters. These clusters acted also as nuclei for the formation of isotropic domains upon heating. Our results promote the fundamental understanding on how colloidal nanospheres behave in an anisotropic fluid, and have a significant potential to be used as a part of database for designing hybrid materials and devices that combine the properties of LCs and magnetic particles.

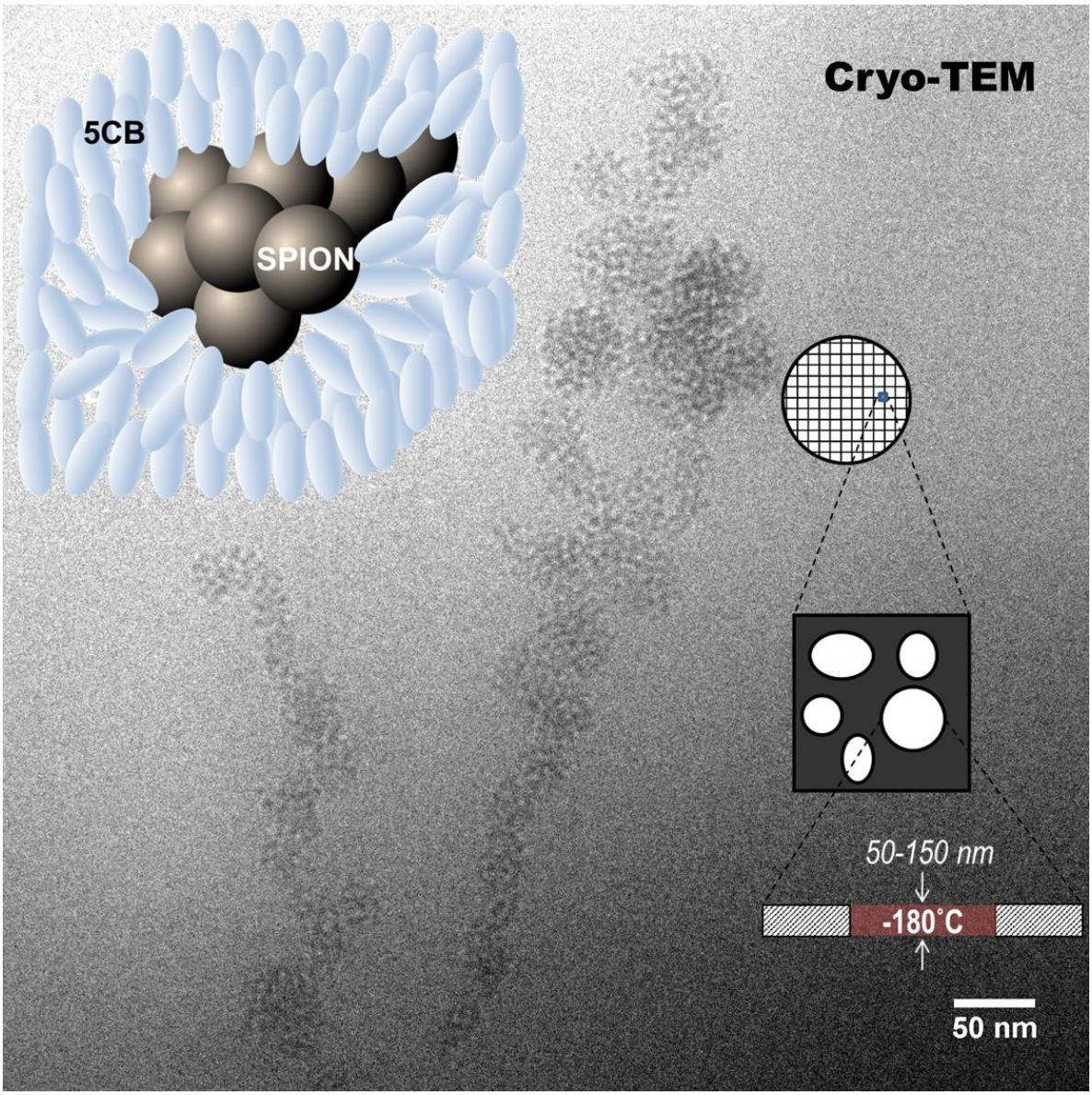

Figure 25. Cryo-TEM image showing the agglomeration structure of SPIONs doped in a 5CB liquid crystal film, which is formed in the micro-perforations of a holey carbon grid. Each electron-dense point represents a single SPION, and the background is the 5CB medium.

[1] Da Cruz C., Sandre O., Cabuil V., "Phase behavior of nanoparticles in a thermotropic liquid crystal", *J. Phys. Chem. B*, *109*, 14292-14299, 2005.

[2] Sung B., Yan H., Kim C., Abelmann L., "Inhomogeneous nematic-isotropic phase transition of a thermotropic liquid crystal doped with iron oxide nanoparticles", *Phys. Lett. A*, *384*, 126927 2020.

[3] Sung B., Abelmann, L., "Agglomeration structure of superparamagnetic nanoparticles in a nematic liquid crystal medium: image analysis datasets based on cryo-electron microscopy and polarised optical microscopy techniques", *Data in Brief*, *34*, 106716, 2021.

41. Advanced nanoscale characterization of lithium ion batteries

Thomas Thersleff[1], Jordi Biendicho[2], Kunkanado Prakasha[2], Evgeniya Khomyakova[3], Jekabs Grins[1], Aleksander Jaworski[1], Gunnar Svensson[1].

[1]Department of Materials and Environmental Chemistry, Arrhenius Laboratory, Stockholm University, SE – 10691 Stockholm, Sweden.

[2]Catalonia Institute for Energy Research-IREC, Sant Adrià de Besòs, 08930 Barcelona, Spain.

[3]Cerpotech, Kvenildmyra 6, 7093 Heimdal, Norway.

Corresponding author: Thomas.thersleff@mmk.su.se

With the performance of lithium ion batteries directly dependent on nanoscale structural and chemical features [1], it is imperative to have a tool that can not only study lithiation chemistry but also directly visualize structure / chemistry relationships with up to atomic resolution. In this work, we outline how we are combining aberration-corrected STEM imaging, EEL and EDX spectroscopies, scanning diffraction, and new data processing methods to address this challenge. We first highlight how integrated Differential Phase Contrast (iDPC) imaging can be used to localize structural domains as well as resolve the lithium / oxygen sublattice in these materials at low dose (see figure 1). Second, we highlight how a new technique developed in-house that we call hypermodal data fusion [2,3] can be used to directly couple multiple spectroscopy and scanning diffraction datasets, permitting relationships between a wide range of materials properties to be quantitatively modelled in morphologically complex systems for the first time (see figure 2). We conclude with a discussion on how these methods can be applied not only to batteries but also to a much broader range of materials and research questions.

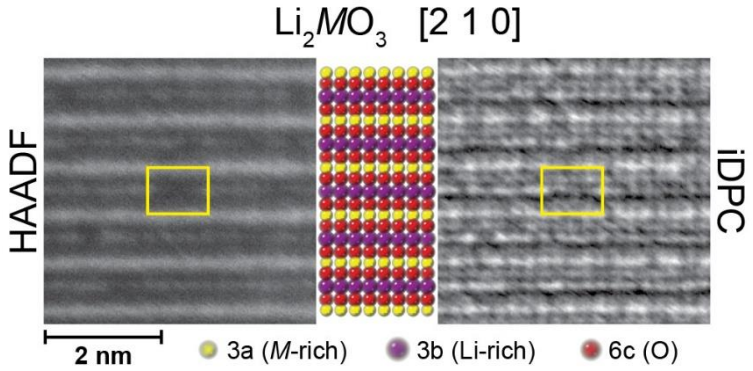

Figure 1 – The layered lithium-rich manganese oxide $Li_{1.1}Mn_{0.54}Al_{0.01}Ni_{0.35}O_2$ splits into nanosized domains consisting of monoclinic $LiMO_2$ and rhombohedral Li_2MO_3 (M = Transition Metal). A region rich in the latter phase was tilted to the [210] zone axis and imaged simultaneously with STEM-HAADF and iDPC detectors. A scaled atomic model of the crystal in this orientation is provided in the middle with Wyckoff positions labelled in the legend at bottom. The contrast for transition metals is bright in the HAADF image, while Oxygen and Lithium columns are additionally revealed with iDPC. The yellow box highlights transition metal disordering on the Lithium-rich 3b site, which is confirmed with the absence of contrast in the HAADF image yet direct visualization of the lithium columns in the iDPC image.

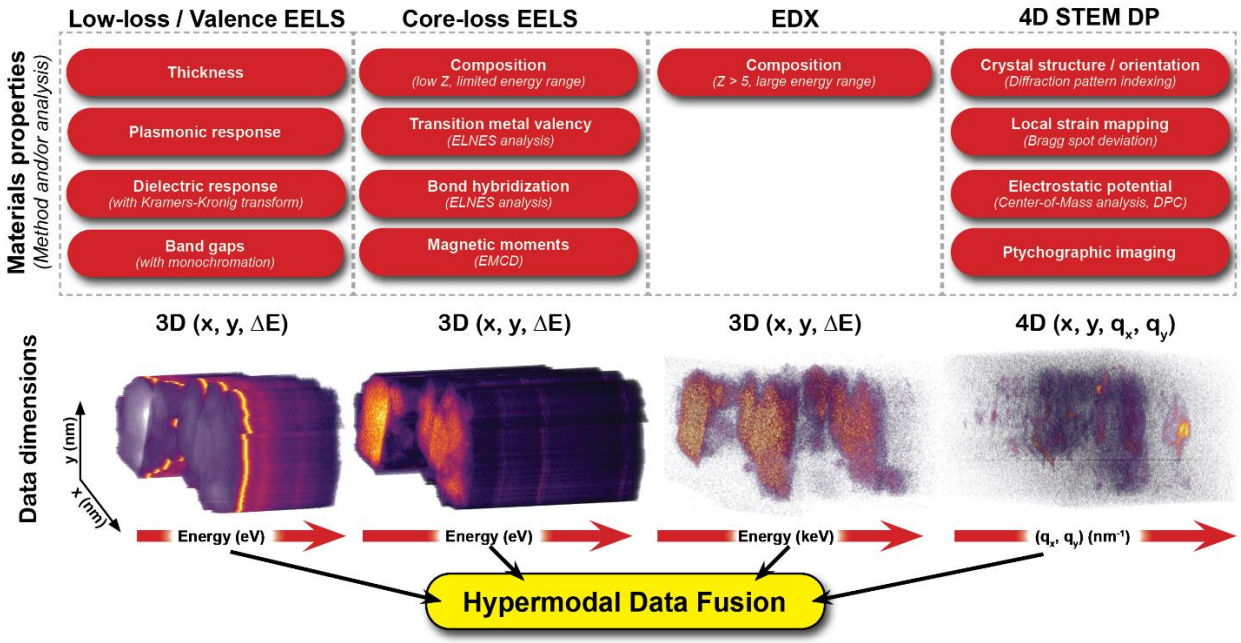

Figure 2 – Schematic illustrating some of the materials properties that can be extracted from various STEM datasets. Hypermodal data fusion is a new method that can reveal how any and all of these properties are related, even if the underlying features overlap along the beam projection. Created from wide field-of-view datasets acquired on $Li_{1.1}Mn_{0.45}Sn_{0.1}Ni_{0.35}O_2$.

[1] K. Rajappa Prakasha, J. Grins, A. Jaworski, T. Thersleff, G. Svensson, L.O. Jøsang, A.D. Dyrli, A. Paulus, D. De Sloovere, J. D'Haen, M.K. Van Bael, A. Hardy, H. Avireddy, J.R. Morante, J. Jacas Biendicho, Temperature-Driven Chemical Segregation in Co-Free Li-Rich-Layered Oxides and Its Influence on Electrochemical Performance, Chem. Mater. (2022). https://doi.org/10.1021/acs.chemmater.1c04150.

[2] T. Thersleff, S. Budnyk, L. Drangai, A. Slabon, Dissecting complex nanoparticle heterostructures via multimodal data fusion with aberration-corrected STEM spectroscopy, Ultramicroscopy. 219 (2020) 113116. https://doi.org/10.1016/j.ultramic.2020.113116.

[3] T. Thersleff, C.-W. Tai, Feature-specific correlation of structural, optical, and chemical properties in the transmission electron microscope with hypermodal data fusion, Under Review. (2022). Preprint: https://doi.org/10.48550/arXiv.2203.11044.

42. Scanning Droplet Adhesion Microscopy

Maja Vuckovac[1], Robin H. A. Ras[1,2]

[1]*Aalto University School of Science, Espoo, Finland*

[2]*Aalto University School of Chemical Engineering, Espoo, Finland*

Corresponding author: maja.vuckovac@aalto.fi

Surface wetting is an important surface property since it will affect the repellence of water droplets from the substrates, adherence of the paints to the surface, and the spreading of cosmetic products on the skin. Furthermore, surface wetting is a complex phenomenon that arises from nano- and microscale. The irregularities at such small scales, either in surface texture or chemical composition, will lead to the spot-to-spot variation of wetting properties and further influence droplet mobility, adhesion and spreading dynamics. However, effective ways to quantify and map microscopic variations of wettability are still missing because existing contact angle and force-based methods lack sensitivity and spatial resolution [1-3]. Here we present a cutting-edge methodology, scanning droplet adhesion microscopy, for evaluating the surface wetting with enhanced accuracy based on the adhesion force measurements. The technique allows measurement of small forces with sensitivity down to nanonewton and mapping of wetting properties at microscale spatial resolution on repellent surfaces [3-5] such as butterfly wings (Figure 1).

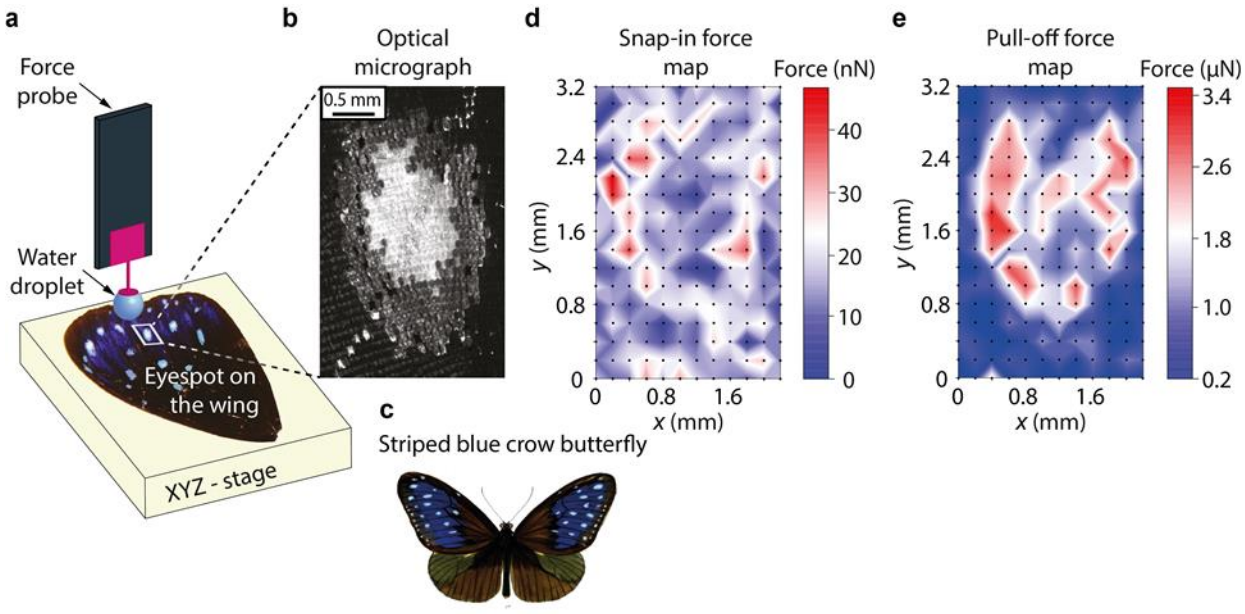

Figure 1. Concept of scanning droplet adhesion microscopy to construct wetting maps showing (a) schematic diagram of the microscope (not to scale), (b) optical micrograph of scanned eyespot area on the wing of (c) striped blue crow butterfly (image by Frederic Moore, PD-1923) with corresponding (d) snap-in and (e) pull-off force maps.

[1] Vuckovac M., Latikka M., Liu K., Huhtamäki T., Ras R. H. A., “Uncertainties in contact angle goniometry”, *Soft Matter*, 15, 7089, 2019.
[2] Liu K., Vuckovac M., Latikka M., Huhtamäki T., Ras R. H. A., ”Improving surface-wetting characterization”, *Science*, 363, 1147–1149, 2019.
Ruska E., Knoll M., “Das Elektronenmikroskop“, *Z. Phys., 78*, 318-339, 1932.
[3] Liimatainen V., Vuckovac M., Jokinen V., Sariola V., Hokkanen M.J., Zhou Q., Ras R. H. A., Scanning Droplet Adhesion Microscopy”, *Nature Communications*, , 8, 1798, 2017.
[4] Hokkanen M. J., Backholm M., Vuckovac M., Zhou Q., and Ras R. H. A., “Force-based Wetting Characterization of Stochastic Superhydrophobic Coatings at Nanonewton Sensitivity”, *Advanced Materials*, 3, 2105130, 2021.
[5] Dong Z., Vuckovac M., Cui W., Zhou Q., Ras R. H. A., Levkin P. A., “3D Printing of Superhydrophobic Objects with Bulk Nanostructure”, *Advanced Materials*, 33, 2106068, 2021.

43. Development and Application of automated experiments in transmission electron microscopy

Taimin Yang[1],

[1]*Department of Material and Environmental Chemistry, Stockholm University, 10691, Stockholm, Sweden*

Corresponding author: Taimin.yang@mmk.su.se

Transmission electron microscopy (TEM) is a core tool to investigate the relationship between the structure and property of a material by visualizing the arrangement of atoms. With the rise of quantitative microscopy, large datasets are needed to increase the representativeness of the results. In addition, each TEM operator has her/his own preference to align the microscope and select region of interest, which could generate inconsistent results and thus reduce data reliability and repeatability. Therefore, an automated TEM is warranted because it can ensure data reproducibility and accelerate characterization by unifying data collection procedures. Over the last three decades, 3D electron diffraction (3D ED) has been developed into a reliable technique for atomic structure determination of micron or nano-sized crystals, which is a complementary method to X-ray diffraction and cryo-EM. The development of semi-automated 3D ED is pioneered by electron diffraction tomography (EDT) and rotation electron diffraction (RED), which automate the step-wise rotation of the sample stage and ED pattern acquisition. In the last six years, new protocols, such as continuous rotation MicroED[1], fast-EDT[2] and continuous rotation electron diffraction (cRED)[3,4] have been developed for determining crystal structures of beam-sensitive materials. They are based on continuously rotating the sample stage at constant speed while collecting ED patterns simultaneously. The data acquisition time for a single crystal was reduced from around 1h to within 5mins[5]. The drastic reduction in acquisition time for single dataset makes high-throughput data collection possible.

In order to move towards fully-automated data collection of 3D ED, we developed a software platform (*Instamatic*) based on Python programming language to communicate with TEM and other related hardware. Based on this platform, we developed experiments and protocols to facilitate 3DED data collection. The development of automated data collection can greatly facilitate the discovery of new materials[6] because it enable us to exam each crystal in a large amount of powders and analyze the possible minor phases in the sample. Furthermore, the experience gained from automating 3DED experiments can be extended to other TEM experiments, such as TEM/STEM imaging, Serial electron diffraction and tomography.

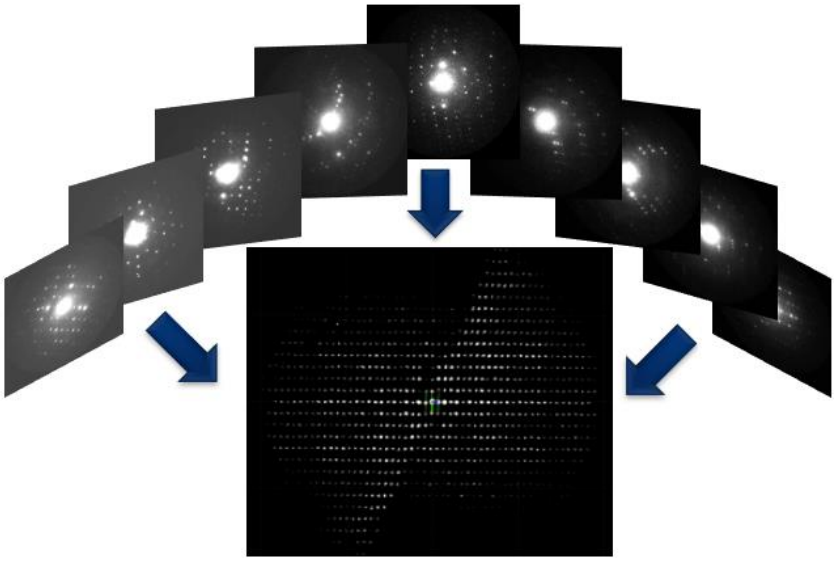

Figure 1. Illustration of 3D electron diffraction

1. Nannenga, B. L., Shi, D., Leslie, A. G. W. & Gonen, T. High-resolution structure determination by continuous-rotation data collection in MicroED. *Nature Methods* **11**, 927–930 (2014).
2. Gemmi, M., La Placa, M. G. I., Galanis, A. S., Rauch, E. F. & Nicolopoulos, S. Fast electron diffraction tomography. *J Appl Cryst* **48**, 718–727 (2015).
3. Wang, Y. *et al.* Elucidation of the elusive structure and formula of the active pharmaceutical ingredient bismuth subgallate by continuous rotation electron diffraction. *Chem. Commun.* **53**, 7018–7021 (2017).
4. Xu, H. *et al.* A Rare Lysozyme Crystal Form Solved Using Highly Redundant Multiple Electron Diffraction Datasets from Micron-Sized Crystals. *Structure* **26**, 667-675.e3 (2018).
5. Nannenga, B. L. & Gonen, T. The cryo-EM method microcrystal electron diffraction (MicroED). *Nat Methods* **16**, 369–379 (2019).
6. Broadhurst, E. T. *et al.* Polymorph evolution during crystal growth studied by 3D electron diffraction. *IUCrJ* **7**, 5–9 (2020).

44. Structural and Microstructural investigation on TBC alumina doped with Titanium Coatings obtained by thermal spray process

Rassim Younes[1], Mohand Amokrane Bradai[1], Youcef Mouadji[2]

[1]*Laboratoire de Mécanique, Matériaux et énergétique (L2ME). Faculté de Technologie, Université de Bejaia, 06000 Bejaia, Algérie*

[2]*Laboratoire de Mécanique, Département de Génie mécanique, Ecole polytechnique Constantine - Algérie.*

Corresponding author: rassim.younes@univ-bejaia.dz

Thermal barrier coating ceramic deposits is an important method of protecting various metal parts, which are exposed to very harsh environments. It consists of input solid particles (a few tens of mm in diameter) into a flame or plasma jet in order to accelerate and melt them before they are crushed on the substrate where they form a deposit. The deposit is in fact a stack of crushed flakes [1-3]. The spraying of TBC offer the potential for improvements in mechanical properties depending on the improvements in physical properties resulting from the microstructure characteristics [4-5]. The use of thermal spraying use to limited to drawable and electrically conductive materials. Recently, however, materials in the form of so-called cored wires have been developed, consisting of a metallic sheath that can be drawn and is conductive, filled with reinforced alloy powders, possibly with ceramic particles. These cored wires allow the flame-wire process to be used to coat superalloys and cermets in order to improve tribological properties

This work is investigation on the microstructural, structural characterisation of a ceramic deposit kind Al_2O_3 doped with 13%TiO_2 (AT-13) deposited on a commonly used low carbon, non-alloyed steel of grade E335 by the thermal flame-wire spraying technique. Microstructural observations showed that the Al_2O_3-TiO_2 (AT-13) deposits exhibit a homogeneous, denser and more compact lamellar morphology with the presence of some porosities. The XRD spectrum of the wire before spraying shows the presence of a some pure corundum majority phase with a rhombohedral structure, a secondary phases which is Al_2TiO_5 under an orthorhombic structure and some traces of TiO_2 (rutile) with a tetragonal structure. The XRD spectrum of the wire deposit revealed the disappearance of TiO_2 and the formation of a new metastable γ-Al_2O_5 phase with a cubic structure.

Key-words: TBC Coatings, SEM Microstructure, X-ray diffraction

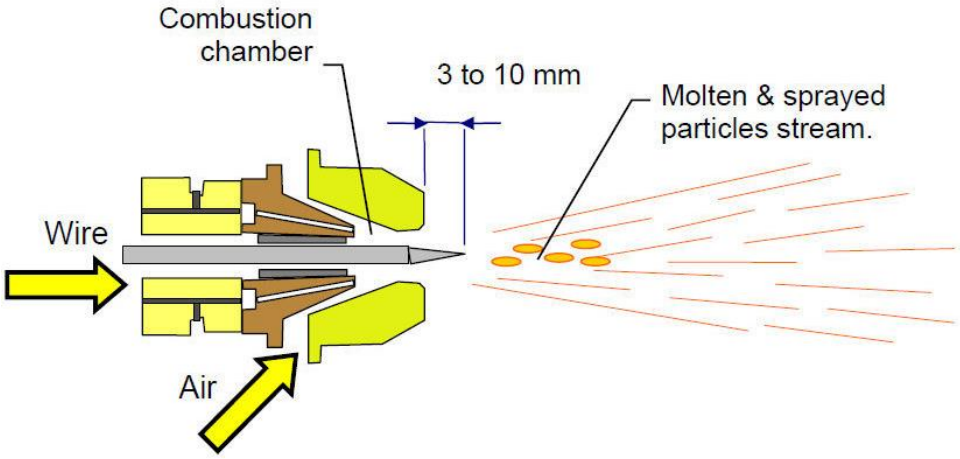

Figure 26 Thermal spray process .

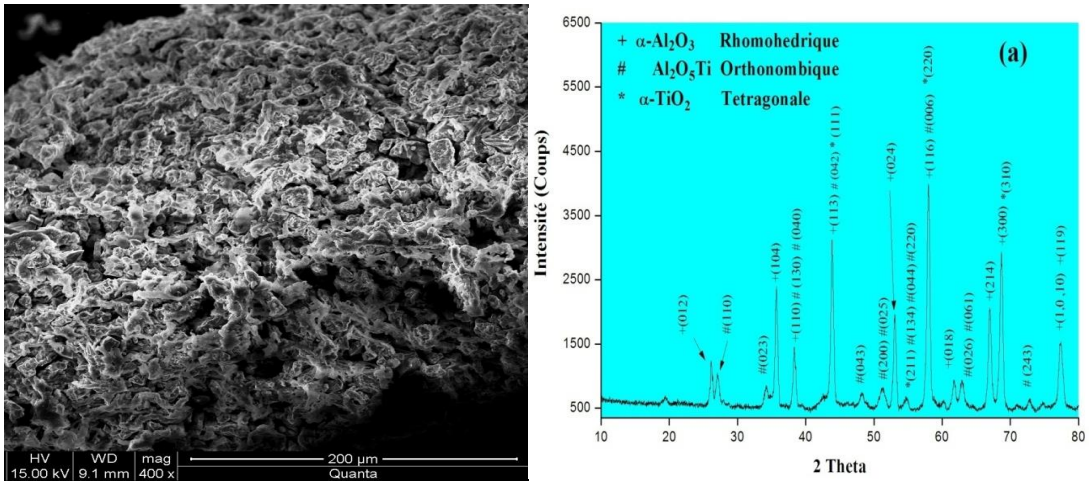

Figure 2: SEM Image and X-ray Diffraction of powder TBC Al2O3- 13%wt TiO2

[1] S. Brossard, P.R. Munroe, A.T.T. Tran and M.M. Hyland, “Study of the splat formation for plasma sprayed NiCr on aluminum substrate as a function of substrate condition,” Surf. Coat. Technol. vol.204 ,pp. 2647-2656, 2010.

*[2] L. Wang, Y. Wang, X.G. Sun, J.Q. He, Z.Y. Pan, Y. Zhou and P.L .Wu, “ Mater, Influence of pores on the thermal insulation behavior of thermal barrier coatings prepared by atmospheric plasma spray**,”** Materials & Design, vol.32, pp 36-47**,** 2011**.***

[3] K. Alamara, S.S. Samandari, P.R. Stoddart and C.C. Berndt , “ Effect of substrate temperature on the splat formation of flame sprayed polypropylene,” Surface & Coatings Technology, vol.206, pp 1180-1187, 2011.

[4] M. Wang and L.S. Leon, “Effects of the powder manufacturing method on microstructure and wear performance of plasma sprayed alumina–titania coatings,” Surface Co at.Technol, vol.202, pp 34-44, 2007.

[5] A. Keyvani , “Microstructural stability oxidation and hot corrosion resistance of nanostructured Al_2O_3/YSZ composite compared to conventional YSZ TBC coatings; Journal of Alloys and Compounds,” vol.623, pp 229-237, 2015.

45. Microscopic characterization of fretting damage in quenched and tempered steel

Amirhossein Zabihi[1], Janne Juoksukangas[1], Jouko Hintikka[3], Mari Honkanen[2], Antti Mäntylä[3], Joona Vaara[3], Tero Frondelius[3,4], Minnamari Vippola[2], Arto Lehtovaara[1]

[1]*Tribology and Machine Elements, Tampere University, Tampere, Finland*

[2]*Tampere Microscopy Center, Tampere University, Tampere, Finland*

[3]*R&D and Engineering, Wärtsilä, Vaasa, Finland*

[4]*University of Oulu, Oulu, Finland*

Corresponding author: amirhossein.zabihi@tuni.fi

Oscillatory tangential loading of in-contact bodies under a micrometer-scale sliding amplitude is termed fretting. Fretting can give rise to significant surface damage accompanied by unforeseen fatigue failure. This study focused on developing a method for the microscopic characterization of fretting-induced damages. The device used in this research caused a reciprocating movement between two annular specimens with large and flat-on-flat contact with no edge effects in fretting motion direction [1]. Under these circumstances, quenched and tempered steel (34CrNiMo6+QT) samples as the self-mated pairs were subjected to the fretting experiments using various normal pressures and sliding amplitudes. Then the microscopic instruments, for instance, the Leica MZ75 stereomicroscope, Alicona InfiniteFocus G5 model 3D optical microscope, and scanning electron microscope (SEM, JEOL IT-500) equipped with an energy dispersive X-ray spectrometer (EDS, EDAX DX4) were employed to investigate the surface and cross-sectional features of the fretted specimens including the protrusions and depressions, wear debris, damaged layers, cracks, and so on. A specific methodology for microscopic examination of fretting degradation was developed as follows:

1. A general view of the whole fretted surface by stereomicroscope.

2. A quantitative measurement of fretting scars through the Alicona InfiniteFocus system to select the areas of interest for further characterization.

3. A compositional and topographical study of the specified regions on the damaged surface and then their cross-section analyses by means of SEM along with EDS analysis to find the elemental distribution. An SEM image of the crack propagation towards the inside of the sample is shown in Fig. 1.

It can be concluded that the above-mentioned microscopic method can be an effective step-by-step technique to characterize the fretting scars by size, depth, surface, and subsurface damages.

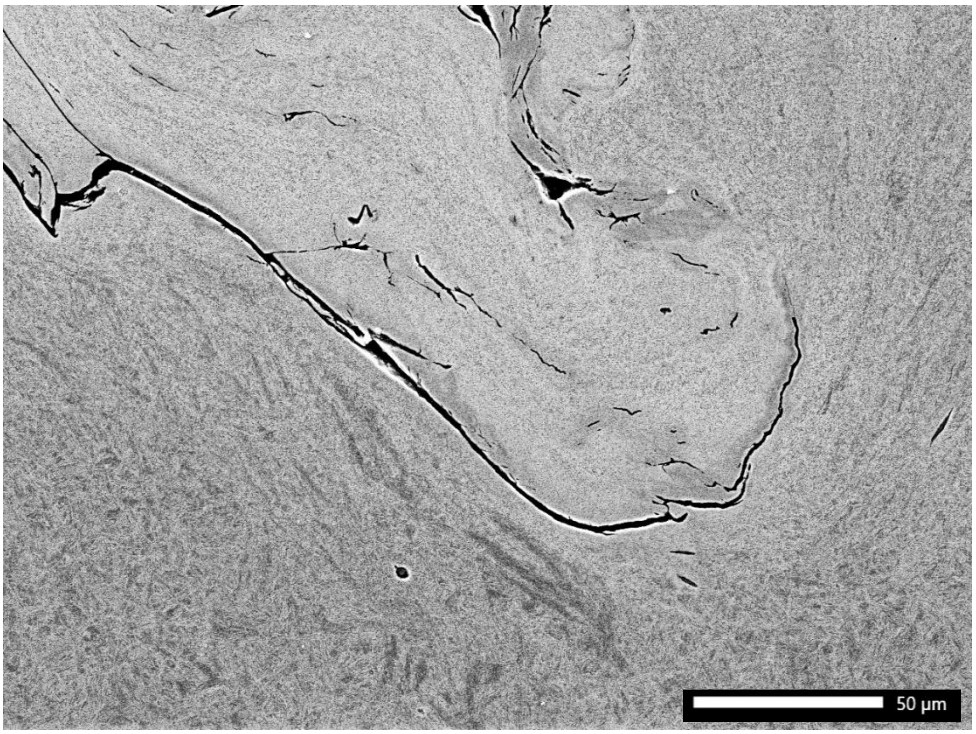

[1] Hintikka, J. et al., “Fretting-induced friction and wear in large flat-on-flat contact with quenched and tempered steel,” J. Tribo. Int., 92, 513-519, 2015.

46. Applications of electron microscopy in additive manufacturing of porous multi-ceramics structures

Setareh Zakeri[1], Mari Honkanen[2], Erkki Levänen[1], and Minnamari Vippola[1,2]

[1]*Materials Science and Environmental Engineering, Faculty of Engineering and Natural Sciences, Tampere University (TAU), Tampere, Finland*

[2]*Tampere Microscopy Center, Tampere University, Tampere, Finland*

Corresponding author: setareh.zakeril@tuni.fi

Ceramic additive manufacturing (AM), also known as ceramic 3D printing, allows the fabrication of 3D ceramic structures with complex geometries that are impossible to be built using traditional shaping methods [1]. Electron microscopy can assist in developing this "long-term game changer for manufacturers" by providing manufacturers with the characterization of the ceramic powders and the quality control of the printed structures. At Tampere University, the advanced electron microscopy techniques available at Tampere Microscopy Center are frequently employed to promote ceramic AM by controlling the quality of the prints and identifying microstructural defects that occur during the printing and heat treatment processes. Our recent study [2] demonstrated the potential of AM to fabricate a new generation of catalytic converters (CCs) by printing self-standing (substrate-less) honeycomb structures out of washcoat materials (gamma-alumina and ceria). Gamma-alumina is a common washcoat material due to its high surface area, however, it loses its surface area at high temperature, and therefore, it requires stabilizers such as ceria to avoid this phenomenon. The structures were printed using stereolithography technique and were sintered at two different temperatures (900 ℃ and 1100 ℃). The homogenous spatial distribution of alumina (orange) and ceria (cyan) powders within the sintered structure at 1100 ℃ was visualized using SEM-EDS mapping (Fig.1(a)). This confirms that ceria did not sediment during the printing process. Hierarchical porosity of the final structure was characterized by SEM, confirming different levels of porosity ranging from $1\,mm$ (open channels intended for gas flow (Fig. 1(b)) to interconnected pores less than $10\,\mu m$ (Fig. 1(c)). The stabilizing effect of ceria on gamma-alumina was studied by surface area measurements and analytical electron microscopy. The STEM and STEM-EDS images shown in Fig. 2(a)-(c) confirmed that no remarkable change in the particle size of alumina can be noticed upon the addition of ceria, indicating that ceria was not effective in stabilizing gamma-alumina at 900 ℃. On the other hand, Figs. 2(d)-(e) show that the presence of faceted ceria particles in the final sintered structure prevented the particle size growth of alumina at 1100 ℃, compared to the pure alumina sintered at 1100 ℃ (Fig. 2(f)).

As the ongoing steps of our research, we are currently using electron microscopy techniques to investigate the effect of organic and inorganic binders on the microstructure of the printed structures and correlate that to the mechanical strength of the structures.

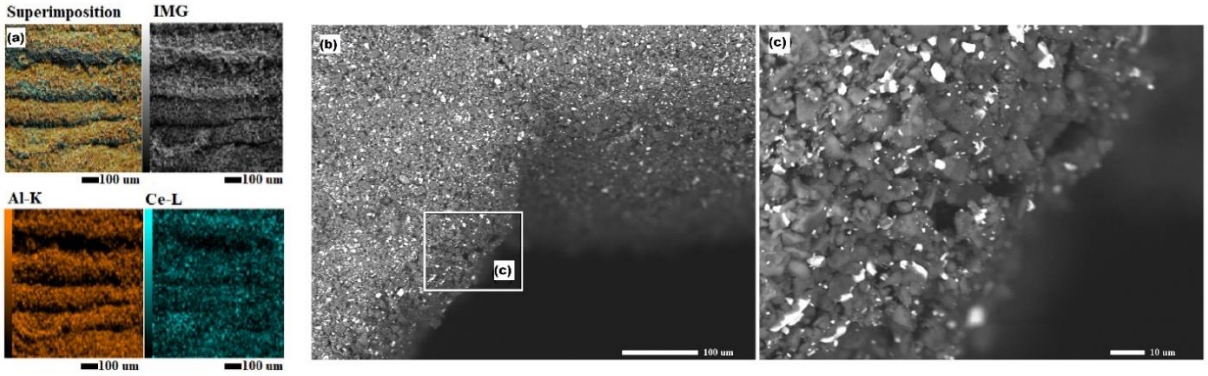

Figure 27 (a) Micro-scale elemental distribution of the sintered structure at 1100 ℃ obtained by SEM-EDS in low vacuum mode (10 Pa) with four sub-images: superimposition of all elemental maps, secondary electron (SE) image of the studied area, and individual elemental maps of Al (orange) and Ce (cyan) shown in the remaining sub-images; (b) Backscattered electron (BSE) image of the sintered structure obtained by with a magnification of 220X; (c) A higher magnification (1000X) BSE image of the marked region in image (b) proposes the presence of interconnected pores in the porous structure [2].

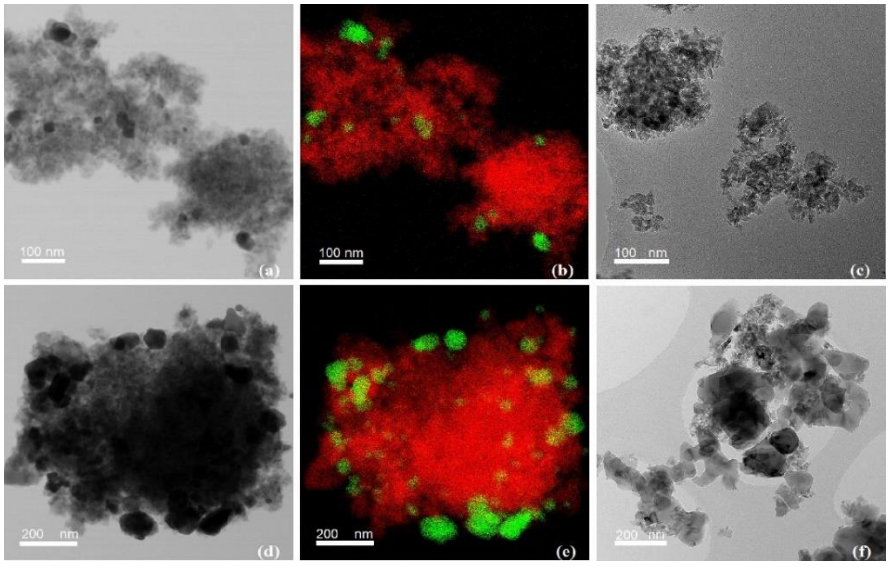

Figure 28 (a) STEM bright field image of the sintered structure at 900 ℃; (b) Elemental distribution obtained by STEM-EDS for the same imaged area as in image (a) with red particles indicating alumina and green particles indicating ceria; (c) TEM image of the pure alumina powder sintered at 900 ℃; (d) STEM bright field image of the sintered structure at 1100 ℃; (e) Elemental distribution obtained by STEM-EDS for the same imaged area in image (d) with red particles indicating alumina and green particles indicating ceria; (f) TEM image of the pure alumina powder sintered at 1100 ℃. Different magnifications have been used for the first (a-c) and second (d-f) row of images [2].

[1] S. Zakeri, M. Vippola, and E. Levänen, “A comprehensive review of the photopolymerization of ceramic resins used in stereolithography,” *Addit. Manuf.*, vol. 35, no. October 2019, p. 101177, 2020, doi: 10.1016/j.addma.2020.101177.

[2] S. Zakeri, T. Vastamäki, M. Honkanen, M. Järveläinen, M. Vippola, and E. Levänen, “Fabrication of self-supporting structures made of washcoat materials (γ-Al2O3-CeO2) by ceramic stereolithography: Towards digital manufacturing of enhanced catalytic converters,” *Mater. Des.*, vol. 210, p. 110115, 2021, doi: 10.1016/j.matdes.2021.110115.

Recent innovations in Scanning Electron Microscope (SEM) in situ Extreme Micromechanics

Remo N. Widmer[1], Nicholas Randall[1], Jean-Marc Breguet[1]

[1]Alemnis AG, Thun, Switzerland

Corresponding author: remo.widmer@alemnis.ch

Micro- and nanomechanical experiments are moving beyond the basic measurement of hardness and elastic modulus thanks to advantages of testing in situ in SEMs. For example, until only recently, high strain rate mechanical testing of materials at strain rates from 100 s-1 – 10'000 s-1 has only been possible using macroscale techniques, such as split Hopkinson bar, Kolsky bars, and plate impact testers. At the microscale, strain rates have typically been limited to approximately 0.1 s-1 or less, owing to limitations in instrumentation, insufficient data acquisition rates and elastic wave propagation conflicts during testing. The latest developments in nanoindentation instruments now allow access to extremely high strain rates up to 104 s-1 and high oscillation frequencies up to 10 kHz at the nanoscale. These state-of-the-art instruments have unlocked access to a wide range of previously unattainable micromechanical properties such as strain-rate sensitivity, fracture-toughness, or high cycle fatigue, by taking advantage of novel piezo-based nanoindentation methods.

This talk will focus on the most recent developments in instrumentation for in situ extreme mechanics testing at the micro and nanoscales. In the focus is a testing platform capable of strain rate testing over the range 0.0001 s-1 up to 10'000 s-1 (8 orders of magnitude) with simultaneous high-speed actuation and sensing capabilities with nanometer and micronewton resolution, respectively. Additionally, the challenges and solutions to performing extreme mechanics over the temperature range from -150 °C to 1000 °C, and the inherent advantages of using small volumes of sample material will be discussed, alongside the presentations of some examples of test data. Finally, future research directions in the field of extreme micromechanics will be discussed.

New abilities in electron microscopy through Laser FIB and sensitive BSE detection

Leif Viskari[1]

[1]*Carl Zeiss AB, Stockholm, Sweden*

Corresponding author: leif.viskari@zeiss.com

In this presentation, we share insight to two recent developments by Carl Zeiss.

Laser FIB (Laser-assisted Focussed Ion Beam milling) allows rapid sample preparation and modification. The use of a femtosecond laser allows high-quality and nearly athermal milling, with milled volumes of cubic millimetres achieved in minutes and surface quality that even allows rudimentary EBSD analysis to be conducted without final FIB-polishing. Here, we provide a technical and methodological overview based on the Carl Zeiss Crossbeam, along with application examples such as cross-sectioning and preparation of micro-mechanical samples.

Improved SEM detectors enable advances in acquisition and workflow. The difference between past- and modern generation BSE detection can literally make or break a study. With the new Carl Zeiss Sense BSD, sensitive and/or low-signal-yielding samples can be studied with better results and less risk of sample damage, as exemplified here in the context of low-voltage imaging of biological and sensitive samples.

Company Webinar JEOL – news from R&D

Philipp Wachsmuth[1], Youssef Akil[1], Gabi Gottstein[1]
[1]*JEOL (Germany) GmbH, Freising, Germany*

Corresponding author: Gottstein@jeol.de

With more than 70 years of experience in research and development, JEOL is today one of the largest manufacturers of electron optical systems and offers a wide range of different analytical and electron optical equipment.

Building on this long history and broad experience in electron optics, JEOL continuous to further develop methods and instrumentation. This is highlighted by the recent releases of new high-end transmission electron microscopes (TEM) like the dedicated and fully automated CryoARM II for life science applications as well as the material scienced focused ultra-high atomic resolution GrandARM II.

We will present a detailed overview of the current line-up covering the newest instrumentation in each of the different product groups JEOL has to offer.

Precession enhanced Electron Diffraction in TEM: From Structure Determination to Orientation & Strain Mapping at nm scale

Athanassios S. Galanis[1]
[1]*NanoMEGAS SPRL, Brussels, Belgium*

Corresponding author: tgalanis@nanomegas.com

Precession Electron Diffraction (PED) technique in Transmission Electron Microscope (TEM) has been first reported by the Vincent and Midgley in 1994 [1]. Since then, and since the commercial availability of beam precession device [2] to the market ten years after, several TEM applications for nanomaterials have been developed based on that technique. It is currently well established that PED enhance dramatically reflections quality (quasi-kinematical) and diffraction data resolution. A significant number of articles (based on PED and our instrumentation) from various laboratories worldwide have been published since 2004, on major scientific microscopy/material science journals.

Due to precession diffraction influence to obtain improved ED data quality, PED was first applied in electron crystallography, where in combination with 3D diffraction tomography in the TEM, has revealed as powerful technique for structure determination of nanocrystals (from complex zeolites and minerals to metals, alloys and organics). In 3D PED TEM tomography method, a series of ED patterns are collected every 1 degree of tilting around the goniometer axis [3, 4]. ED intensities can be extracted automatically towards the crystal structure solution of nanocrystals.

Most popular technique in materials science that uses PED, is the TEM automatic orientation and phase mapping analysis [5,6]. This technique (ASTAR) is like the traditional EBSD method in SEM, and the major benefit is the enhanced spatial resolution that can be up to 1-3 nm (FEG-TEM). With ASTAR, PED spot diffraction patterns are recorded while the sample area of interest is scanned by the precessed electron beam. [2]. Crystallographic orientation and / or phases are observed through comparison of recorded ED patterns with pre-calculated (simulated) templates [7]. ASTAR method has been successfully applied to several materials as metals, alloys, minerals, semiconductors, ceramics, nanowires, ion batteries, organic compounds, etc

PED has been recently successfully applied to obtain strain mapping analysis of several semiconductor materials at 1-4 nm resolution (sensitivity 0.02%), based on comparison of PED-NBD patterns of strained areas with a reference - non-strained area. This technique (TopSPIN) is critical to monitor the designed and unintended strain distributions. Beam Precession is applied in strain mapping analysis, as ED reflections become insensitive to thickness and minor orientation variations, the dynamical effect is reduced, and the number of higher order reflections is increased, improving strain map accuracy.

The recent launched application of e-PDF (electron Pair Distribution Function) approach [8] allows the characterization of nanocrystalline or amorphous materials. e-PDF technique analyze the interatomic distances, bonding and possible short/large scale order of nanocrystalline /amorphous materials at nm scale, enabling to monitor in situ solid state reactions, structure of glassy materials, layered thin films quality and amorphous/ re-crystallization studies in semiconductor devices.

[1] R. Vincent and P. Midgley, Ultramicroscopy **53** (1994), p. 271

[2] www.nanomegas.com

[3] E. Mugnaioli *et al*, Ultramicroscopy **109** (2009), p. 758.

[4] U. Kolb *et al*, Ultramicroscopy **107** (2007), p. 507.

[5] E.F. Rauch *et al*, Zeitschrift für Kristallographie **225** (2010), p. 103.

[6] A. Kobler *et al*, Ultramicroscopy. 2013 May;128:68-81

[7] E.F. Rauch and M. J. Veron, Mater. Sci. Eng. Tech. **36** (2005), p. 552.

[8] T.Egami, S.Billinge Underneath the Bragg Peaks Pergamon vol.16

Bringing EDS to life! Multi-colour electron microscopy on biological samples.

Louise Hughes[1]
[1]*Oxford Instruments, Bucks, United Kingdom*

Corresponding author: louise.hughes@oxinst.com

What if we could change the way we analyse biological sample in an electron microscope? What if we could use EDS as a true imaging tool to help us interpret data from our samples?

Multi-colour electron microscopy using energy dispersive x-ray spectrometry (EDS) combines ultrastructural electron data with elemental information about sample composition. The additional ultrastructural differentiation can improve interpretation of features within samples and highlight regions of interest not easily determined using the electron signal alone.

Recent key developments in EDS technology have increased the speed of accurate analysis of light elements in biological samples. A major task remains in selecting the best methods for specimen preparation and determining the influence that choice has on the data we can obtain. This webinar will discuss the workflows involved, from sample prep considerations through to rapid analysis, and highlight how EDS is rapidly becoming a key technology for your biological and biomaterial research questions.

A New Large-Array Direct Detector for Ultra-Fast 4D STEM 4D

Robert Monteverde[1]
[1]*Direct Electron, San Diego, The United States*

Corresponding author: bmonteverde@directelectron.com

STEM is a technique that is becoming increasingly widespread, with a broad range of applications including electric and magnetic field mapping, crystal grain and strain mapping. In contrast to conventional, 2D STEM, where electrons scattered over a large range of angles are collected using a detector that outputs a single intensity value at each probe position, 4D STEM employs a pixelated detector to record a complete scattering pattern at every probe position, yielding an information-rich 4D dataset. One current limitation of 4D STEM is thoughput. Pixelated detector frame rates limit 4D STEM to acquisition speeds that are 1-2 orders of magnitude slower than conventional 2D STEM. Certain 4D STEM applications, particularly crystal grain mapping, may benefit from the use of a detector with a relatively large ~ 1 megapixel array size, and this array size can give the detector the flexibility to perform non-4D STEM applications, such as fast in situ TEM imaging. However, to achieve a megapixel array size, microscopists are limited to a choice between using detectors optimized for low-dose biological TEM imaging, or using detectors that consist of tiled 256 x 256 pixel chips, with areas of missing information between tiles.

Here, we describe Celeritas, a new, ultrafast monolithic active pixel sensor (MAPS) type direct detector specifically designed for 4D STEM. The physical sensor is 1024 × 1024 pixels in size, with 15 µm pixel pitch. At full frame size, the detector readout speed exceeds 2,100 frames per second (fps) Higher speeds are achieved through sub-area readout, with maximum of up to 87,000 fps 256 × 64 pixels, a speed approaching that of conventional 2D STEM. The flexibility of Celeritas allows the user to choose pixel count and speed to suit a variety of different applications and imaging modes.

A New Event-Based Direct Detector for Cryo-EM

Michael Spillman, Benjamin Bammes*, Hongjiang Wu+, Robert Bilhorn*, Zhao Wang+, Robert Monteverde

** Direct Electron, LP, + Baylor College of Medicine*

Corresponding author: bmonteverde@directelectron.com

Over the past 10 years, electron counting with direct detection cameras has become the de facto standard for cryo-EM data acquisition. However, since its initial demonstration in 2009, the technology for electron counting has remained fundamentally unchanged: Electron counting is performed computationally, by thresholding and centroiding blobs on each of a large number of integrating mode frames acquired under a strictly limited TEM beam current. Every new camera generation from each of the three direct detection camera companies has used this brute force counting strategy, featuring only moderate increases in size, speed, and price.

One of the most significant bottlenecks for cryo-EM is the restrictive imaging conditions imposed by electron counting. Maintaining sparse illumination within each frame from the camera is necessary to avoid coincidence loss stemming from the inability to discriminate multiple coincident electrons as separate events. The limited exposure rate imposed by current cameras has two consequences: (1) it places an upper limit on throughput, and (2) it eliminates the microscopist's flexibility to optimize imaging conditions for new methods.

Here, we describe new direct detection technology that-for the first time-performs electron counting in hardware with a 4kx4k sensor, enabling high-quality image acquisition across a wide range of exposure rates with minimal coincidence loss. The resulting camera-called Apollo-delivers the quality of electron counting, while offering the flexibility and easy-of-use of an integrating-mode camera.

Combined WDS-EDS analysis on the SEM

Rosie Jones[1]
[1]*Oxford Instruments, Bucks, The United Kingdom*

Corresponding author: rosie.jones@oxinst.com

Wavelength Dispersive Spectrometry (WDS) and Energy Dispersive Spectrometry (EDS) utilize the same X-ray signal, generated by bombarding a solid sample with a beam of electrons, to determine elemental composition and distribution. These two microanalytical techniques, which can be employed on electron beam instruments (e.g., scanning electron microscope (SEM)), have different advantages/disadvantages. A higher spectral resolution can be achieved with WDS, and therefore it is possible to resolve X-ray peaks that overlap in the EDS spectrum, resulting in more accurate element identification and quantification. The higher spectral resolution of WDS also brings higher peak to background ratios, and therefore, lower detection limits allowing the accurate quantification of trace elements (>0.1 wt%). A comparative disadvantage of WDS is, unlike EDS, which generates a spectrum for the whole possible range of energies instantaneously, WDS can only measure X-rays of one energy at a time and therefore measurements are typically slower. The count rate achievable with a large area EDS detector is also typically higher, again making analysis via EDS quicker.

On this basis, a highly favourable solution is to combine the two techniques for fast and accurate results, and to do this on a highly flexible instrument for imaging and microanalysis – the SEM. Major – minor elements present in a sample can be measured using EDS, and WDS can be utilized where it is most advantageous – for the accurate quantification of trace elements, or those impacted by peak overlaps. This presentation will demonstrate the advantages of adding a WD spectrometer, with Rowland circle geometry and fully focussing crystals, to an SEM and conducting analysis in combination with EDS. We outline our method and show how using this approach can achieve results that are comparable with those collected on an electron microprobe (EPMA) with multicollection WDS.

Gain the maximum throughput with artifact-free surfaces for sample characterization by using high current plasma FIB-SEM

Petr Klímek[1]
[1]*TESCAN, Brno, Czechia*

Corresponding author: petr.klimek@tescan.com

The standard procedure for preparing cross sections using the FIB-SEM technique is to use high currents to remove material quickly, then reduce the FIB current to obtain better beam profile and consequently, a better quality for the final surface. Reducing the maximum current used for final polishing of the section surface, however, results in a longer preparation process. For small cross sections with sizes in the tens of µm, this current reduction method is acceptable. However, as the size of the cross-sectional area to be polished increases, the analysis time increases substantially; therefore, this method is not suitable for preparing cross sections with sizes in the hundreds of µm. To overcome this limitation for large cross sections, plasma FIB was introduced to deliver higher beam currents than those achievable with conventional Ga FIB-SEMs.

Plasma FIB-SEM provides several advantages for sample characterization. First, its high current ion beam is capable of high material sputtering rates which enables efficient preparation of large trenches or cross sections. Plasma FIB also can be used for polishing large surface areas, thereby enhancing sample features and providing more detailed contextual information about structure and composition. about the sample. This can help to reveal material distribution, obtain better statistical information, and link the microscale to the nanoscale sample characterization.

Several technologies have been introduced that improve the implementation of high current plasma FIB for large scale materials characterization. In this webinar, we will walk through the typical plasma FIB cross-sectioning workflow and discuss high current polishing methods. We will present TESCAN's TRUE X-Sectioning TESCAN Rocking Stage, which were developed to suppress artifacts and improve the final cross section surface quality when using high beam currents for final polishing. Finally, we will show how plasma FIB-SEM speeds not only cross section preparation, but also enables a greater understanding of your materials by improving 3D FIB-SEM tomography analyses.